University of South-Eastern Norway
Faculty of Technology, Natural Sciences and Maritime Studies
—
Doctoral dissertation no. 167
2023

Guozhen He

Point of Care COPD Diagnostics Based on Paper-based Assay and Biofluid Sensing

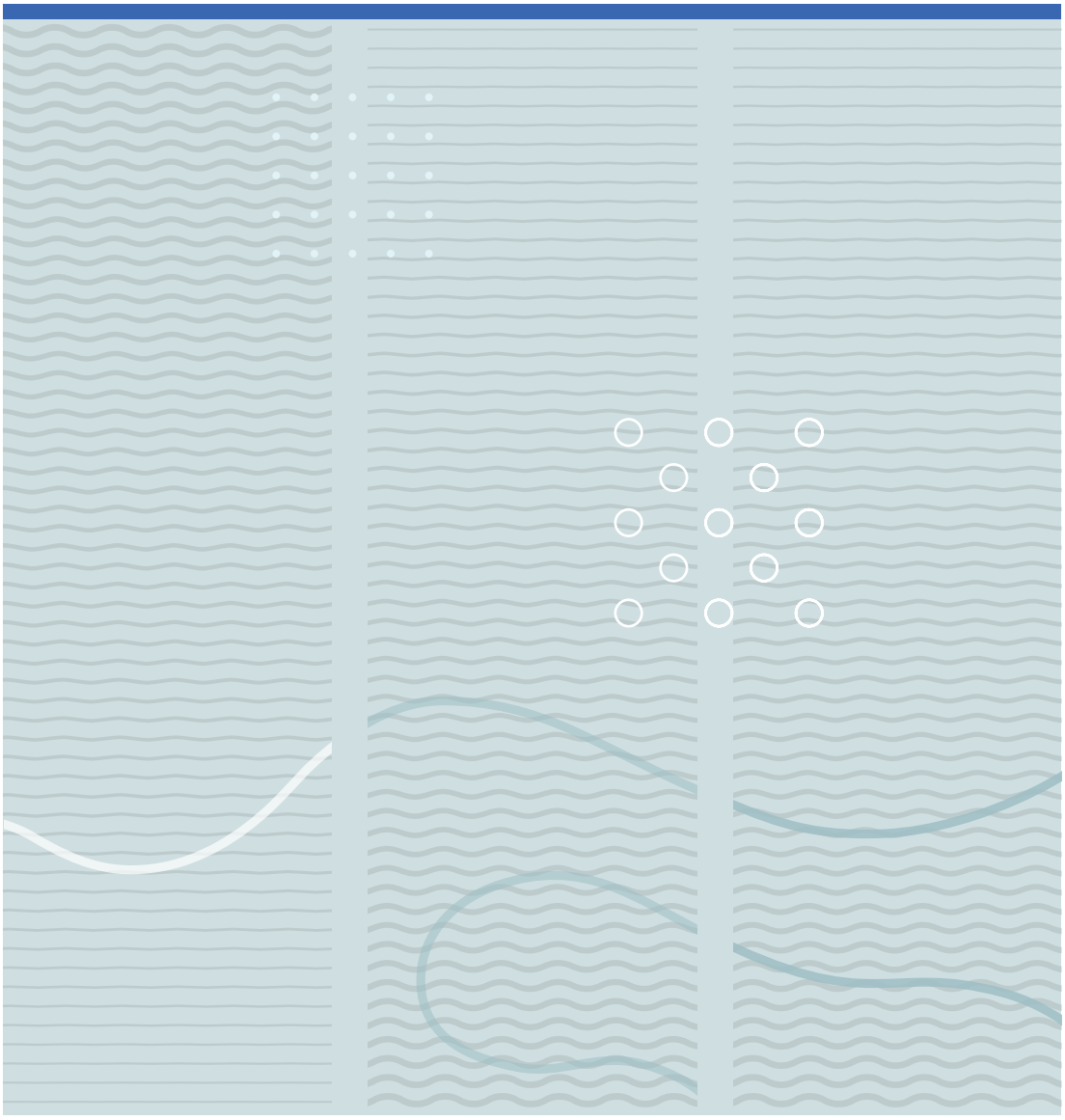

Guozhen He

Point of Care COPD Diagnostics Based on Paper-based Assay and Biofluid Sensing

A PhD dissertation in
Applied micro- and nanosystems

Faculty of Technology, Natural Sciences and Maritime Studies
University of South-Eastern Norway
Horten, 2023

Doctoral dissertations at the University of South-Eastern Norway no. 167
ISSN 2535-5244 (print)
ISSN 2535-5252 (online)

ISBN 978-82-7206-783-9 (print)
ISBN 978-82-7206-782-2 (online)

Print: University of South-Eastern Norway

Dedication

To my beloved parents Yong and Jin,

Thank you is never enough to express my gratitude to your everlasting love and solicitude.

Preface

The thesis is submitted for the degree of Philosophiae Doctor from the Department of Microsystems, Faculty of Technology, Natural Sciences and Maritime Sciences, University of South-Eastern Norway.

The doctoral study was conducted from October 2018 to September 2022 with Professor Tao Dong, PhD., as the primary supervisor.

This work was also supported by co-supervisors Professor Per Alfred Øhlckers and Dr. Zhaochu Yang.

Financial support:

- Sensovann AS
- RFF Forskningsfond. Oslofjordfondet, Praktisk og effektiv oppflging av KOLS-pasienter i kommunene (Project No. 285575)
- Regionalt forskningsfond Vestfold og Telemark (Project No. 321814)

Acknowledgements

I would like to firstly express my gratitude and appreciation to my primary supervisor, Professor Tao Dong, for his guidance and motivation. Thanks for giving me the opportunity. I learnt the attitude and methodology towards both life and research.

I wish to express my thanks to my co-supervisors, Dr. Zhaochu Yang and Prof. Per Øhlckers for their insightful discussions on my research and articles. I appreciate the help from Dr. Nuno Pires, Dr. Zhongyuan Shi, and Dr. Haakon Karlsen, Joao Carlos for their discussions on bioelectronics and biosensors.

I wish to thank all my group members and my close friends in Norway, China, the United States, Germany, and the United Kingdom, for making my study period full of joy.

Abstract

Chronic obstructive pulmonary disease (COPD) has always been the one of the top four major death causes during the last ten years. During the era of covid-19 pandemic, COPD patients faced higher mortality rates than ever before. Inefficiency in COPD diagnosis and exacerbation monitoring leads to tremendous medical costs and economic burden. Decentralized point-of-care (PoC) diagnostics based on disposable paper-based biosensors emerge as a cost-effective approach, which requires sensitive detection of COPD biomarkers in human saliva and blood as a prerequisite. When testing biological samples, it also needs to consider matrix effects resulted from samples and handling protocols. Biofouling is the most noticeable and deleterious effect of untreated saliva or serum that happens simultaneously on most interfaces that results in blocking and passivation of the sensing surface with non-specific adsorbed proteins.

This dissertation work focuses on the following challenges: (i) demonstrate sensitive electrochemical and optical biosensing of COPD biomarkers in human saliva based on lateral flow assays; (ii) investigate solutions to resolve hook effect in sandwich LFAs and redesign the LFA structure; (iii) control defects in emerging nanomaterials, taken 2-dimensional black phosphorus as an example, for the development of future biosensors that contact human saliva and blood; and (iv) an anti-biofouling strategy to overcome non-specific protein adsorption and matrix effect of body fluids.

Keywords

COPD, PoC diagnostics, Lateral flow assay, Hook effect, Salivary assay, Defects, Two dimensional materials.

List of papers

The thesis is based on the following articles:

Article 1

He, G., Dong, T., Yang, Z., Branstad, A., Huang, L., Jiang, Z., (2022). Point-of-care COPD diagnostics: Biomarkers, sampling, paper-based analytical devices, and perspectives, Analyst, 147, 1273-1293. Doi: 10.1039/D1AN01702K

Article 2

He, G., Dong, T., Yang, Z., Jiang, Z., (2022) Mitigating hook effect in one-step quantitative sandwich lateral flow assay by timed conjugate release, Talanta, 240, 123157. Doi: 10.1016/j.talanta.2021.123157

Article 3

He, G., Dong, T., Yang, Z., Ohlckers, P., (2019) Tuning 2D Black Phosphorus: defect tailoring and surface functionalization, Chemistry of Materials, 31(24), 9917-9938. Doi: 10.1021/acs.chemmater.9b03639

Article 4

He, G., Dong, T., et al. (2023) Surface oxygen deficiency enabled spontaneous anti-protein-fouling in WO_3 nanosheets.

Article 5 (IEEE Conference)

He, G., Dong, T., Yang, Z. (2022) Probe sonication to prepare homogenous WO_3 nanosheet inks for energy conversion and biosensing applications, 20th International Conference on Mechatronics-Mechatronika, pp. 1-4. IEEE. DOI: 10.1109/ME54704.2022.9982863.

Articles 1,3,4 and 5 are omitted from online publication

Table of contents

1 Introduction

1.1 COPD prevalence and outcomes

During the past decade, chronic obstructive pulmonary disease (COPD) has consistently ranked among the top four leading causes of death around the world.[1,2] It affects around 10 percent of the world population and led to an annual mortality of 3.2 million lives in 2017, while the yearly mortality increased by 13.2 from 2007 to 2017.[3] In Norway, COPD is known as **kronisk obstruktiv lungesykdom (KOLS)**. It affects around 6 percent of the Norwegian people over 40 years old.[4] As life expectancy extends, there is a tendency that more people are likely to suffer from COPD in the future. Moreover, in this post-covid era, COPD patients are more vulnerable than ever before. People suffering from COPD are 4 times more risky to severe COVID-19 disease and suffer poor outcomes.[5,6] A multicentered study showed that 62.5% of the severe COVID-19 cases and 25% of deaths were COVID patients.[7]

The prevalence and outcomes of COPD have led to tremendous direct medical costs and indirect economic costs including sick leave and lost productivity. In the United States, studies estimated that the annual direct cost exceeded 30 billion U.S. dollars and the total cost reached 50 billion U.S. dollars in 2010.[8] In Norway, COPD, together with other respiratory diseases, annually led to 11.1 billion Norwegian Kroners (NOK) of direct medical expenditures and 17.2 billion NOK of total economic loss in 2013.[9] According to Folkehelseinstituttet (FHI) data[10], the county of Vestfold and Telemark has a higher number of COPD medicine users than the Norwegian average (see Table 1). The medical care expenditures and total cost sharply increase as COPD exacerbates into late stages while the survival rate of patients decreases.[11]

Thus, early diagnosis and timely follow-up of COPD status together play a crucial role in treating COPD patients as well as reducing COPD-related losses.

Table 1. Prevalence of major chronic diseases in Norway.

Chronic disease	Vestfold og Telemark	Norway (average)
COPD/Asthma medicine users	120	114
Heart disease medicine users	101	103

*Per 100 000 people. Data obtained from FHI website.[3]

1.2 Advances in PoC diagnostics of COPD

The traditional definition of COPD is irreversible airway limitation caused by environmental pollution and smoking. COPD stages and exacerbation were monitored based on spirometry together with a symptom questionnaire.[3,12] In recent years, researchers argued that COPD is resulted from environment-gene interactions.[12–15] According to Global Initiative for Chronic Obstructive Lung Disease (GOLD) report published in 2022, host factors were included as part of the COPD causes,[16] consequently indicating that diagnostics and monitoring based on spirometry is not sufficient to manage COPD. Discovery and systematically studies of COPD biomarkers have shed new lights on the COPD diagnostics and monitoring. Researchers argued that biomarker plays a critical role in identifying the causative COPD endotypes and predicting declines of lung function associated with exacerbation.[3,12] Therefore, the detection and quantification of proteins in human body fluids is extremely important. Biomarkers—especially proteins produced by human organs and subsequently transported into body fluids—can reproducibly indicate medical states of the patients,[17–19] e.g. c-reactive protein (CRP), interleukins (ILs), and matrix metalloproteinases (MMPs) for COPD diagnosis.[19] By detecting levels of protein biomarkers in body fluids, it potentially offers a simple, fast, affordable, and non-invasive solution to largely boost the early screening and monitoring of COPD.

Saliva or blood? Blood, urine, interstitial fluid, and saliva are the commonly targeted body fluids in the measurements of protein biomarkers.[19,20] As a lung disease, biomarkers related to COPD are mostly accessible in saliva and blood. The dissertation briefly illustrated the biological pathways of these protein biomarkers since releasing from the lungs to entering blood and subsequently into saliva (figure 1), in concentrations ranging from sub-picomolar to micromolar. This thesis summarized representative biomarkers related to COPD and acute exacerbation of COPD into table 2 and table 3 in section "4.1.3 salivary and blood biomarkers". The levels of these COPD protein biomarkers were found to be correlated between blood and saliva. Detection of these protein levels in either blood or saliva can be applied to prevent COPD exacerbation. Nevertheless, sampling blood requires invasive needle or needle-equivalent technology, which is still not adequate for the daily assay. On the contrary, sampling saliva is harmless and more accessible than testing blood, which matches perfectly to routinely monitoring of COPD exacerbation. The collection of samples is non-invasive, fast and economic. It poses lower risk of infection and is easy to handle for multiplexed tests. In addition, the concentration of target biomarker in saliva often correlates well to blood. The saliva assay would offer a perfect test allowing convenient diagnostics and follow-up checks at point of care scenarios, which may effectively lower the medical cost in long-term treatment of COPD.[21] Despite of the promising future, it needs a combination of multiple biomarkers to accurately predict the exacerbation of COPD against other diseases or simple inflammation. This problem has motivated the development of protein biosensors[3,22] which can provide detection results in minutes and are amenable to analyze proteins in settings outside a clinical laboratory. However, modern biosensors still face an important challenge[3,22]: diagnosis of diseases requires detecting several protein biomarkers simultaneously while their concentrations in the biological fluids vary by several orders of magnitude. It poses a strict requirement for the detection range of biosensors. Readers may refer to Article 1 included in the dissertation for detailed discussions on the COPD biomarkers, sampling technologies, and evaluation of point-of-care COPD diagnostic strategies based on biomarkers.

Methods like Western Blot, ELISA, electrophoresis, and chromatography are often applied to detect protein biomarkers in saliva. These conventional techniques still need professionals to operate in labs, contrary to the goal of early screening and monitoring from accessible body

fluids like saliva. The urgent need for a robust protein biosensing technology motivates the development of biosensors.[23]

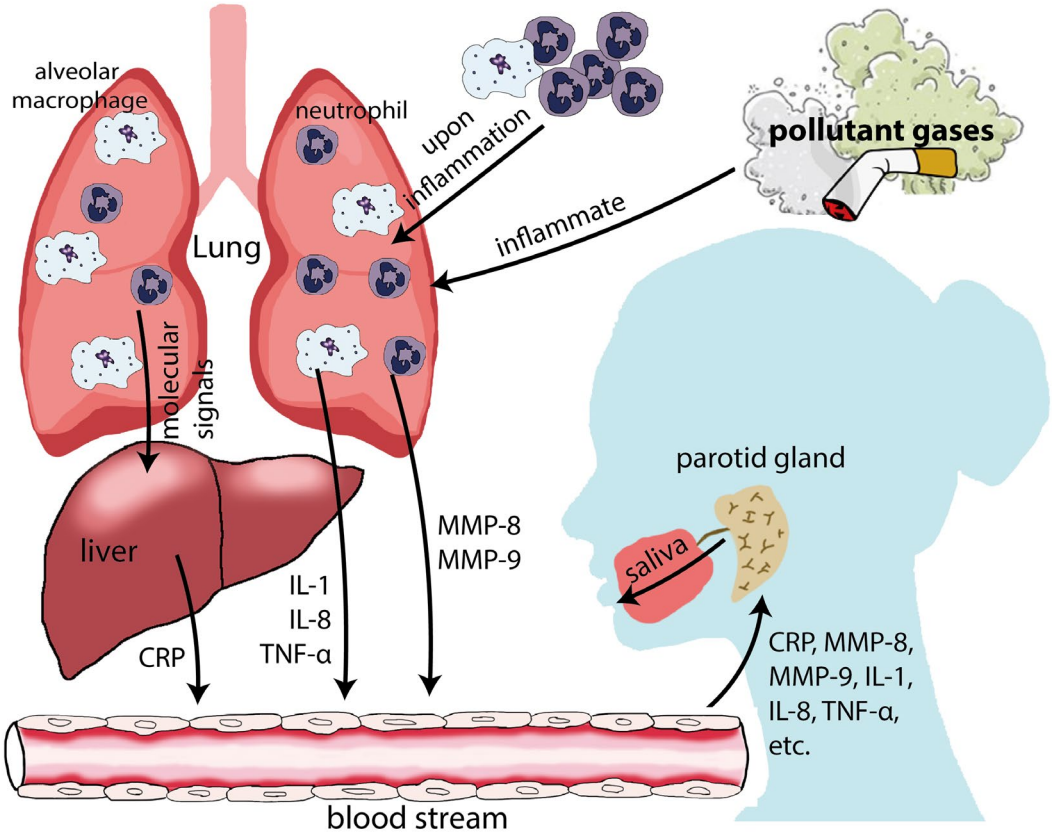

Figure 1. A scheme representing generation of COPD-related protein biomarkers and their biological pathway toward blood and saliva. Selected COPD protein biomarkers are produced by different organs, transported to parotid gland via blood, and secreted into saliva.

1.3 Biosensor strategies for COPD

Current biosensors to detect proteins are consisted of three essential components—a biological recognition element (bioreceptor) that selectively responses to single or multiple the target analytes, a transducer that produces a measurable signal upon bio-recognition events, and finally a signal processor that collects, amplifies, and displays the signal. Transducer is the key biosensing part in biosensors, which is based on the principles of optics,[24] magnetics,[25] colorimetry,[26] electrochemistry,[27] acoustics[28], photoelectrochemistry[29],

etc. To improve the level of automation, biosensors are coupled with either disposable or non-disposable microfluidic platforms. Article 1 discusses disposable microfluidic platforms for COPD diagnostics through human body fluids. Since label-based biosensors have been well-studied and intensively reviewed by other researchers,[30] this dissertation only covers the development of label-free biosensors that detects protein biomarkers, especially photoeletrochemical biosensors as an emerging genre and comparison between electrochemical and photoelectrochemical biosensors. When these two biosensors are testing real human samples, either in vitro or in vivo, co-existing proteins will simultaneously adsorb to the electrode surfaces, known as the biofouling phenomenon. Article 4 presents development of an antifouling strategy by modifying electrode surface with WO_3 nanosheets that are rich in oxygen vacancies.

1.3.1 Research progress on label-free protein-sensing biosensors

Label-free biosensor consists of a recognition unit and a sensing unit. Typical recognition units for specific protein detection include: (1) Single biological receptors as antibodies, phages, affibodies, molecularly imprinted polymers, and aptamers. Binding of target protein to these receptors (by molecular affinity) triggers the signal of protein detection. The detection signal can be either dependent or independent of intrinsic electronic properties of these receptors. (2) Dual biological receptors as aptamer-complementary oligonucleotide probes[31,32] and hairpin-triplex oligonucleotide probes[33]. These probes may have two mechanisms of recognition: one involving dissociation of the probes in which the aptamer binds to the protein with higher affinity against the complementary sequence. The structure of the probe is destroyed and leads to the detection signal; second involving the adsorption of the target protein to the dual oligonucleotide probe. This mechanism occurs if the protein possesses redox groups, and the detection signal is achieved via DNA-mediated charge transport. The intrinsic charge transport properties of double stranded oligonucleotides were characterized by researchers of Professor Barton's group at California Institute of Technology.[34,35] For electrically inert proteins, such as CRP, ILs and MMPs, the use of DNA-mediated charge transport can be adapted with the aid of redox molecules adsorbed or intercalated to DNA base pairs.[36]

1.3.1.1 Label-free electrochemical biosensor

Amperometric, potentiometric and impedimetric sensors are the types of EC sensors commonly reported in the literature. The corresponding label-free sensing schemes for protein detection in saliva are shown in figure 2. An amperometric sensor with a "sandwich" type assay conducted on top of the working electrode was studied to detect salivary TNF-α. Atop a gold working electrode immobilized capture antibody. Horseradish peroxidase (HRP) was chosen as the label and linked to detection antibody. HRP catalyzed the redox reaction of a redox mediator on top of the working electrode. The current was measured as a function of time using a chronoamperometric technique in where the excitation voltage applied to the working electrode was swept with time using pulses. The technique exhibited fast response (within seconds) for bio-detection and low detection limits (picomolar levels).[27] Field effect transistors (FETs) were reported in potentiometric sensor to detect cytokines in saliva as demonstrated by Xuezeng´s group at Harbin Institute of Technology[37]. The FET channel made of graphene had immobilized single-stranded oligonucleotides, and the capture of protein had induced changes of channel conductivity detected by an increase of potential difference between source and drain electrodes. The concept showed a detection limit of 12 pM. On the other hand, an impedimetric sensor was developed by Kim et al. to detect salivary cortisol.[38] The sensor was run as a chemiresistor using reduced graphene oxide as the resistor channel which immobilized antibody specific to cortisol. The sensor exhibited limit of detection as low as 27.6 pM, and the low limit was explained by the feature of the reduced graphene oxide channel to sharply vary its impedance due to the capture of the antigen.

Despite the advances, further development of label-free EC biosensors is limited by a number of factors. (1) The EC sensors need to introduce an electrical perturbation or electrical excitation (fixed DC or AC potential) when measuring the protein concentration. Because the measurement relies on electrical bias, the EC sensors are susceptible to high background noise. This explains the narrow detection range (only two orders of magnitude) of the biosensors.[27,38,39] (2) The potentiometric FET sensor is hindered by false-positives results due to high susceptibility of the detection area (Debye length) to interferences from any charged substances in the biological sample. These interferences are independent from applied electrical perturbation. (3) Most of label-free amperometric sensors relied on antibody to

controlling electron transfer between a redox mediator and an electro-catalyst onto the electrode surface, while the impedimetric sensor also depends on the electronic properties of the antibody. However, typical antibody exhibits low conductivity and high impedance, which also contributes to the narrow detection range.

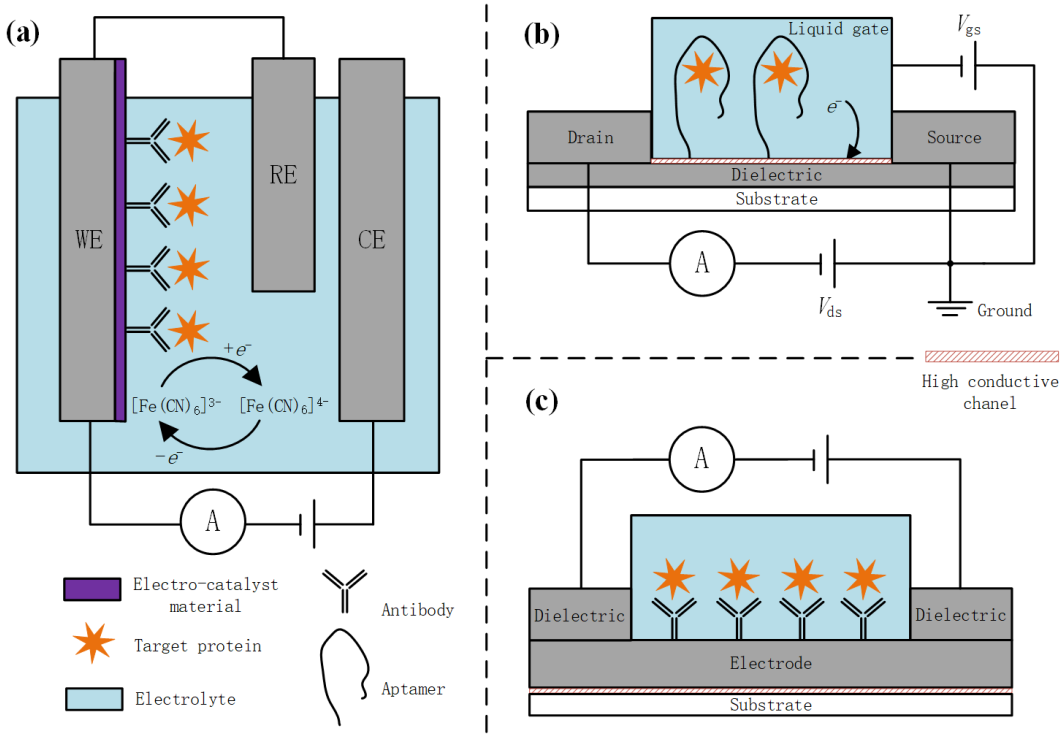

Figure 2. electrochemical sensor for label-free protein detection can be classified into three types in terms of working principles: (a) amperometric type; (b) potentiometric type; (c) impedimetric type.

1.3.1.2 Photoelectrochemical biosensor

The PEC biosensor has been showing great research prospects in recent years. Comparing to the EC sensors, the PEC sensor reduces the background signal interferences by the use of excitation light signals as the input, instead of electrical bias, which improves significantly the detection range of the biosensors.[40] The structure of PEC sensor is similar to that of a photoelectrochemical cell. A working electrode (photoelectrode) is made of a semiconductor as a photosensitizer and connected to a counter electrode. When the working electrode is immersed into the electrolyte, the photogenerated carrier pairs are separated under the built-in electric field, and through the photoelectrode/electrolyte interface, catalyze redox reactions of charge scavenging species generating an output electrical response. Hole-

electron exchange at the interface generally follows Marcus´ law. Most works on PEC biosensors focused on exploring new materials for working electrodes, sensor structures, and sensing mechanisms.

Working electrode: the most common photoelectrode in PEC sensors is the photoanode which catalyzes the redox reaction of a hole scavenger (HS). The photoanode comprises a n-type semiconductor which ensures the conversion of light to a driven potential. The n-type semiconductors WO_3 (E_g=2.7 eV), Fe_2O_3 (E_g=2.1 eV), TiO_2 (E_g=3.0–3.2 eV) among other binary transition metal-oxide semiconductors, as well as ternary oxides such as $BiVO_4$ (E_g=2.4 eV) and $CuBi_2O_4$ (E_g=2.0 eV) have majorly been used in PEC sensors.[41] The photoanodes of TiO_2 and WO_3 have the advantages of simple preparation and stable chemical properties. Researchers have also studied emerging nanomaterials for the photoanode, namely cadmium-based quantum dots (CdS, CdSe, CdTe, etc), despite their toxicity, and graphene quantum dots (E_g=2.2–3.1 eV).

Sensor structure: the bio-photoanode is currently the most studied structure of PEC biosensor, in which the photoanode surface is modified with recognition elements. The structure of bio-photoanode is shown in figure 3. When the bio-photoanode detects a biological sample with complex composition, the redox non-target compounds present in the sample can also be oxidized onto anode surface leading to significant interference to the measured signal. Wang et al. studied the surface modification of a p-type semiconductor by recognition elements and built a bio-photocathode to replace the bio-photoanode.[42] The negative potentials of bio-photocathode prevent the diffusion and adsorption of non-target components that exist simultaneously onto the working electrode, thereby solving the problem of background interferences to the detection signal. In a single bio-photoanode or bio-photocathode structure, the photogenerated electron-hole pairs outside the built-in electric field are easily be recombined before reaching surface[43]. Therefore, Han et al. studied the bio-heterostruture PEC sensor whose photoelectrode was made of a WO_3@BiOI heterojunction modified with antibody[44]. The heterojunction played a role in enhancing the electron-hole separation, thereby suppressing undesired recombination. The heterojunction

can be applied to either photoanode or photocathode, or both so as to improve current response.[45]

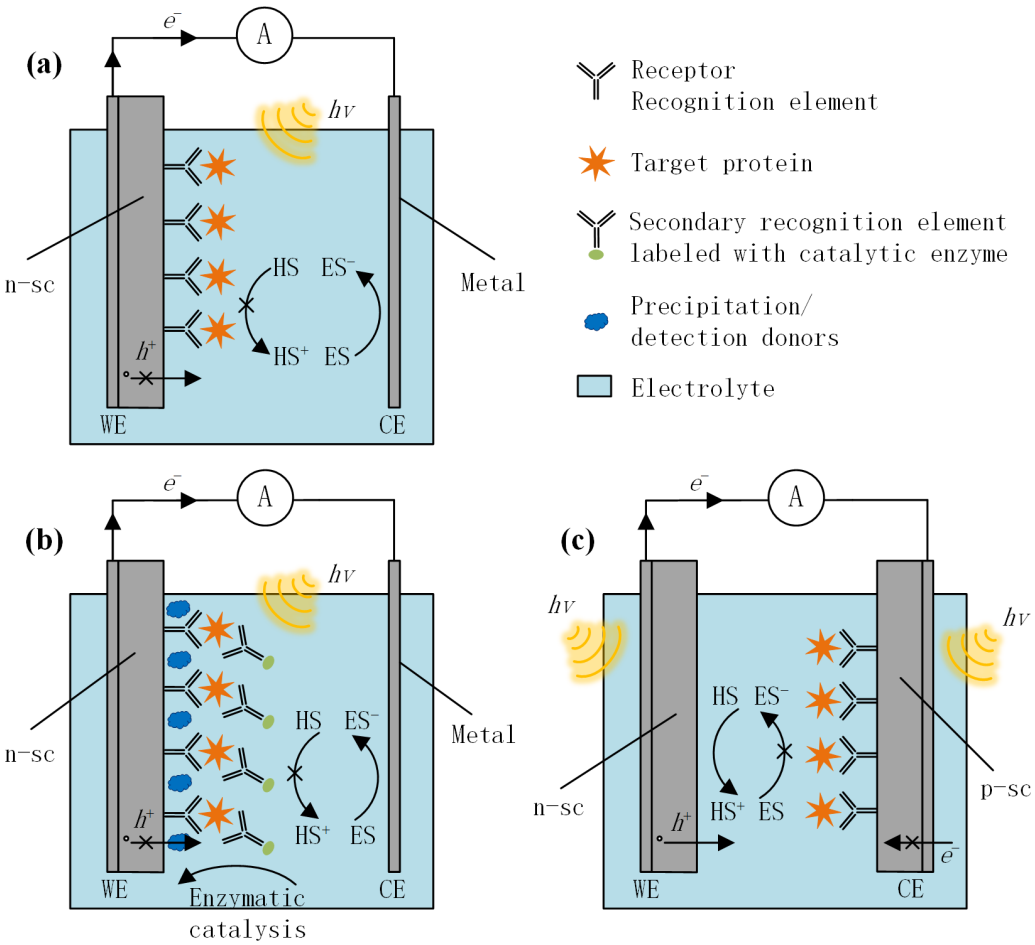

Figure 3. PEC sensor for protein detection can be classified into three categories: (a) bio-photoanode type coupled to steric hindrance; (b) bio-photoanode type coupled to in-situ generation of PEC-promoting/hindering species; (c) bio-photocathode type coupled to a photoanode. n-sc and p-sc may comprise heterojunction of semiconductors.

Sensing mechanism: it is related to effects of protein binding to bioreceptors causing the variation in the detection signal. Nevertheless, labelling methods are still used to realize the sensing mechanism for PEC sensors, including in-situ generation of electron donor/acceptor[46], biocatalytic precipitation,[47] etc. These mechanisms generally make use of enzyme labels which catalyze reactions generating electroactive or insulating species to either promote or hinder the response of the photoelectrode, respectively.

Among the current sensing mechanisms, only the mechanism of steric hindrance can truly realize the label-free detection in PEC sensors. In a sterically hindered PEC sensor, the resulting protein-bioreceptor complex hinders the diffusion of the hole/electron scavenging species in the electrolyte to the photoelectrode, resulting in a change in output J-V response. Although the attractive simplicity of the mechanism, the sterically hindered PEC sensor rarely achieved detection sensitivities below nanomolar levels while maintaining a large range of detection.[48] The reason is that output J-V response does not depend on the change in charge-transfer dynamics, but instead dominated by the thermodynamic mass transfer (diffusion) process from the target electron/hole scavenger to the photoelectrode surface. By increasing the proportion of the output response with charge-transfer dynamics control, it is expected to further improve the sensitivity and detection range of the biosensor.

The current studies on label-free photochemical sensors have not yet explored the electronic properties of the bioreceptor itself. As introduced above, the works done in Professor Barton´s group have shown that dual oligonucleotide probes exhibit properties of charge transport that can control charge-transfer kinetics of redox species. Charge transport mediated by double-strand DNA is conferred by the pi-stack of the base pairs. When the pi-stack is disturbed by absence or dissociation of base pairs, a 100-fold decrease in current across the oligonucleotides can be achieved.[34,35] If these probes are immobilized onto an electrode, great variation on charge-transfer dynamics can be expected. However, the principle of DNA-mediated charge is not compatible to existing PEC sensor structures. When the dual oligonucleotides are immobilized onto a semiconductor or heterojunction, the intrinsic electronic properties will significantly be damaged by the effect of either photooxidation or photoreduction of oligonucleotide bases (i.e. guanine).[49]

Compared to electrochemical sensors for protein detection, the PEC sensor exhibits better sensitivity and detection range. On the other side, the current studies have shown that the existing label-free photoelectrochemical biosensor technology[48] still do not achieve the requirements of detection range to simultaneously detect multiple protein biomarker levels in bio-fluids such as the case of COPD biomarkers in saliva. In addition, research was limited to measurement of device performance, and the systematic study of the

photoelectrochemical sensing principle with experimental verifications, theoretical calculations and/or comparison of numerical models and experiments has not yet been conducted. The challenges of developing new PEC biosensors are summarized as follows:

1. There is a gap between photovoltaic parameters (quantum efficiency, photocurrent stability, etc.) and models of interfacial redox processes (charge-scavenging efficiency, overpotentials, etc) for modelling charge-transfer dynamics in the PEC sensor. The disconnection of models prevents the control of sensor response and subsequent detection range and sensitivity of the biosensor.

2. For the working electrode, most PEC sensors for protein detection are still limited to wide bandgap semiconductors such as TiO_2 and WO_3, which exhibits high charge transport losses in bulk and interface comparing to emerging low bandgap semiconductors[43], besides reducing use of light to only high-energy wavelengths.

3. Absence of a sensing mechanism for enhancing change on charge-transfer dynamics and maximizing J-V response. In the few works combining the PEC sensor with dual oligonucleotides as the bioreceptor[31,32], the research was limited to the mechanistic behaviour of competitive binding between oligonucleotides and proteins while the intrinsic charge transport properties of the dual oligonucleotides have not been touched.

4. Majority of PEC sensors measure the concentration of protein in buffered electrolytes or lab-prepared ionic solutions, while the direct detection in bio-fluids was rarely demonstrated.

1.3.2 Paper-based disposable biosensors for PoC diagnostics

To avoid self-plagiarism, readers may find detailed review and discussions in section 4.1 of this thesis and section “5. Paper-based diagnostics to detect COPD-related biomarkers in saliva and blood” in Article 1.

Section 5 in Article 1 reviewed studies on lateral flow assays (LFA) and microfluidic paper-based analytical devices (µPADs) to detect COPD biomarkers. To summarize, only a limited number of studies have investigated the detection of COPD biomarkers from human biofluids. Few paper-based biosensors have been developed and optimized using untreated saliva or

blood samples. Real biofluidic samples were only used for functional validation, and in small quantities. Effective concentrations of analytes in biological samples may differ from that in lab-prepared buffers. Multi-centered clinical validation involving numerous tests using samples collected from real patients and comparison with the GOLD standard is also necessary. Current clinical studies have reported the use of lateral flow assay for identifying bronchiectasis severity, airway infection, risk of exacerbation, and periodontitis. Preliminary clinical validation suggests that point-of-care paper-based biosensors may be efficient tools for screening diseases and identifying bronchiectasis patients at high risk of disease exacerbation. Despite fruitful progress in recent years, it still faces several challenges to achieve paper-based biosensors for COPD PoC diagnostics.

First of all, matrix effects are present in different human samples. For example, in saliva, viscosity may differ based on various factors such as the individual's health status, food consumption, and when saliva samples are collected. Mucin has been identified as a COPD biomarker that increases during exacerbation while its increase also leads to high viscosity of the biofluid sample. High viscosity results in significant biases in assay results and thus requires sample treatment. Detailed discussion can be found in sub-section 3.1 “Advances and perspectives on point-of-care diagnostics of COPD, from sampling biomarkers to paper-based disposable biosensors” and Article 1.

Secondly, it requires further study to enable quantitative paper-based sensors by coupling sensing mechanisms beyond colorimetric sensing to paper substrates. Most commercial LFAs are based on colorimetric sandwich assay and offer qualitative tests, while binary results cannot be used to determine COPD stages and COPD exacerbation. To successfully monitor COPD at low cost, it is required to develop quantitative LFAs, and incorporating sensing mechanisms like electrochemical or fluorescence sensing is one of the most promising approaches. Furthermore, as sandwich assay is widely applied and compatible to current industrial fabrication chain, it also requires solutions to resolve the hook effect in sandwich LFAs which causes false-negative results in LFAs at high concentrations of analytes. Relevant studies are presented in subsection “Lateral flow immunosensors to analyze salivary C-reactive protein” and Article 2.

Third of all, biofouling happens and deteriorates sensor performance when sensors contact biological samples unless preventive measures are taken. Biofouling is a result of non-specific adsorption of proteins and adhesion of cells, which interferes not only analyte-receptor binding but signal transduction across sensing interfaces as well. Elaboration of this topic can be found in sub-section “Emerging Functional Nanomaterials and Their Potential in Body Fluid Biosensing, examples of 2D Black Phosphorus”, sub-section “Tungsten trioxide coatings with oxygen vacancies for biomedical sensor surfaces with ultra-high resistance against adhesion of fouling proteins”, and Article 3 to 5.

Last but not the least, reliable bioreceptors with high specificity and low production cost are crucial for the commercialization of point-of-care paper-based biosensors. Current research in both lab and commercial products primarily relies on antibodies, which are produced in mice, goats, rabbits, etc. However, products from different suppliers often exhibit different binding affinity and specificity, which can vary between batches and need to be measured specifically for each batch. Before developing an assay, it is necessary to screen commercial antibodies available in the market to compare binding affinity, specificity, and stability between products between different batches.

2 Aims, Tasks, and Contributions of the Thesis

2.1 Aims and Tasks

This thesis aims to develop paper-based disposable biosensors and their protocols, in order to detect COPD biomarkers in saliva and to provide solutions for COPD PoC diagnostics. This thesis also aims to investigate novel anti-biofouling approaches by controlling defects in emerging nanomaterials, which would be a key technology in body fluid biosensing. The thesis involves following major tasks:

Task 1. Review latest advances in COPD biomarker identification and their role in predicting and monitoring of COPD and its exacerbation. This task is covered by sub-section “3.1.3 salivary and blood biomarkers” in chapter 3 of this thesis and section “salivary and blood biomarkers related to COPD and COPD exacerbations” in Article 1. Relevant chapters

concluded a salivary biomarker panel of C-reactive protein, procalcitonin, and neutrophil elastase as one of the most promising combinations to monitor COPD and its acute exacerbation. This panel was selected as the targeted analytes in the KOLS project.

Task 2. Review sampling technology and paper-based disposable biosensing technology, which served the aims of this thesis. This task is accomplished by sub-sections “3.1.4 state-of-the-art saliva and blood sampling technologies” and “3.1.5 paper-based disposable biosensors to salivary and blood biomarkers related to COPD” of this thesis, as well as by sections “4. Saliva and blood sampling technologies” and “5. Paper-based diagnostics to detect COPD-related biomarkers in saliva and blood” in Article 1. Based on the above work, development of salivary sampling and quantitative lateral flow assay was chosen as the technical route in the KOLS project.

Task 3. Develop paper-based biosensor to detect salivary biomarkers related to COPD and resolve associated hook effect. This task is covered by section “3.2 lateral flow immunosensors to analyze salivary C-reactive protein”, in which a fluorescence LFA and an electrochemical LFA were both detected to detect CRP in saliva. In addition, a modified structure to the conventional LFA structure was studied to mitigate the hook effect in LFAs. Selected parts of the above studies were published as Article 2.

Task 4. Investigate anti-biofouling technology to resolve non-specific protein adsorption to sensor surfaces when detecting COPD biomarkers in body fluids. To develop novel anti-biofouling electrodes in sensors, the thesis first reviewed defect-engineering in 2D black phosphorus and tungsten oxide as two representative emerging functional materials. Based on the survey, the thesis further studied preparation of homogeneous WO_3 nanosheet ink by solvothermal synthesis and probe-sonication, engineering of oxygen vacancies in WO_3 by calcination, effect of oxygen vacancies on protein adsorption and biocompatibility of WO_3 nanosheets. These works were also reported in Articles 3, 4, and 5.

2.2 Contributions of the Thesis

Chapter 3.1 comprises a comprehensive review on the COPD PoC technology, which serves as one of the guidance of the technical approach selected in the dissertation and the KOLS

project. Successful PoC diagnostic requires synergetic advances in salivary and blood biomarkers, sampling technology and paper-based biosensors. To evaluate the process in the complete PoC procedure, chapter 2 includes three aspects: (1) specific blood and salivary biomarkers related to COPD exacerbation and different COPD endotypes, (2) sampling technology to acquire blood and saliva samples which will be analyzed throughout paper-based PoC diagnostics, and (3) paper-based biosensors that inspect human blood samples and saliva samples to measure levels of COPD biomarkers. The first sub-section reviews the history of COPD, COPD exacerbation, their diagnostics, and biomarkers identified in salivary and blood. It includes the generation, transport, and clinical verification of different biomarkers in blood and saliva. This sub-section focuses on summarizing the advances in identifying COPD biomarkers, biomarkers' relationships with different COPD endotypes, and evaluating the accuracy and reliability of different biomarkers. The second sub-section discusses latest achievements and our own perspectives on technologies to sample human saliva and blood. It further discussed the development of sampling protocols for blood and saliva, respectively. For blood sampling, it focuses on the fabrication, material selection, and shape design of microneedles. For saliva sampling, it focuses on saliva sampling kits with an evaluation of the pros and cons of different designs. The third sub-section introduces advances in paper-based disposable biosensors to detect blood and salivary biomarkers which was reviewed in the previous sub-section. It also discusses the hook effect in paper-based biosensors and matrix effects of human samples. Chapter 4.1 ends by proposing the author's own point-of-view on the challenges and perspectives in terms of COPD PoC diagnostics. It envisions the impact of saliva and blood matrix effect, necessity of development and validation using human samples, difficulties in paper-based biosensor development, and potential directions to innovate paper-based biosensors and COPD PoC systems.

Chapter 3.2 studies "hook" effect in one-step sandwich LFA and a method to resolve it while quantitative detecting CRP in saliva. The hook effect causes false-negative results in sandwich assay when biomarker concentrations exceeded predetermined range of detection. This work introduced a sucrose-treated intermediate pad which hindered sample flowing between the conjugate pad and the nitrocellulose membrane, and thus delay releasing conjugate antibody and subsequent reaction between conjugates and analytes to avoid the hook effect. It

exhibited a 10 times improvement in range of detection than conventional LFAs. Chapter 3.2 also describes an attempt integrating electrochemical biosensors with LFAs. A novel chronoamperometric immunosensor combing lateral flow strips was developed to detect a representative COPD biomarker, CRP, in saliva. Enzymatic catalyzation of TMB oxidation was demonstrated on nitrocellulose membranes in order to realize electrochemical LFA. The immunosensor exhibited a limit of detection of 0.07 nM with high reproducibility. It also exhibited a linear range of detection covering 0.5 nM to 10^5 nM. Such range fulfilled the requirement for monitoring of chronic disease like COPD.

Chapter 3.3 reviews defects and manipulation of defects in emerging functional nanomaterials, i.e., 2D black phosphorus, to boost development of biosensors and PoC devices to detect COPD biomarkers in human body fluids. It includes methods to control its properties by defect-tailoring and surface functionalization, and its applications in biosensors and disease diagnostics. It also presents critical insights on the future synthesis, modification, and further applications in biosensor.

Chapter 3.4 studies an anti-biofouling strategy by controlling oxygen vacancies in WO_3 to change its surface wetting behavior. Generation of surface oxygen vacancies improved the hydrophilicity of WO_3 thin films, resulting in less non-specific protein adsorption and longer electrode lifetime.

The main scientific contributions of this work are as follows:

1. It systematically reviewed essential technologies to develop a PoC system for COPD, including (1) specific blood and salivary biomarkers related to COPD exacerbation and different COPD endotypes, (2) sampling technology to acquire blood and saliva samples to be used for paper based PoC diagnostics, and (3) paper-based biosensors that specifically detect COPD biomarkers in human blood and saliva samples.

2. It developed an electrochemical LFA and a fluorescence LFA to detect CRP as a representative COPD biomarker in huma saliva.

3. It presented a novel strategy to resolve high-dose hook effect in lateral flow assay without addition manual operation based on introducing a sucrose-treated intermediate pad.

4. Different from previous electrochemical LFA which utilized toxic substrates for signaling, the author utilized 3,3',5,5'-tetramethylbenzidine (TMB) as a non-toxic indicator in amperometric detection of CRP.

5. It reviewed different approaches towards tuning of BP properties, covering cutting-edge studies on controlling defects in BP, in order to extend applications of functional nanomaterials in biosensors.

6. Antifouling strategies based on oxygen-vacancy-controlled hydrophilicity in WO_3 thin films were studied.

7. It developed an optimized protocol to synthesize WO_3 nanosheets, to prepare WO_3 inks and to spin-coat WO_3 thin films.

3 Summary and elaboration of articles

3.1 Advances and perspectives on point-of-care diagnostics of COPD, from sampling biomarkers to paper-based disposable biosensors

3.1.1 Background

In the KOLS project, we are developing a point-of-care biosensing system together with a protocol, which can be performed by patients without training. Thus, we need to decide biomarkers, sampling techniques, biosensing technical routes. From the vast library of protein biomarkers discovered by medical researchers, we have to determine a feasible panel of protein biomarkers that not only reveals the COPD endotypes but also predicts COPD exacerbation. Until now, COPD biomarkers have been mostly identified in either blood or saliva.[13,19,50] To set foundations for biosensor development and associated protocol, we also

reviewed progress of saliva sampling, blood sampling, and paper-based diagnostic technology to detect blood or salivary biomarkers, in order to predict and monitor COPD and COPD exacerbation.

3.1.2 Objectives

- Identify the panel of salivary protein biomarkers which indicates the occurrence and exacerbation of COPD.
- Evaluate the PoC solutions which best suit the purpose of COPD diagnostics.
- Extract thesis to be further studied in regard to direct detection of proteins in human body fluids.

3.1.3 salivary and blood biomarkers

We surveyed 15 biomarkers related to COPD, including C-reactive protein (CRP), neutrophil elastase (NE), matrix metallopeptidase 9 (MMP-9), serum amyloid A (SAA), alpha$_1$-antitrypsin (AAT), eosinophil, interleukins, tumor necrosis factor-alpha (TNF-α), mucin (MUC) 5AC, MUC5B, procalcitonin (PCT), and serum C-X-C motif chemokine 10 (CXCL10). By reviewing numerous literatures, we summarized key figures of merit that are of our concern and based on which the reliability was evaluated. In table 2, we summarized salivary and serum biomarker concentrations in healthy controls, COPD patients in stable stages (SCOPD), and COPD patients undergoing acute exacerbation (AECOPD). To our knowledge, only a few of them has been clinically verified to predict AECOPD in terms of cut-off values and related sensitivity and specificity (table 3).[51–53] Detailed discussions on each biomarkers can be found in Article 1. To distinguish the current 4 types of exacerbation, we believe the following biomarkers are reliable. CRP in either saliva or serum indicates overall inflammation.[54] CRP is also useful in prescribing during exacerbation that it reduces antibiotic use.[54] PCT, NE, and IL-1b are biomarkers for bacterial-predominant inflammation.[51] Increase in serum CXCL10 predicts viral-predominant inflammation,[51,55] while increase in serum eosinophils predicts eosinophilic-predominant inflammation.[51]

Table 2. Median concentrations of COPD biomarkers in saliva and serum. Adapted from Article 1.

Biomarker	Saliva (ng/mL)			Serum (ng/mL)			Ref.
	Healthy	Stable	AE	Healthy	Stable	AE	
CRP	0.89	1.61	7.35	2.1×10^3	3.9×10^3	36.8×10^3	[56,57]
PCT	0.09	0.09	0.50	NA	NA	0.06	[56,58]
NE	152	189	769	46.89	69.29	NA	[56,59]
IL-6	1.8×10^{-3}	5.1×10^{-3}	NA	2.25×10^{-3} (Tunisian)	3.13×10^{-3} (Tunisia) 27.68 (Chinese)	80.93 (Chinese)	[52,59,60]
SAA	Unknown	Unknown	Unknown	Unknown	21.58	40.68	[52]
MMP-9	Unknown	Unknown	Unknown	156.95	258.68	NA	[59]

Note: AE stands for acute exacerbation.

Table 3. Biomarkers verified in AECOPD patients.

	Cut-off value	Sensitivity	Specificity	Ref.
SAA	10.06 g/L	82%	69%	[52]
IL-8	82 mg/L	72%	62%	[53]
CXCL10	56 pg/mL	75%	65%	[51]

3.1.4 State-of-the-art saliva and blood sampling technologies

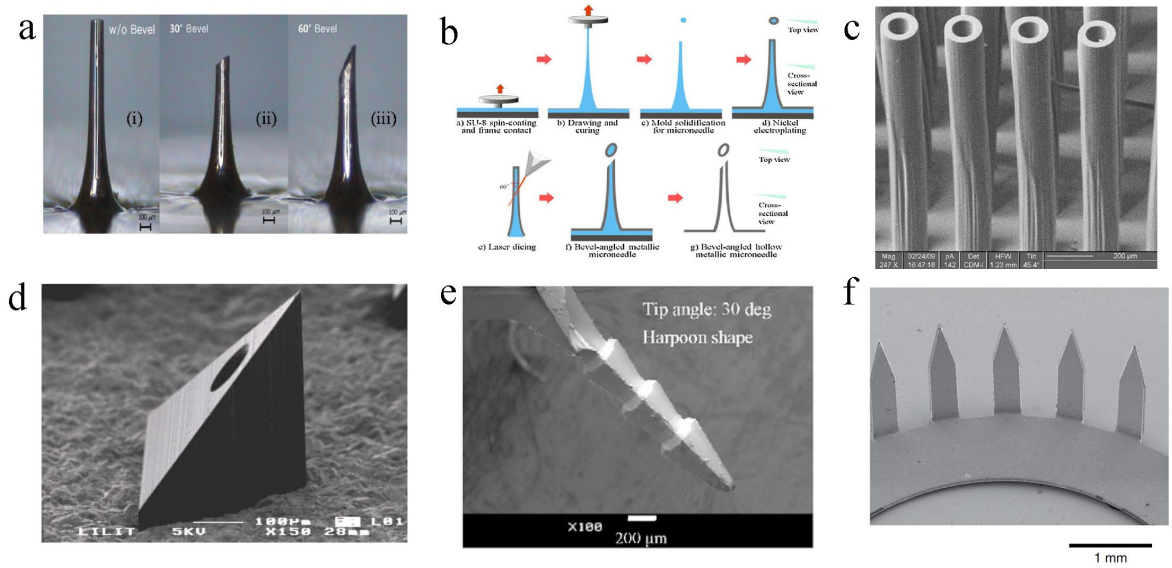

Figure 4. Examples of microneedles developed for blood sampling (reprinted from Article 1). (a) Nickel hollow microneedles and (b) its fabrication by electroplating.[67] (c) A hollow microneedle array made of SU-8.[69] (d) A PMMA hollow microneedle in a pyramidal shape.[70] (e) A solid microneedle in harpoon-shape.[72] (f) A microneedle array made of stainless-steel.[73] Permissions have been granted from the publishers respectively.

The ASSURED criteria published by World Health Organization (WHO) have been widely accepted by the PoC community as a benchmark of ideal test.[61] It affected our decision in choosing the body fluid from which to detect COPD biomarkers. As summarized above and reviewed in Article 1, most of COPD biomarkers exhibit lower concentrations in saliva than in blood.[13] High concentrations make them easy to be detected by biosensors. On the other hand, blood sampling technology is invasive and requires microneedles. Blood samples are collected by either venipuncture, arterial blood, or capillary puncture. In PoC scenarios, capillary puncture is the most desired since it induces less pain and only small amounts of samples are needed. Capillary puncture at fingertips requires microneedles to be as long as 800 µm to 2200 µm.[62,63] Study of microneedles started in the 1990's with an original purpose for drug delivery, where both solid and hollow ones were used.[64] Blood sampling is more difficult than drug delivery because it requires longer hollow ones.[62,63] Negative pressure is applied to acquire large volumes of samples while capillary force and blood pressure are enough to obtain small volumes. Hollow microneedles are also more sophisticated to fabricate

compared to their solid counterparts. Microneedles need to be biocompatible, mechanically robust, and with high aspect ratio. To our knowledge, current microneedles are mostly fabricated by stainless steel,[65] platinum[66,67], titanium, [68] SU-8,[69] poly(methyl methacrylate) (PMMA),[70] and silicon.[71] They are usually fabricated by electroplating,[66,67] deposition,[68] and lithography.[70] In general, blood sampling as an invasive method is not ideal according to the ASSURED criteria because it exerts pain and risk of infection to the patients as well as requires professionals to operate.

Saliva samples are obtained from whole saliva or certain glands.[74–77] Saliva collection from a specific salivary gland was invasive in the beginning, because it was performed by ductal cannulation inserted into the gland.[78] Later, ductal cannulation was replaced by non-invasive methods like Lashley cup, [79,80] gentle suction,[81] and customized collectors[82]. Unstimulated whole saliva was widely used in recent PoC studies.[83–90] Unstimulated whole saliva samples were collected by swab-based method, spitting method, and passive drool method. The passive drool method is simple and free from food debris nor flow rate changes, while it takes a long sampling duration. It is also difficult to collect samples from elderly patients with dry mouths. Spitting reduces the collection time, but it is subjected to stimulation and results in sample heterogeneity as a foam layer often appears on the top of the saliva. Currently, more and more researchers tend to collect unstimulated whole saliva with oral swabs. Commercial swab kits are now available for saliva collection, including Salivette, Salivabio, Super Sal, Quantisal, Intercept, and Versi Sal. Salivette, Salivabio and Super Sal swabs are in rod shape. Samples need to be extracted from the swab by centrifugation. Super Sal kit combines a swab with a syringe-like compression tube and a collector. Quantisal, Intercept, and Versi Sal kits include pad swabs and buffer solution. They were designed for drug tests, not saliva collection.

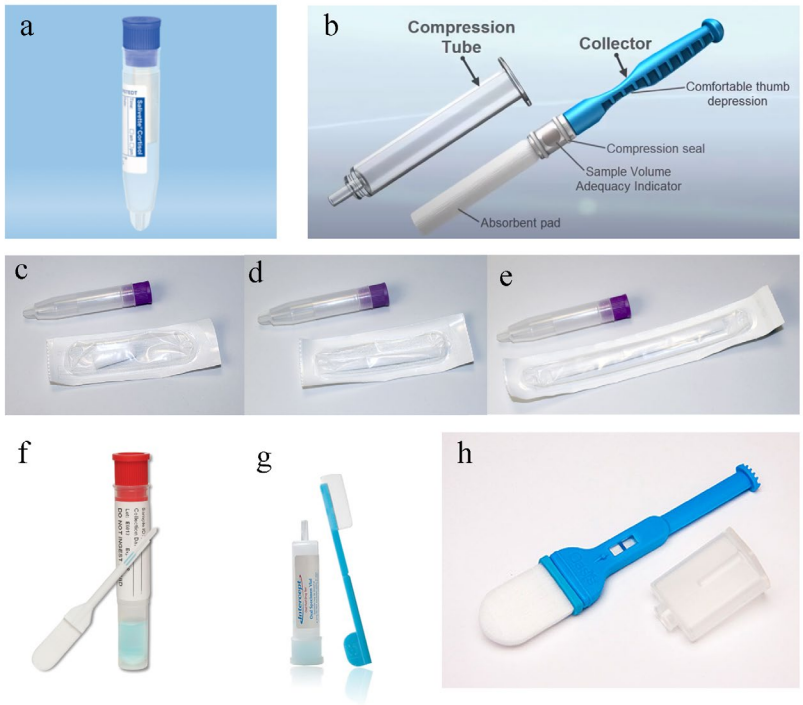

Figure 5. Examples of commercial oral swabs to sample whole saliva: (a) Salivette® Cortisol kit, (b) Super SAL™, (c) SalivaBio swabs for adults, (d) infants, and (e) children, (f) Quantisal®kit, (g) Intercept® kit, and (h) Versi SAL® kit. Adapted from Article 1.

3.1.5 Paper-based disposable biosensors to salivary and blood biomarkers related to COPD

Lateral flow assay exhibits advantages including convenience, rapid response, ease of use, and low cost, hence being widely commercialized in the PoC market.[91] The majority of commercialized colorimetric LFAs offer qualitative tests, which are enough for applications such as pregnancy test, infectious disease test, drug abuse assay.[92] Nevertheless, qualitative LFA does not satisfy requirements of COPD diagnostics, because COPD screening and monitoring require quantitative detection of multiple biomarkers.[93] Conventional qualitative LFAs rely on metallic nanoparticles and their localized surface plasmon resonance effect.[94–96] To enable quantitative LFAs, results are obtained by calculating color intensity ratios of test line intensity over control line intensity.[97,98] Some studies also replaced plasmonic nanoparticles with fluorescent nanoparticles such as organic fluorophores and quantum dots to improve sensitivity.[99,100] Comparing to colorimetric LFAs, fluorescence LFAs can be easily

affected by stray light or other environmental interferences.[92] Current quantitative LFAs are able to analyze COPD biomarkers like CRP,[99,101–104] SAA, [101] PCT,[104,105] and IL-6.[106] Blood has been more explored than saliva. Dilution is a common operation to get rid of matrix effects in serum samples.[102–104,106] µPADs have been seldom developed to analyze salivary or blood biomarkers that related to COPD, as only detection of MMP-9 and CRP were reported.[107,108]

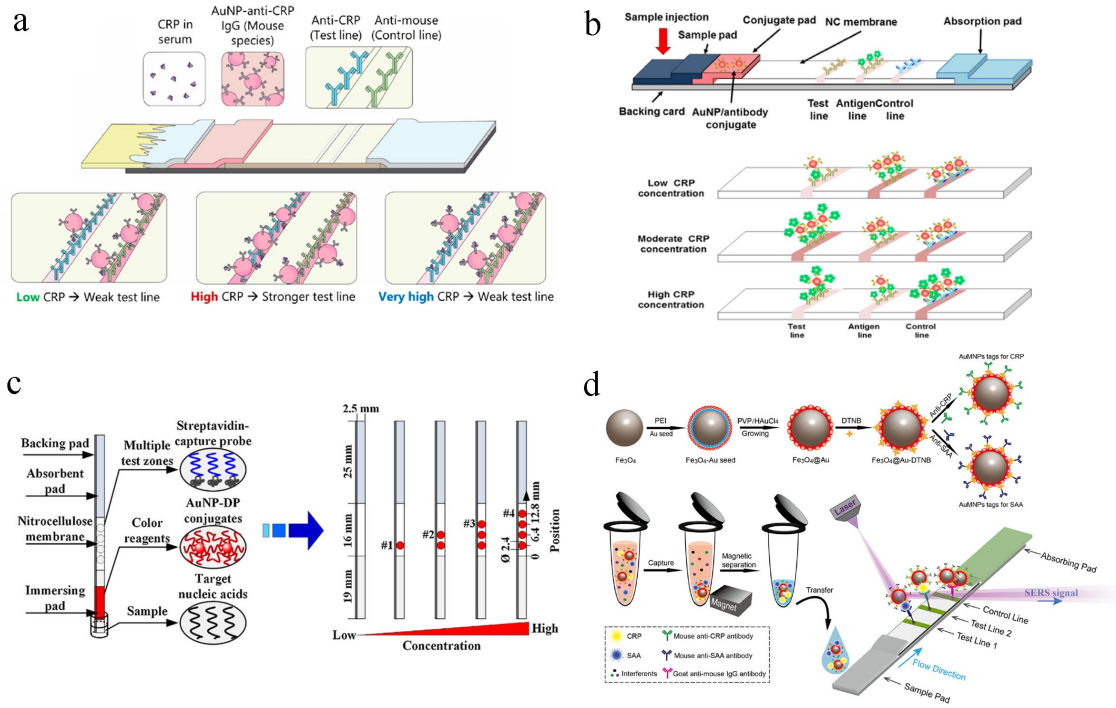

Figure 6. Representative schemes of selected LFAs to detect COPD biomarkers (reprinted from Article 1). (a) A classical "two-line" LFA strip and suggested cause of hook effect.[102] (b) A hook-effect-mitigated LFA strip with an additional antigen line.[98] (c) A hook-effect-mitigated LFA with multiple test zones.[109] (d) A multiplexed LFA strip to detect CRP and SAA.[101] Adapted from article 1.

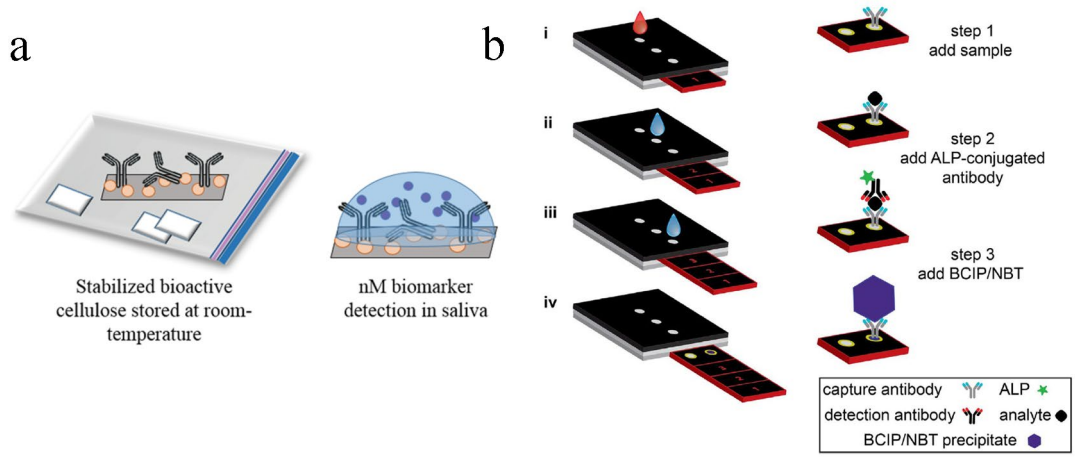

Figure 7. Adapted from Article 1. (a) A colorimetric disposable biosensor made of cellulose to detect salivary MMP-8 and MMP-9.[107] (b) A 3D µPAD to detect blood CRP.[108] Permissions have been granted from the publishers respectively.

3.1.6 Conclusions and perspectives of paper-based biosensors for COPD PoC diagnostics

Since most of the reported works still detect analytes in treated saliva samples which were centrifuged and diluted with buffer, we targeted to detect CRP in untreated saliva. Detecting CRP in saliva by LFA has to overcome salivary matrix effect. First of all, saliva samples can be contaminated by blood or food debris. Blood is resulted from oral bleeding during mouth inflammation, while mouth inflammation increases CRP concentration. Food debris potentially reacts with antibodies and thus induces interferences. Secondly, saliva obtained at different flow rates exhibit variations of biomarker concentrations and pH values. Under stimulation, saliva flow rate increased up to 70 times higher than without simulation, while pH ranges from 7.8 at the highest flow rate to 5.3 at the lowest rate.[77] Thirdly, presence of mucin increases the viscosity of saliva samples and hinders sample transport in LFAs. Fourthly, handling of saliva samples also affects their viscosity. It was reported that saliva viscosity decreased after sequential centrifugation, freezing, and unfreezing.[107] Fifthly, hook effect happens in LFAs using sandwich immunoassay, where high concentrations of analytes result in false negative results. Last but not the least, co-existing proteins in saliva result in biofouling phenomena as a result of unspecific adsorption of proteins, which hinders electrochemical detection.

Based on the critical review in Article 1, we selected salivary CRP as the model biomarker to start developing our lateral flow assay, in order to meet the ASSURED criteria. We coupled different biosensing mechanisms to LFAs in order to detect CRP in saliva. Followingly, we introduced a unique LFA design to mitigate the hook effect. To minimize interferences from saliva collection, we adapted swabs to collect unstimulated whole saliva while avoiding saliva treatment, transportation or storage.

3.2 Lateral flow immunosensors to analyze salivary C-reactive protein

3.2.1 A strategy to resolve hook effect in LFA

3.2.1.1 Background

Hook effect described the false-negative results happened in sandwich LFAs when high concentrations of analytes present.[102,109–114] As analyte concentration increases in quantitative sandwich LFAs, T/C intensity raises monotonically in the beginning but abnormally decreases as the concentration of analyte excesses a critical level, resulting a "hook" in the diagrams T/C intensity ratios vs. concentration of analyte. The hook effect makes LFA unreliable in the clinical scenario, because biomarker levels in untreated human body fluids can dramatically increase from the normal values. For instance, serum CRP level in healthy people is usually lower than 1 ng/mL[56,57] while it can go up to 250 µg/mL in patients with severe infection.[115]

The common solution is to introduce addition sample treatment in LFA protocols, e.g., washing steps[116] and sample dilution,[117] which makes the process inconvenient. Some increase the concentration of detection antibody,[118] thus increases manufacturing cost and sacrificing limit of detection due to high background noise. Other attempts include adding a third conjugate-binding line,[98] adding multiple test zones,[109] kinetic measurement.[102]

To resolve hook effect without increasing manufacturing costs nor adding manual operations, we developed a strategy of delay releasing labelled detection antibody to evade the

competitive reaction between labeled and unlabeled C-reactive protein to the capture antibody immobilized at the T line. The strategy was realized by regulating the sample flow rate with a sucrose-treated intermediate pad below the conjugate.

3.2.1.2 Objectives

- Develop a fluorescence sandwich LFA to detect CRP in saliva.
- Study the mechanism hook effect.
- Redesign LFA structure to resolve hook effect.

3.2.1.3 Experimental

A typical LFA in our study was assembled according to figure 5. We prepared the detection antibody by EDC-NHS linking anti-CRP antibody C6 with a commercial polyethylene glycol (PEG) modified quantum dot (QD). We immobilized detection antibody onto a conjugate pad made of glass fiber. Excitation wavelength of the CdSe QS was from 365 nm to 450 nm. Intermediate pads were made of cellulose and immersed into sucrose water solution of different concentrations. Treated intermediate pads were subsequently dried in a vacuum. CN140 NC membrane from Sartorius was immobilized with goat anti-mouse IgG to capture antibody C6 and anti-CRP antibody C2 (500 μg/mL) as the capture antibody. The jetting rate was optimized to be 0.5 μL/cm. After C2 immobilization, we blocked NC membranes after immobilization. Detailed fabrication process was explained in detail in the experimental section in Article 2.

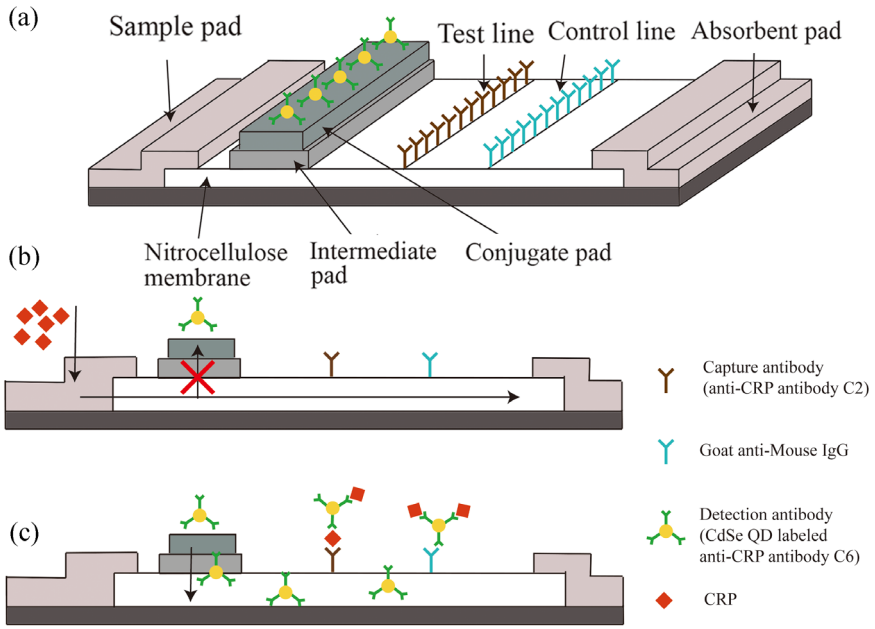

Figure 8. Schematics of (a) the improved LFA structure. (b) The intermediate pad was treated with sucrose to delay the fluid, thus (c) delay releasing the detection antibody in order to resolve the hook effect. Adapted from Article 2.

We collected unstimulated whole saliva samples using SalivaBio kits. Three volunteers consented us to use their saliva and participated in the sampling procedure. Volunteers were prohibited to eat food, drink alcohol or carbonated drinks, smoke, or exercise before sampling. Detailed saliva sampling process and ELISA procedure can be found in Article 2. Salivary CRP concentrations were measured by ELISA. We also prepared artificial saliva to develop LFA. We measured fluorescence intensity at T and C lines by converting colored pictures taken from a single lens camera into grayscale via ImageJ software. We normalized the intensities by our algorithm which was explained in detail in Article 2.

3.2.1.4 Results

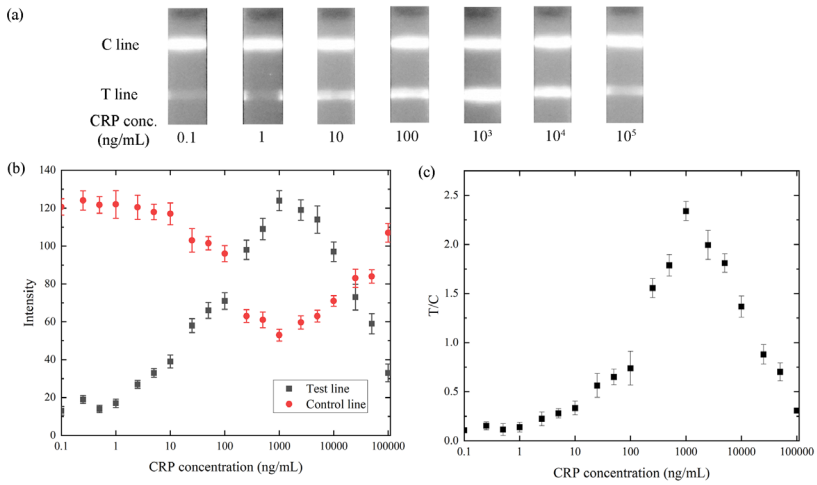

Figure 9. (a) Photos of fluorescence intensity in grey scale at T and C lines measuring CPR in artificial saliva solutions, converted to greyscale. f (b) test line and control line fluorescence intensities, and (c) T/C ratios versus increasing CRP concentrations. (n=3). Adapted from Article 2.

In LFAs without the intermediate pad, both figure 9a and 9c exhibited “hook” shapes. When CRP concentration was below 10^3 ng/mL, both T line intensity and T/C ratio increased monotonously as CRP concentration goes up and the C line intensity gradually goes down. When CRP concentration exceed 1000 ng/mL, fluorescence intensity at T line and T/C ratio started to decrease while C line intensity started to bounce back. The LFA achieved a range of detection between 0.5 ng/mL to 1000 ng/mL. False-negative results were obtained when CRP concentration was above 1000 ng/mL.

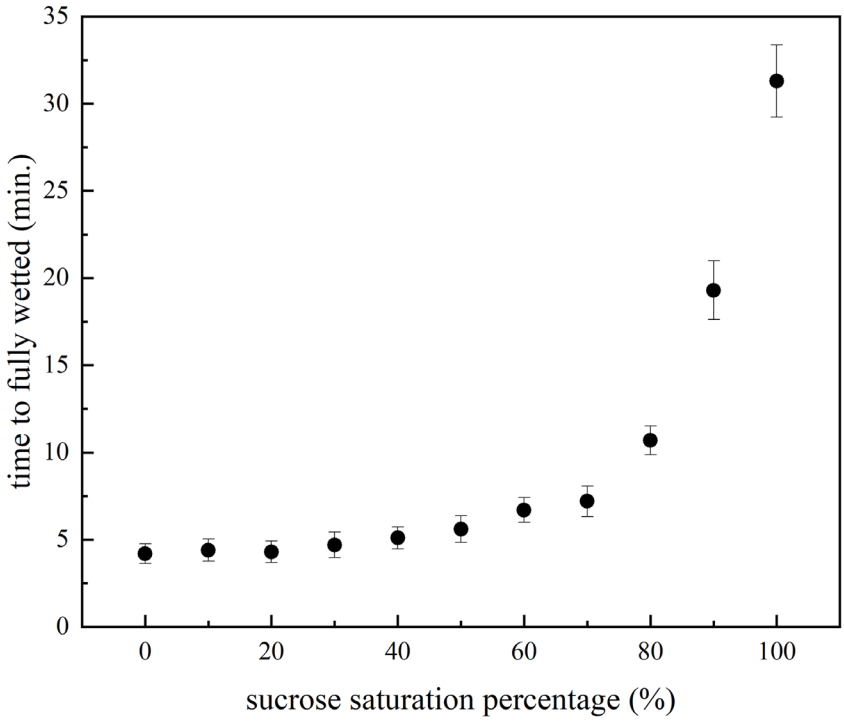

Figure 10. Wetting behavior of sucrose-treated intermediate pads. As concentration of sucrose increases, it takes more time to fully wet the intermediate pad (n=3). Adapted from Article 2.

An ideal intermediate pad should regulate the flow rate while not interfering with antigen-antibody reactions. We selected sucrose because of its affordable cost and good biocompatibility.[119] In addition, sucrose was reported to stabilize protein immobilized on paper substrates.[120] We measured the time needed for sucrose solutions at different concentrations to wet a cellulose intermediate pad (figure 7). It took approximately 4 min for DI water to fully wet the cellulose pad. By increasing the sucrose concentration, the wetting time gradually increased. When the sucrose saturation was above 70%, the wetting time significantly increased. At 70% sucrose saturation, it took around 7.2 min to fully wet the intermediate pad, while the wetting time increased to 31.3 when sucrose saturated solution was applied. For our LFAs without an intermediate pad, it took 15 min to 20 min for fluorescence intensities at T line and C line to be stable. Thus, we select sucrose saturation between 70%, 80%, and 90% (19.3 min) for further investigation.

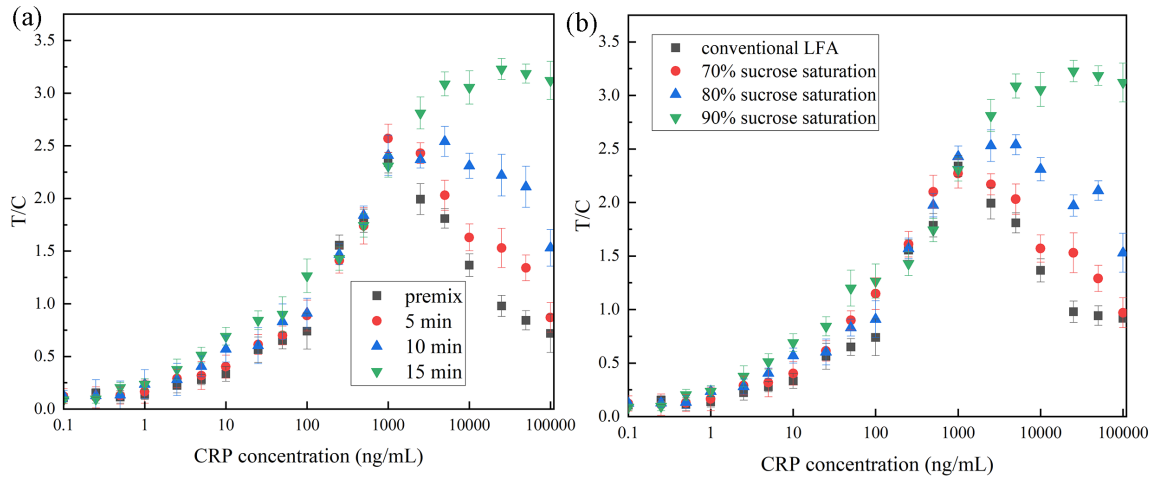

Figure 11. (a) Ratios of fluorescence intensities at T and C lines in conventional LFAs without an intermediate pad nor a conjugate pad. By manually delaying addition of CRP and detection antibodies, the hook effect starting from 1000 ng/mL of CRP gradually disappeared. (b) Ratios of fluorescence intensities at T and C lines from LFAs with sucrose-treated intermediate pads (n=3). The hook effect was mediated when intermediate pads were treated with 90% sucrose saturated solution. Adapted from Article 2.

We assume that the hook effect will be mitigated by avoiding competitive reaction between labeled CRP (QD-C6-CRP) and unlabeled CRP at the test line. To validate our assumption, we investigated the effect of adding CRP and C6-CdSe complex in sequence onto LFAs without the conjugate pad (figure 11a). When CRP were premixed with detection antibody before adding to a the LFA and QD-C6-CRP were fully reacted, T/C ratio exhibited a trend similar to that in conventional LFAs without an intermediate pad (figure 9). T/C ratio reached its maximum at 1000 ng/mL of CRP concentration and a hook was observed. As we set an interval of 5 min between adding CRP and adding the detection antibody, the hook was elevated when CRP concentration was above 1000 ng/mL. By increasing the time interval, the saturate point of T/C ratios moved to higher CRP concentrations and the hook started to disappear. We applied intermediate pads treated with sucrose solution of different concentrations to mimic the manual procedure (figure 11). As sucrose concentration increased, it took a long period for the sample solution to pass the intermediate pad and wet the conjugate pad above. When sucrose is of 70% saturation, T/C ratio increased monotonically as CRP concentration increased from 0.1 ng/mL to 1000 ng/mL and decreased with CRP concentration increased from 1000 ng/mL to 10^5 ng/mL. As the sucrose concentration increased, the saturation points

of T/C ratio moved to higher CRP concentrations. At 90% sucrose saturation, the T/C ratio reached its plateau when CRP concentration exceeded 10^4 ng/mL.

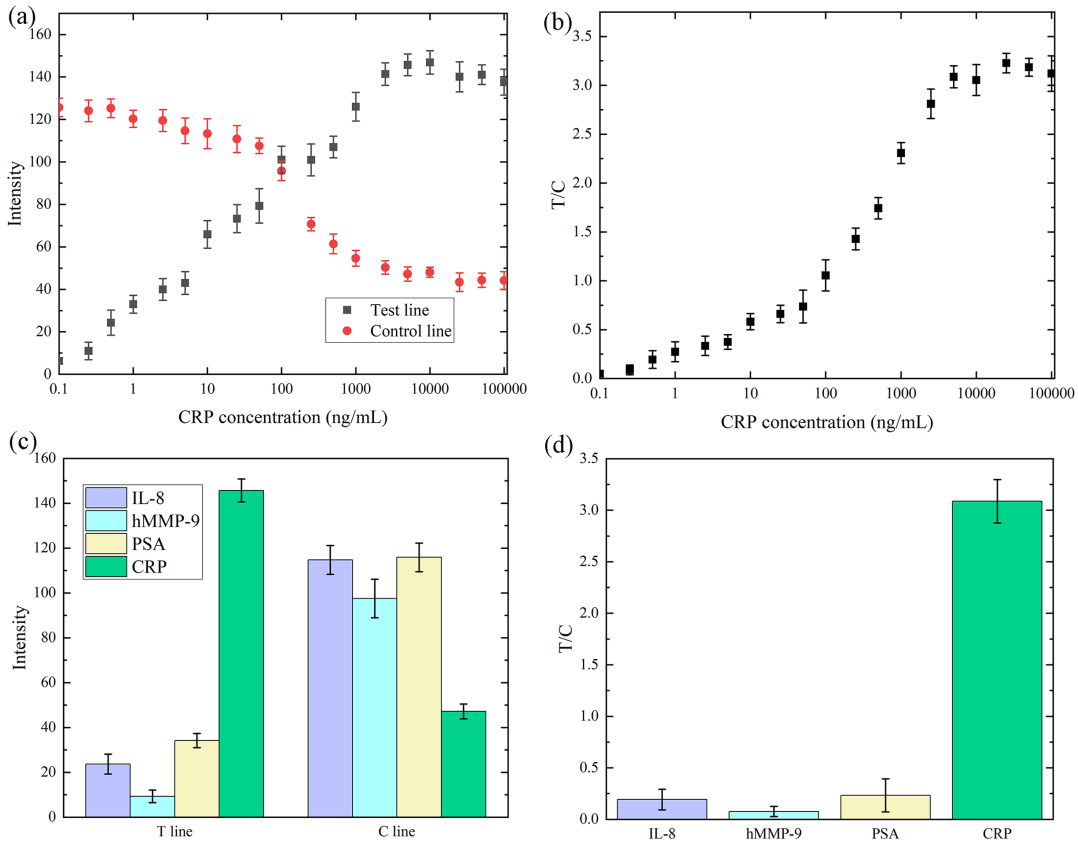

Figure 12. (a) Fluorescence intensity and (b) T/C ratios from LFAs with sucrose-treated intermediated pads without the hook effect. (c) Fluorescence intensity at T and C lines and (d) T/C ratios testing selected interfering proteins that co-exist in saliva from typical COPD patients. (n=3). Adapted from Article 2.

The variations of fluorescence intensities are shown in figure 12. The intensity at the T line increased monotonically as CRP level rose from 0.1 to 10^4 ng/mL and reached a plateau when CRP concentration was between 2.5×10^4 to 10^5 ng/mL. The T/C ratio showed a comparable tendency to the intensity at the T line, while C line intensity was the opposite. We didn't observe any hook effect in this LFA. Besides being free from hook effect, the improved LFA also exhibited good specificity against other COPD biomarkers like PSA, hMMP-9, and IL-8. In the end, we verified our modified LFA with untreated human saliva (figure 12). A similar trend was observed as in figure 9. The accuracy was compared with ELISA results (table 4). Relative errors of all the samples were less than 11%.

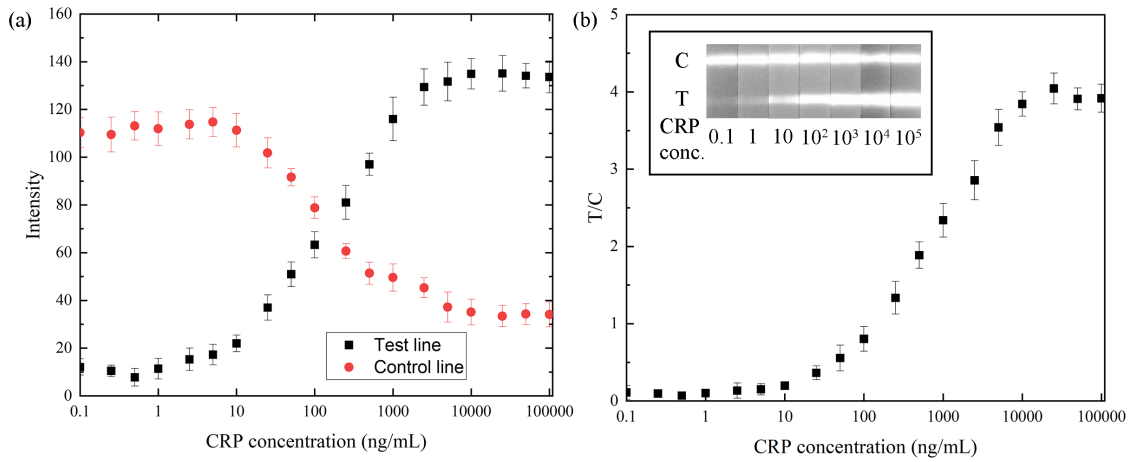

Figure 13. Fluorescence intensity at the T line and (b) T/C ratios from LFAs with sucrose-treated intermediated pads when human saliva samples were tested. Saturated sucrose solution was diluted with 10 vol.% water. Adapted from Article 2.

Table 4. Accuracy of the modified LFA testing saliva (n=3).

Sample (ng/mL)	1	2	3
CRP concentration (Standard deviation)	47.3 (3.1)	88.6 (9.4)	114.1 (12.7)
Concentration measured by ELISA	50	77	103
Relative error (%)	-5.4	15.0	10.8

3.2.1.5 Discussion

The hook effect appeared when excess analytes were reacted with capture antibody at the test line where otherwise captures labelled antibodies. In our protocol, one CdSe QD was bounded to three detection antibodies in average, which might result in higher-order CRP-antibody complexes and different configurations. Additionally, a transient complex state might exist during the CRP-binding.[121] To simply our model and analysis, we assumed that CRP-antibody associations were one-step reactions and their products only maintained one configuration. Thus, we only needed to discuss four association constants related to the reaction at the test line, which are associations between immobilized capture antibody C2 and unlabeled CRP (K1), detection antibody QD-C6 and CRP (K2), QD-C6 and CRP at the T line (K3), and labelled QD-C6-CRP and capture antibody C2 (K4). Through calculation and reference[122], these four association constants ranked from large to small were K3, K1, K2, and K4. K1 and K2 were around the same level while they were 3 to 4 magnitudes larger than K4. As a result, more unlabeled CRP would react with capture antibody C2 which was immobilized at the T

line than they bound to detection antibody. In LFAs without the intermediate pad when CRP concentration increased from 0.5 ng/mL to 1000 ng/mL, fluorescence intensity at the T line increased as more QD-C6-CRP-C2 complexes were formed while intensity at the C line decreased because of less QD-C6 could bind to goat anti-mouse IgG at the C line. When CRP concentration exceeded 1000 ng/mL, QD-C6-CRP complex exhibited the lowest binding affinity with capture antibody C2, hook effect would always happen when detection antibody was not enough to label all the free CRP in the sample and the test line intensity was governed by K4. By separating these reactions with an intermediate pad, unlabeled CRP could be captured at the test line without interference. The test line intensity was determined by K2.

Sucrose in the intermediate pad did not interference antibody-CRP binding, while hindering fluid sample flowed into the conjugate pad to release detection antibody. Dried sucrose blocked the pores inside the cellulose membrane and gradually dissolved after encountering the sample, resulting in an area with temporarily high viscosity which exhibited high resistance to the flow.

3.2.1.6 Conclusions

We mitigated the hook effect by re-designing the lateral flow assay with a sucrose-treated intermediated pad. Our modified LFA exhibited a CRP detection range of 0.5 ng/mL to 10^4 ng/mL which was ten times wider than the LFA without intermediate pad. It provided a cost-effective method to resolve hook effect without adding manual operations to LFA.

3.2.2 A chronoamperometric lateral flow immunosensor to detect C-reactive proteins in saliva

3.2.2.1 Background

The background of the LFA and its problems are discussed in detail in section 5 and section 6 of Article 1. In this sub-section, we report a novel chronoamperometric immunosensor combing lateral flow strips to detect CRP in saliva. For demonstration, enzymatic catalyzation

of TMB oxidation in presence of HRP and H_2O_2 was selected to generate chronoamperometric current signals. Screen-printed electrode chips are applied to acquire chronoamperometric signals. Experimental results exhibited that the assay is capable of performing quantitative tests to detect CRP in human saliva.

3.2.2.2 Material and methods

3.2.2.2.1 Reagents and instruments

Reagents and most of the instruments used in this part were the same in Article 2. A Metrohm Multi Autolab/M204 potentiostat/galvanostat was used in electrochemical tests. A customized connect was applied to connect SPEs to the electrochemical workstation.

3.2.2.2.2 Preparation of the lateral flow strips

The basic structure and fabrication process is similar to what was described in Article 2. In addition, HRP conjugated anti-CRP antibody C6 (HRP-C6) was prepared according to the protocol provided by Abcam.

3.2.2.2.3 Detection of CRP in PBS and in saliva based on chronoamperometric LFA

Preparation of CRP in PBS and Saliva samples was the same in Article 2. We defined a test zone on the NC membrane by drawing two hydrophobic lines on both sides of the test line using a liquid blocker pen. There is 10 mm distance between the two hydrophobic lines. 20 µL of TMB substrate was added onto the test zone using pipettes. Subsequently, an SPE chip was placed onto the test zone. Its current signals were recorded by an Autolab potentiostat. The concentration of CRP captured by anti-CRP antibodies was measured by chronoamperometry with an applied potential of -0.1 V versus the Ag/AgCl reference electrode.

3.2.2.2.4 Sampling of human saliva samples

Saliva were samples using the protocol described in Article 2.

3.2.2.3 Results and discussion

3.2.2.3.1 chronoamperometric detection of HRP label on NC membranes

Prior to chronoamperometry studies, cyclic voltammetry (CV) was applied to study the reduction and oxidation of commercial TMB substrates loaded onto NC membranes using SPE

chips. The scan rate was set to 100 mV/s. Clear oxidative/reductive signals were obtained on wet NC membrane using SPE chips. Two groups of redox peaks are observed in figure 14, which were the two-step oxidation or reduction. In order to avoid noise signals due to redox reactions of TMB under applied potentials, the applied potential at the working electrode during chronoamperometric assay was set to -0.1 V against an Ag/AgCl screen-printed reference electrode.

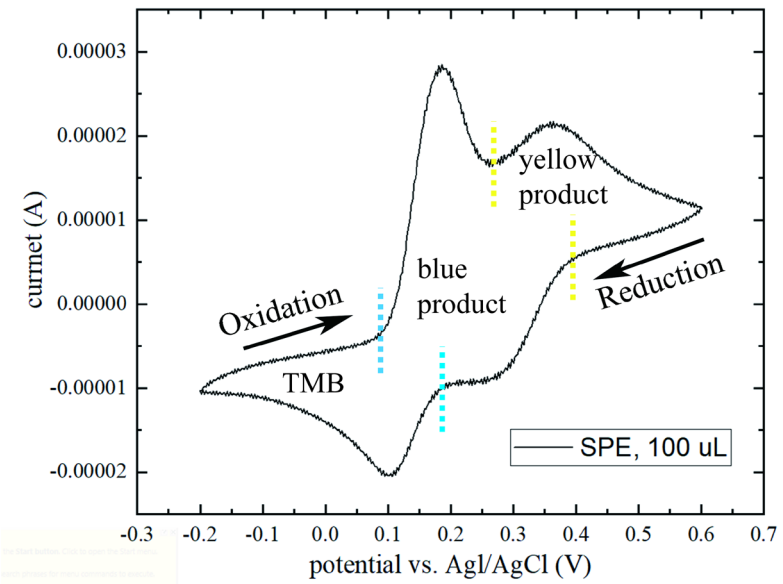

Figure 14. Characterization of commercial TMB substrate on NC membrane using SPE chips. The scan rate was set to 100 mV/s.

To validate the detection of HRP labels on NC membranes, chronoamperometric detection of HRP-C6 conjugate was first studied. According to earlier studies of TMB oxidation[123] and our study (figure 3.1), without stopping agents, TMB substrate is first oxidized by HRP/H_2O_2 into a blue product which subsequently turns into an orange solution which is consisted of the blue product and the yellow product within 5 minutes. We eventually allow 30 s for the incubation of HRP-C6 and TMB substrates before CA measurements.

3.2.2.3.2 paper-based chronoamperometric CRP detection in PBS solution

The LFA was constructed according to figure 15. During our experiments, glass fiber exhibits the best compatibility to saliva samples when comparing to other commercial materials including cellulose filters and surface-modified polyester. A sandwich format based on

antibodies was adapted in this work to recognize CRP in different samples. The conjugated pad is loaded with HRP-conjugated anti-CRP antibody C6.

During a typical assay (figure 3.2), HRP-conjugated C6 interacted with CRP in the sample and migrated along NC membrane. Approximately 15 minutes after adding the sample, HRP-C6-CRP complexes would be captured at the test line by immunoreaction between CRP and antibody C2, while HRP-C6 which were not combined with CRP would eventually migrate into the absorption pad. The test zone was defined by two hydrophobic lines drawn on both sides of the test line, with 10 mm in between. Before the chronoamperometric detection, we added TMB substrate was added to the test zone, covered the test zone with a SPE chip. HRP catalyzes the oxidation of TMB into two products, which is a two-step oxidation involving two electrons [123,124].

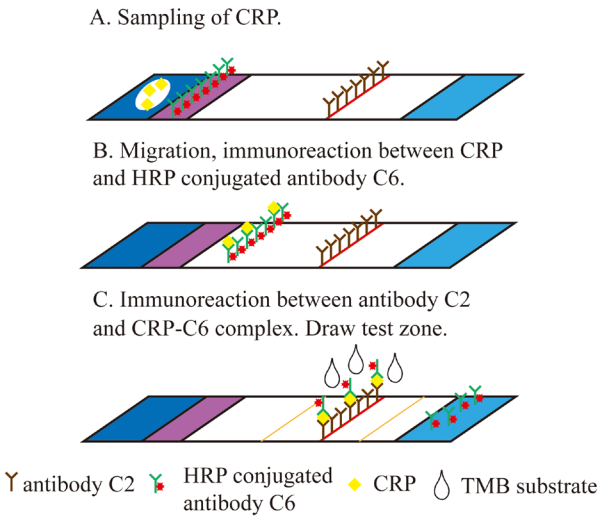

Figure 15. Workflow of the chronoamperometric lateral flow immunosensor in this work. CRP was first added to the sample pad. Followingly, two hydrophobic lines were drawn at two sides of the test line and an SPE chip was placed atop to measure CRP concentrations.

The chronoamperometric detection of CRP on lateral flow strips was first carried out using PBS solution spikes with desired concentration CRP. As shown in figure 3.3a, different concentrations of CRP (from 0.5 to 10^5 nM in PBS at pH 7.4) were detected using a SPE chip. With increasing concentrations of CRP in PBS solutions, the amounts of HRP-C6-CRP-C2 complexes formed in the test region increased, resulting in significantly stronger current

signals. Linear regression was applied to study the performance of the immunosensor (figure 3.3 b). The linear range of detection was determined as 0.5 nM to 10^5 nM, with a standard deviation smaller than 5% and a correlation coefficient $R^2 = 0.976$.

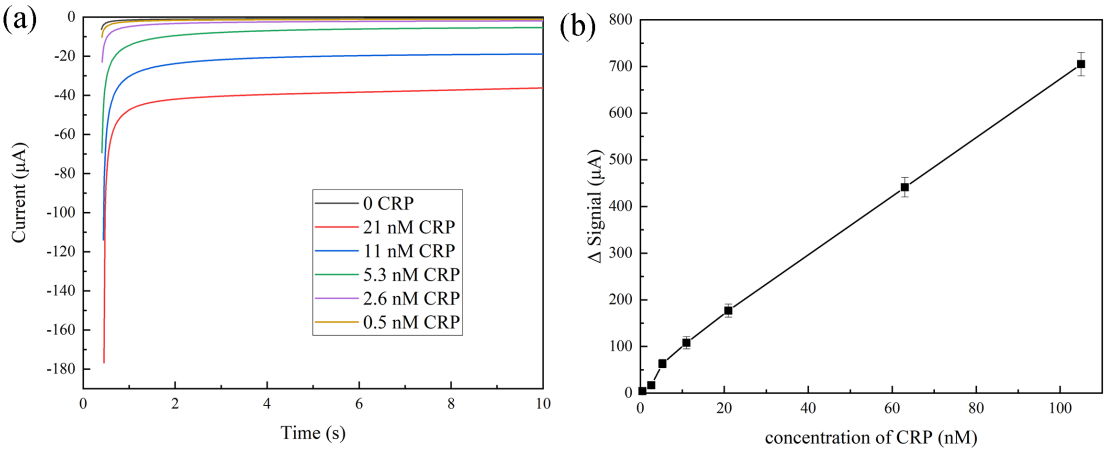

Figure 16. (a) Chronoamperometric measurements of CRP at different concentrations and (b) plot of the current intensity variations against CRP concentrations in PBS solution using amperometric LFA.

Proteins other than CRP were also spiked into PBS solutions (pH 7.4) and added onto lateral flow immunosensors respectively to characterize the specificity. IL-8, hMMP-9, and PSA were selected as models of study because they are common analytes in saliva, associating with progression of chronic diseases.[19] As shown in figure 3.4, the peaks of current signals from samples containing 5.3 nM CRP were approximately 10 times of samples containing 5.3 nM of analytes other than CRP. According to the results, the immunosensor exhibited good reproducibility and specificity.

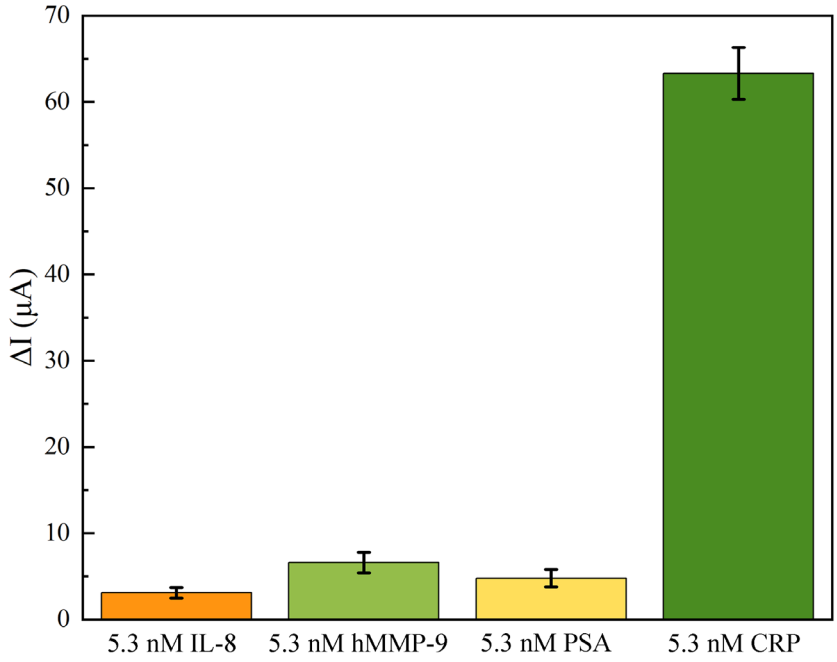

Figure 17. Specificity of the chronoamperometric LFA using different proteins. Each protein was tested three times.

3.2.2.3.3 Study of chronoamperometric CRP detection in real saliva

After verification of biosensing principle and performance of the chronoamperometric lateral flow immunosensor in PBS solution spiked with different analytes, real human saliva samples were used to optimize the configuration of the test strips. Saliva samples were obtained from a nominally healthy volunteer. The procedure of saliva sampling was described in detail in section 2 materials and methods. We analyzed salivary CRP concentrations of CRP using ELISA kits. The human saliva samples were spiked with 0.5 nM to 10^5 nM of CRP respectively to determine the linear range of immunosensor when testing real saliva. As shown in figure 3.5, the first curve corresponds to the human saliva without addition of CRP. With addition of CRP into saliva, the current peak gradually increased. The linear range of detection was determined as 0.5 nM to 10^5 nM, with a relative standard deviation less than 10% and a correlation coefficient R^2 = 0.996. Signals obtained from human saliva was lower than the results obtained from PBS solutions, which may be possible resulted from the complicated composition and high viscosity of real saliva [21].

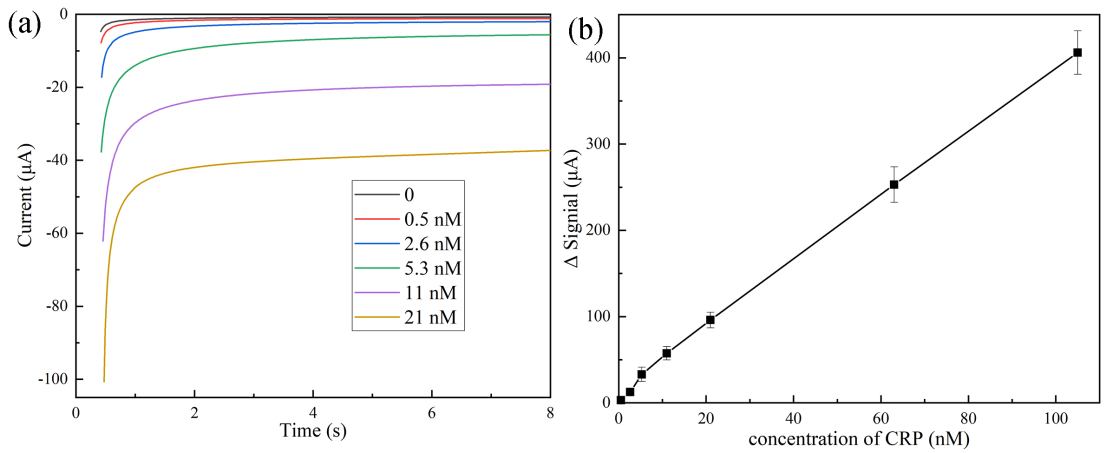

Figure 18. (a) Chronoamperometric measurements of CRP at different concentrations and (b) plot of the current intensity variations against CRP concentrations human saliva spiked with CRP using LFA. Our LFA achieved a linear detection range covering 0.5 to 10^5 nM in saliva.

Comparing to other reported colorimetric, fluorescence, and electrochemical LFAs which all directly measurement labels conjugated to the secondary antibody, we measured the faradaic current resulted from the reduction of TMB's first oxidation product. As shown in conventional ELISA, the concentration of TMB's first oxidation product corresponds to the concentrations of antibody C6 captured at the test line. Comparing to LFAs based on colorimetry and fluorescence, electrochemical LFAs are less sensitive to the environmental interferences. Thus, electrochemical LFAs don't need dedicated encapsulation with well-designed light paths. By introducing the TMB substrates, we successfully extend the range of detection from previously reported picomolar level[125] to nanomolar level which is relevant to medical applications including monitoring of chronic diseases[102]. Additionally, TMB substrates will turn blue within a few seconds in case of successful detection.

On the other hand, there are still improvements that need to be accomplished before our LFAs can be directly used in practical scenarios. Our LFA still needs additional manual operations to draw water-prove lines and add TMB substrates between the lines. When detecting CRP in real saliva samples, the current intensities were lower than results obtained from PBS solutions. The limitation in LOD of CRP may be attributed to limited convective mass transfer on porous fibrous materials.[126,127] Some researchers studied electrochemistry on cellulose paper with and without hollow channel.[126] They argued that the presence of the cellulose matrix reduces rates of convective mass transfer and hence limits the performance of paper-

based electrochemical sensors. The high viscosity of saliva will also significantly decrease the diffusive transport all CRP and antibodies as well as TMB substrate during chronoamperometric measurement.[128]

3.2.2.3.4 Conclusions

In summary, a chronoamperometric immuno-LFA was reported to detect CRP in both PBS solution and human saliva. The chronoamperometric lateral flow immune-LFA achieved a linear detection range covering 0.5 nM to 10^5 nM in both PBS solution and human saliva. It also shows a limit of detection of 0.07 nM CRP in PBS solution a limit of detection of 0.32 nM in saliva. Despite the reported results, efforts still need to be taken to broaden the range of CRP detection, especially at micromolar levels. It also needs to minimize manual operations of adding substrates during the assay as well as to realize multiplexed detection of different analytes. In future works, attempts will be made to integrate an additional pad on which TMB substrates are dried. Nevertheless, nitrocellulose is never the perfect substrate for LFAs. Electrochemical LFAs may be improved by studying novel porous fibrous materials cooperating with physical or chemical treatment to create hollow channels in LFAs by defining hydrophobic and hydrophilic regions to obtain stable electrochemical measurement.

3.3 Emerging Functional Nanomaterials and Their Potential in Body Fluid Biosensing, examples of 2D Black Phosphorus

3.3.1 Background

Through the ongoing KOLS project, we recognized biofouling as one of the major challenges in directly sensing biomarkers in untreated human body fluids both in-vivo and in-vitro. We insighted that, by controlling the defects in semiconducting nanomaterials, superhydrophilicity could be achieved to prohibit unspecific adsorption of proteins onto electrode surfaces. A detailed background can be found in Article 3.

3.3.2 Objectives

- Evaluate state-of-the-art techniques to generate defects in emerging nanomaterials.

- Evaluate characterization and application of defects in biosensing area.
- Determine the material to be used in the anti-biofouling application.

3.3.3 Results

A detailed review of the relevant aspects can be found in Article 3.

3.4 Surface oxygen deficiency enabled spontaneous anti-protein-fouling in tungsten trioxide nanosheets

3.4.1 Background

Biofouling is a universal issue to biosensors and other medical devices that contact untreated biological fluids.[129–132] It happens simultaneously on most interfaces unless antifouling strategies haven been applied. Blocking the contacting surface is an essential step in fabricating biosensor electrodes. However, for decades, it is still challenging to achieve truly antifouling interfaces between micro-/nano-systems and biological fluids. Biofouling is often characterized as non-specific adsorption of proteins and cells to liquid/solid interfaces, after continuous operation in biological fluids.[129,133] When contacting bloods, biofouling can even lead to clotting.[131] Unlike artificial solutions prepared in lab, even the simplest biological fluids may be consisted of countless molecules and cells that would lead to biofouling. Based on current studies, protein adsorption is believed to be the very first step of biofouling, and subsequently mediates cell adhesion and thrombus formation,[134] especially for plasma-contacting surfaces.[132,135,136] Adsorbed proteins are believed to form a layer between 2 to 10 nm thick, where protein concentration can be 1000-fold higher than the concentration in plasma far from the surface.[134] Biofouling degrades the performance of devices that operating in biological fluids. Taken electrochemical biosensors as an example, molecules and cells adsorbed to electrode surfaces will not only screen selective biorecognition, but also block electron transfer between redox species and electrode surfaces. Such adsorption results in blocking and passivation of the sensing surface, and ultimately degrades the biosensor performances in various aspects, including accuracy, reproducibility, selectivity, sensitivity, limit of detection, etc. Similar degradations have been observed in other types of

biosensors.[137] As the area of biosensors continues to prosper, preventing non-specific adsorption is becoming a more and more critical challenge to be resolved, especially as new applications like implantable sensors and brain-computer interfaces continue to rise.

Even since the emergence of biosensors, researchers have been developing antifouling strategies to eliminate non-specific protein adsorption.[138] These numerous attempts can be classified into following categories: (1) sample processing, (2)porous membranes, (3) surface modifications through physical, chemical, biological approaches, and (4) combined approaches. For in vitro detection, a common strategy is to process complex biological samples with dilution, centrifugation, and additions of various agents including surfactants,[129] anticoagulants,[139] antiplatelet agents,[140] etc. Sample treatment is not always the ideal solution since it adds extra manual operations and it is not suitable for continuous, in-vivo detection in biological fluids. Beyond sample treatment, it requires different measures to detect small molecules and relatively large molecules like proteins. Semi-permeable membranes have been applied in electrochemical biosensors to detect small molecules like glucose[141], doxorubicin, kanamycin, gentamicin, and tobramycin[142] in blood. Nanopore[143] and composite of bovine serum albumin (BSA) and gold nanowire[144] have been developed to detect proteins. Comparing to filtration approaches, huge efforts have been made in developing surface modification approaches, majorly through chemical coating with organic molecules and biological molecules.[145] George M. Whitesides' group is one of the pioneers in researching antifouling chemical coating, which set foundations in two major categories as organic molecules rich in hydrogen bonds, e.g., poly(ethylene glycol)[138], and zwitterions.[146,147] By mimicking zwitterions with biomolecules, S. Jiang et al. developed peptides maintaining both positive and negative charges.[148]

Despite fruitful achievements in the past decades, antifouling in complex biological fluids still remains a major challenge to biosensors and other medical devices. Developed approaches bear different shortages that hinder their applications. Semi-permeable membranes cannot be used in biosensors that detect proteins. Chemical modification with molecules like albumin and PEG passivates the surface of the electrode and hinders electron mobilization from redox species in solution to the electrode. Biosensors with such chemical modification are usually

not sensitive enough to reach low detection limits. In addition, adsorbed albumins mediate platelet aggregation in blood and thus cause thrombus formation.[131,133] PEG has been reported to reduce non-specific protein adsorption, however, it a non-biodegradable polymer that generates multiple side effects[149,150] and leads to development of PEG antibodies.[151] Biocompatible zwitterions were developed to replace PEG, but Some of them are still subjected to fouling when operating in biological fluids for extended periods.[152]

3.4.2 Objectives

- Solvothermal synthesis of WO_3 nanosheets with various oxygen vacancies.
- Fabrication of superhydrophilic sensor surfaces by spinning coating WO_3 thin film.
- Investigation of antifouling behavior of as-prepared WO_3 thin films.

3.4.3 Experimental

In a typical procedure of solvothermal synthesis, we added 0.2 g of WCl_6 and 2.0 g of oxalic acid into 40 mL of absolute ethanol. After stirring for 30 mins at room temperature, we relocated the mixture into an autoclave which was of 100 mL volume, then sealed it and let the mixture react at 100 °C for 24 h. The product was cooled inside the autoclave to 25 °C and subsequently collected by centrifugation in deionized water and absolute ethanol respectively. Collected powder, which was hydrogen tungsten oxide hydrate, was further calcined in different atmosphere like air, N_2, and 20% H_2/Ar at 300 °C for 1 h using a CVD furnace. We heated up the furnace at 10 °C/min until required temperatures were reached.

Calcined WO_3 nanosheets were dispersed into isopropanol to reach a concentration of 50 mg/mL. The mixtures were kept in a water bath and probe sonicated at 20 °C, 400 W with a pulse of 1 s on and 2 s off for various durations (8 h, 12 h, 16 h). Sonicated mixtures were filtered by 0.45 µm syringe filters to reach WO_3 inks. Before spin-coating, 1 x 1 cm^2 ITO glasses were cleaned by bath sonication sequentially in water, isopropanol (IPA), and ethanol, for 15 mins each sonication. ITO glasses were further treated by a UV Ozone cleaner. As prepared 90 µL/cm^2 of WO_3 inks were spin coated onto ITO glasses at a spinning speed of 5000 rpm for 30 s by a dynamic dispense technique. WO_3 thin films were dried on a hot plate at 65 °C.

Characterization methods were omitted here to avoid self-plagiarism and were described in detail in Article 4 and Article 5.

Specific plasma protein detection by ELISA and micro-BCA assay. The samples were placed in PBS solution for 8h and then transferred to protein solution (1 mg/mL). We incubated the protein solution at 37°C for 2 h. After the protein solution was sucked out, the sample surface was cleaned with PBS solution five times. To desorb the protein coat, the samples were transferred to a concentration of 1 wt% SDS/PBS solution for ultrasonic treatment for 20 min, to desorb the protein coat. For the protein concentration in the eluent, the kit was used following the instructions of the manufacturer. The absorbance (OD) of the protein solution was measured at 562 nm using a microplate reader, and the protein adsorption capacity is calculated.

3.4.4 Results

Solvothermal synthesis of WO_3 nanosheets and probe sonication to prepare homogeneous WO_3 inks. WO_3 nanosheets were synthesized following an optimized solvothermal method which was developed in Article 5. The XRD pattern of the solvothermal product (figure 19c) corresponded to monoclinic hydrogen tungsten oxide hydrate ($H_{0.12}WO_3 \cdot 2H_2O$, PDF#40-0693). As-synthesized hydrogen tungsten oxide hydrate powder contained agglomerates consisting of nanoparticles of 20 nm diameters. The agglomerates were as large as 200 nm in dimension (figure 19d). To obtain stoichiometric tungsten trioxide, solvothermal products were calcined in air. The XRD patterns of air-calcined products (figure 19c) corresponded to cubic tungsten oxide (WO_3, PDF#41-0905). Probe sonication was applied in the attempt to reduce the agglomerates and improve the homogeneity. Crystal structure and phase of calcined products were not changed after 12 hours of probe sonication. With help from probe sonication in isopropanol, all of the agglomerates were dispersed into free-standing nanoparticles with size of 20 nm. Since the morphology of solvothermal synthesized WO_3 were reported to be sensitive to the procedure,[153,154] adding sequences of WCl_6 and oxalic acid into ethanol before solvothermal reaction were also studied. By altering the adding sequence, the precursor could be $WCl_3(OC_2H_5)_2$ or $WCl_3(OCH_3)_2$ in ethanol solution with $W_2Cl_4(OC_2H_5)_6$ precipitates, however, the air-calcined products were all identified as same cubic tungsten

trioxide (PDF No.41-0905). Different precursors exhibited little impact on the final air-calcined products. Detailed discussion on the effect of adding sequence and probe sonication can be found in Article 5.

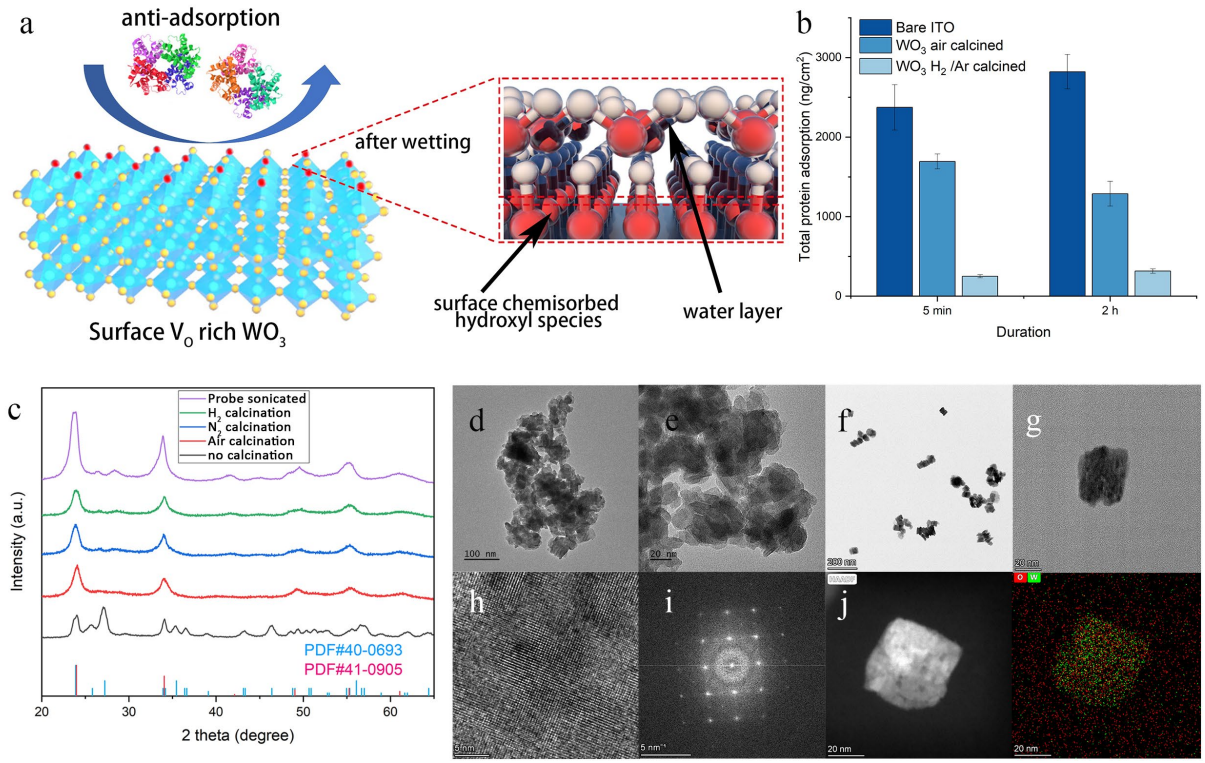

Figure 19. (a) XRD patterns of the solvothermal synthesized hydrogen tungsten oxide hydrate, and tungsten oxide after calcination by air, N_2, and 20% H_2/Ar. Air-calcined sample was also processed by probe ultrasonication for 12 hours. (d,e) TEM figures of the solvothermal synthesized hydrogen tungsten oxide hydrate. (c,d) of the air-calcined WO_3 after probe sonication. (e,f) HRTEM, FFT. (g) Mapping of air-calcined cubic WO_3. Adapted from Article 4.

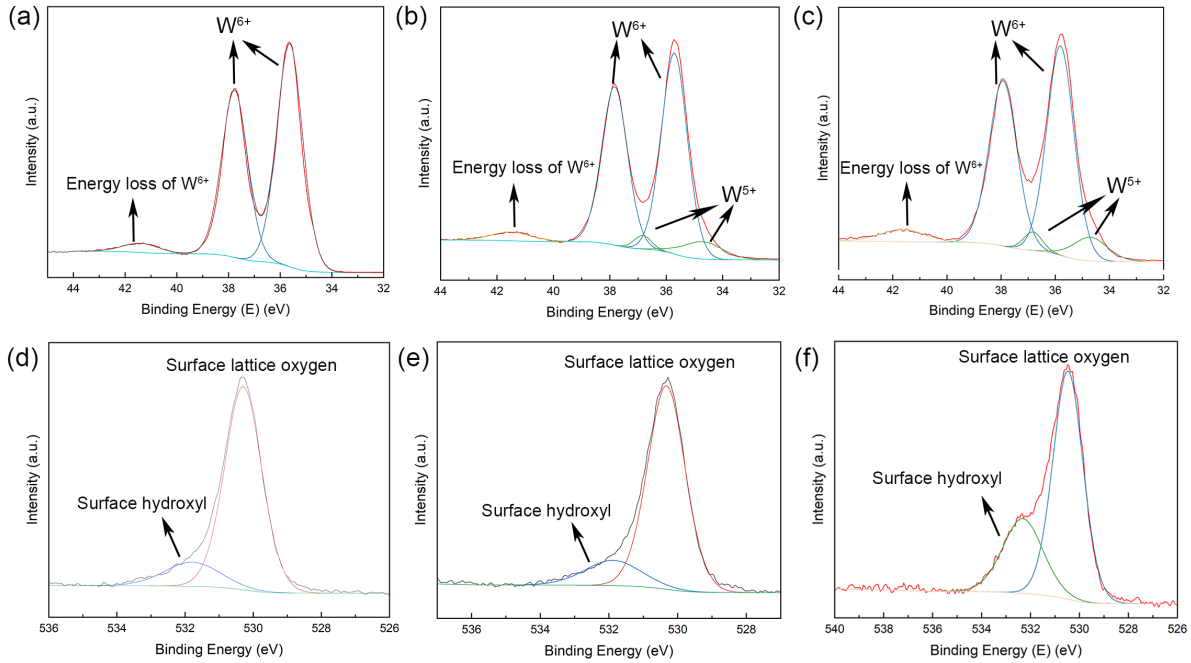

Figure 20. High resolution W 4f and O 1s XPS spectra of WO_3 nanosheets calcined under (a, d) air, (b, e) N_2 atmosphere, and (c, f) 20% H_2/Ar atmosphere. The increasing areas of W^{5+} and surface hydroxyl peaks indicate generation of surface oxygen vacancies. Adapted from Article 4.

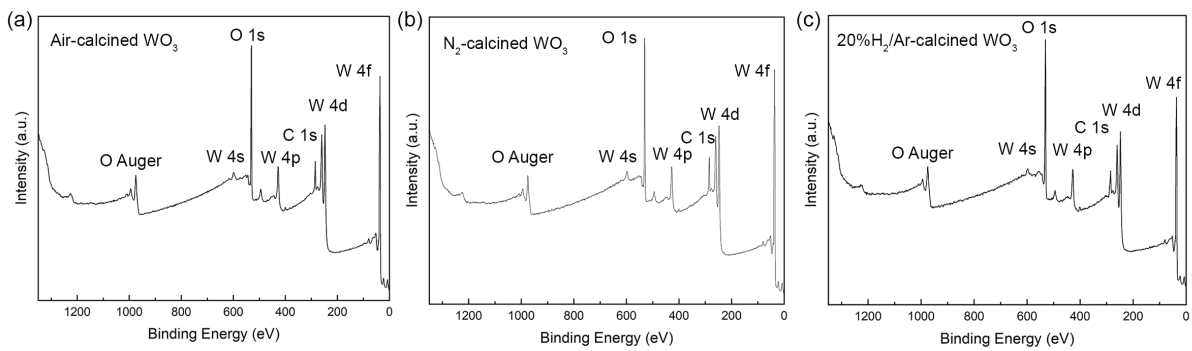

Figure 21. XPS spectra of WO_3 calcined under (a) air, (b) N_2 atmosphere, and (c) 20% H_2/Ar atmosphere. Adapted from Article 4.

Table 5. Binding energy of tungsten and oxygen peaks summarized from XPS spectra.

Sample	Peak binding energy (eV)					
	W^{6+}		W^{5+}			
	$4f_{7/2}$	$4f_{5/2}$	$4f_{7/2}$	$4f_{5/2}$	Surface oxygen	Surface hydroxyl radical
WO_3	35.65	37.79			530.29	531.79
N_2-calcined WO_3	35.71	37.83	34.71	36.83	530.33	531.88

H_2-calcined WO_3	35.81	37.93	34.71	36.83	530.47	532.31

Table 6. The percentage of W^{6+}, W^{5+}, surface lattice oxygen, and surface hydroxyl radical calculated from XPS spectra.

Sample	atomic %			
	W^{6+}	W^{5+}	Surface lattice oxygen	Surface hydroxyl radical
WO_3	100	0	0.82	0.18
N_2-calcined WO_3	0.90	0.10	0.81	0.19
H_2-calcined WO_3	0.89	0.11	0.57	0.43

Generation of oxygen vacancies in WO_3 nanosheets. To generate oxygen vacancies (V_O) in WO_3 nanosheets, the solvothermal product underwent calcination in 20% H_2/Ar, and N_2. XPS spectroscopy provided a semiquantitative evaluation on the oxygen vacancies in the surface regions of WO_3 nanosheets. In W 4f XPS spectra (figure 20a, 20b, and 20c), the peaks of binding energies at 37.79–37.93 eV represented the W $4f_{5/2}$ peak of W^{6+} and the peaks at 35.65–35.81 eV corresponded to W $4f_{7/2}$ of W^{5+}.[155] The broad peak at around 45.1 eV corresponded to the energy loss feature of W^{6+}. In XPS spectra taken from N_2-calcined WO_3 samples and H_2-calcined WO_3 samples, another two peaks at 36.8 eV and 34.7 eV represented W $4f_{5/2}$ and W $4f_{7/2}$ of W^{5+}, indicating the presence of oxygen vacancies in the surface regions. The O 1s spectra showed the peaks of surface lattice oxygen at 530.29–530.47 eV and the peaks of hydroxyl radicals at 531.79–532.31 eV on the WO_3 surfaces.[155] The percentage of surface hydroxyl radical sharply increased in H_2-calcined WO_3 comparing to samples calcined in air or N_2. Previous work suggested that hydroxyl radical was chemisorbed at to surface oxygen vacancies for stabilization.[156] A larger area of the hydroxyl radical in the XPS spectrum indicated more oxygen vacancies on the sample surfaces. The calculated percentage of hydroxyl radical was more than twice of the ones in either air-calcined WO_3 or N_2-calcined WO_3. It suggested that oxygen vacancies were largely generated on the surface sites. Electron spin resonance (ESR, a.k.a., electron paramagnetic resonance) spectroscopy further supported the results from XPS spectra. ESR/EPR spectroscopy showed a peak at g=2.0024 which corresponded electrons trapped at surface oxygen vacancies.[155,157] A higher peak indicated more surface oxygen vacancies in the samples (figure 21). In general, calcination by

air, N_2, or 20% H_2/Ar did not change the crystal structure of solvothermal synthesized WO_3. WO_3 nanosheets calcined in air exhibited no oxygen vacancy. WO_3 nanosheets calcined in 20% H_2/Ar were rich in oxygen vacancies while N_2 calcination resulted in moderate levels of oxygen vacancies (table 6).

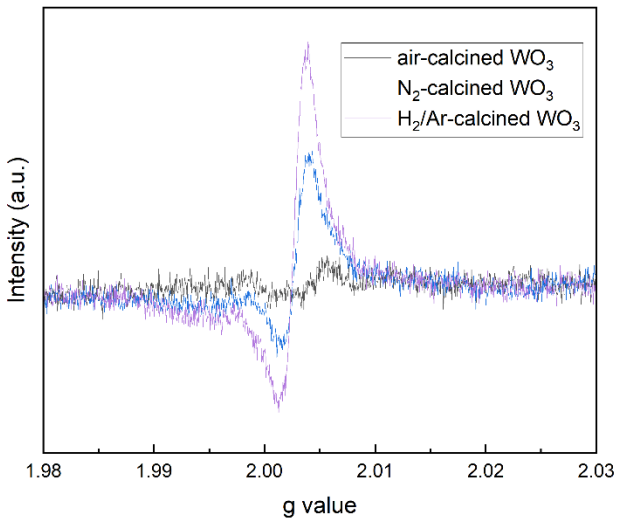

Figure 21. ESR/EPR spectra of WO_3, peak at g=2.0024. A large peak indicates higher concentration of oxygen vacancies in the sample. Adapted from Article 4.

V_O enabled superhydrophilicity and anti-protein-adsorption of WO_3 thin films. Water contact angle is an important benchmark to characterize wetting behavior of thin films. A plane is considered superhydrophilic if its optical water contact angle is below 10°. WO_3 inks were prepared by dispersing WO_3 nanosheets with controlled oxygen defects into isopropanol, based on an optimized protocol. Electrodes covered with WO_3 thin films were further fabricated by spin-coating WO_3 inks onto commercial ITO/SiO_2 substrates. The commercial ITO/SiO_2 substrate exhibited an average optical water contact angle of 36.2 ± 2.3°. Air-calcined WO_3 thin films exhibited an average water contact angle of 17.5 ± 0.6°. The optical contact angles of water on N_2-calcined WO_3 thin films and H_2-calcined ones were further decreased to 13.7 ± 1.1° to 8.38 ± 0.7°. Such results indicated that rich surface V_O led to superhydrophilicity of in WO_3 thin films. Fibrinogen (FIB), human serum albumin (HSA),

immunoglobulin G (IgG), and lysozyme (LZM) were selected as model proteins to study their irreversible adsorption on ITO substrate, WO_3 thin film with no V_O and rich in V_O. Individual model protein was incubated with different thin films for 5 minutes and 2 hours. The adsorption of HSA, FIB, and IgG to tungsten trioxide thin films without V_O was much lower than their adsorption to ITO. The adsorption of HSA and IgG to WO_3 thin films saturated after 5 minutes, while the adsorption of FIB continued to increase with extended incubation. At 5 minutes, the adsorption of LZM to WO_3 thin films was double that of the adsorption to ITO. Optical water contact angles were decreased to 8.38 ± 0.7 ° for WO_3 thin films rich in V_O, and the adsorption of HSA, FIB, LZM, and IgG was significantly reduced. Adsorption of HSA, LZM, and IgG remained at the same levels below 5 ng/cm^2 as the exposure time extended from 5 minutes to 2 hours, while the adsorption of FIB decreased from 17.3 ng/cm^2 to 5.6 ng/cm^2. Adsorption of HSA, FIB, LZM, and IgG onto WO_3 thin films rich in surface V_O was reduced by 95.5%, 95.8%, 98.6%, and 98.7% compared to ITO substrate. Adsorption of HSA, FIB, LZM, and IgG was reduced by 79.8%, 92.7%, 98.8%, and 82.2% compared to WO_3 with no surface V_O. To further examine the properties of WO_3 films, different WO_3 films were treated with human plasma. Adsorption of HSA, FIB, LZM, and IgG from human plasma was quantified using the micro-BCA method. The trends of protein adsorption from plasma between bare ITO, ITO coated with air-calcined WO_3, and H_2/Ar-calcined WO_3 were the same as the adsorption from as-prepared solutions, except for LZM. The decrease in protein adsorption at longer exposure may be attributed to the Vroman effect. Compared to bare ITO, the adsorption of HSA, FIB, LZM, and IgG onto WO_3 thin films rich in surface V_O were reduced by 71.4%, 75.2%, 49.7%, and 50.0%. Compared to WO_3 with no surface V_O, the adsorption of HSA, FIB, LZM, and IgG was reduced by 63.4%, 87.4%, 60.5%, and 26.3%.

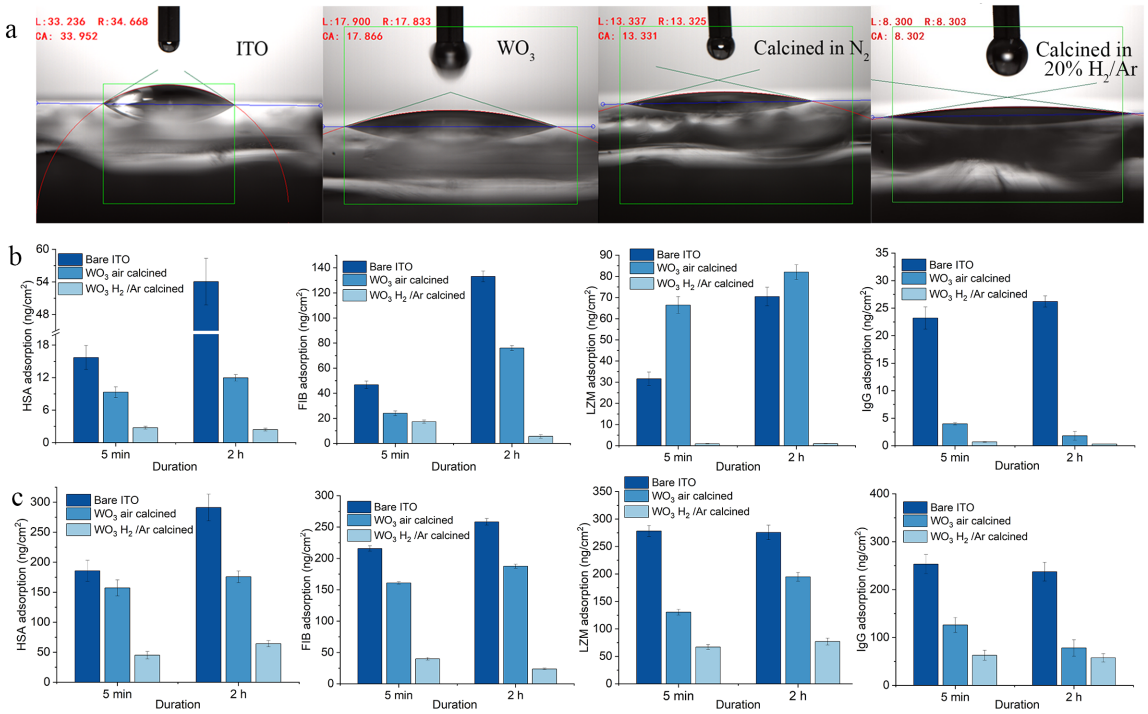

Figure 22. (a) Optical contact angles of water on ITO substrate, air-calcined WO_3, N_2-calcined WO_3, and H_2-calcined WO_3 thin films. Adapted from Article 4. (b) Irreversible adsorption of HSA, FIB, LZM, and IgG to ITO/SiO_2 substrates, WO_3 thin film with no oxygen vacancy (air calcination), WO_3 thin film rich in oxygen vacancy (20% H_2/Ar calcination). Adsorption was characterized by ELISA. (c) Irreversible adsorption of 4 proteins for human plasma, measured by micro-BCA.

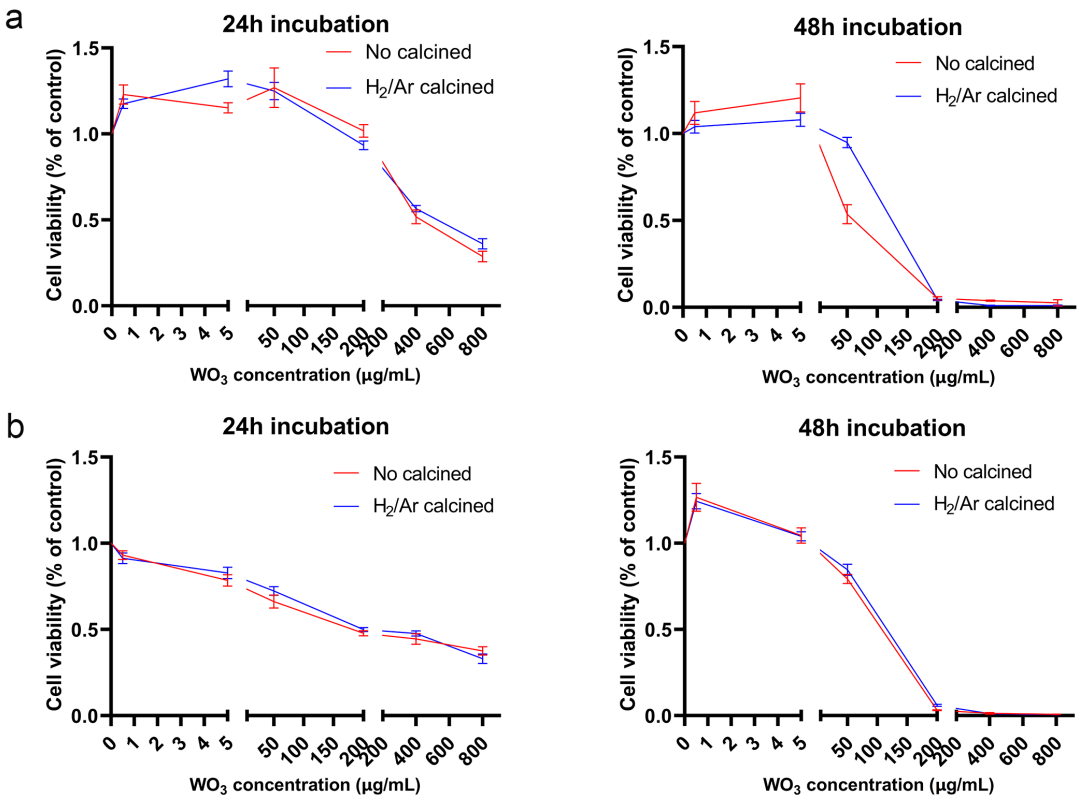

Figure 23. Cellular toxicity of WO_3 nanosheets. HUVECs were incubated with WO_3 nanosheet for 24 h and 48 h, with its cell activity measured by (a) CCK-8 assay and (b) CTG assay. Adapted from Article 4.

The influence of tungsten trioxide on human somatic cells remains largely unexplored, particularly in the context of its use as electrodes in implantable sensors, where the detachment of WO_3 nanosheets from the thin film could potentially pose a risk to human health via adsorption in blood vessels. To address this knowledge gap, we evaluated the toxicity of WO_3 nanosheets on human umbilical vein endothelial cells (HUVECs). We exposed HUVECs to WO_3 nanosheets with varying concentrations from 0 to 800 µg/ml for 24 and 48 hours and analyzed the resulting cytotoxicity using both CCK-8 and CTG assays. CCK-8 results (figure 23a) revealed that HUVECs exhibited a significant decline in cell activity when HUVECS were exposed to 200 ng/mL WO_3 nanosheets for 24 hours, with near-total cell death observed after 48 hours, thus indicating a time- and dose-dependent relationship. Interestingly, we observed a modest increase in cell activity at low WO_3 concentrations (0.5 and 5 µg/mL), suggesting a biphasic effect of WO_3 on cells. To further verify our findings, we utilized the CTG method (figure 23b), which relies on ATP activity for cell counting, and found that exposure to 200 µg/mL WO_3 nanosheets for 24 hours resulted in a 50% reduction in cell activity. While

low-concentration WO_3 treatment did not show an effect on cell growth after 24 hours, an increase in cell activity was observed after 48 hours, indicating that low-dose WO_3 can promote cell growth. Our findings suggest that WO_3 nanosheets have a biphasic effect on HUVECs, with concentrations below 0.5 μg/mL promoting cell growth and higher concentrations leading to significant apoptosis. Detailed discussion can be found in article 4.

4 Conclusion and outlook

This dissertation focuses on developing COPD PoC diagnostics of COPD through human saliva and blood samples, as well as studying the potential of using emerging functional nanomaterials in biosensors. The thesis reviewed the COPD PoC technology, which includes (1) specific blood and salivary biomarkers related to COPD exacerbation and different COPD endotypes, (2) sampling technology to acquire blood and saliva samples to be used for paper based PoC diagnostics, and (3) paper-based biosensors that specifically detect COPD biomarkers in human blood and saliva samples. The thesis also reviewed defects and their manipulation in emerging functional nanomaterials, i.e., 2D black phosphorus, to boost development of biosensors and PoC devices to detect COPD biomarkers in human body fluids. It includes methods to control its properties by defect-tailoring and surface functionalization, and its applications in biosensors and disease diagnostics. It also presents critical insights on the future synthesis, modification, and further applications in biosensor. The prior reviews contributed to KOLS project, selected salivary CRP, PCT, and NE as the biomarker combination to monitor COPD and its progression, and selected quantitative LFA to detect these biomarkers in saliva. It also recognized major challenges including the hook effect, matrix effect, and biofouling that interfered detection of biomarkers in human biofluids. These challenges were tackled in the following papers. From the second review, tungsten oxide rich in oxygen vacancy was selected as the electrode coating to minimize biofouling from non-specific proteins in biofluids.

The thesis studied a novel hook-effect-free design in one-step sandwich LFA which quantitative detected CRP in saliva. The hook effect causes false-negative results in sandwich assay when biomarker concentrations exceeded predetermined range of detection. This work introduced a sucrose-treated intermediate pad which hindered sample flowing between the

nitrocellulose membrane and detection antibody immobilized on the conjugate pad, and thus delay releasing conjugate antibody and subsequent reaction between conjugates and analytes to avoid the hook effect. It exhibited a 10 times improvement in range of detection than conventional LFAs. The thesis further described an attempt integrating electrochemical biosensors with LFAs. A novel chronoamperometric immunosensor combing lateral flow strips was developed to detect a representative COPD biomarker, CRP, in saliva. Enzymatic catalyzation of TMB oxidation was demonstrated on nitrocellulose membranes in order to realize electrochemical LFA. The immunosensor exhibited a linear detection range covering 0.5 nM to 10^5 nM and a detection limit as low as 0.07 nM with high reproducibility. Such range covered the requirement for monitoring of chronic disease like COPD. This work studied two quantitative biosensing mechanisms in LFA. It also studied the origin of the hook effect in sandwich LFAs and mitigated the hook effect by adding an intermediate pad between the nitrocellulose membrane and the conjugate pad. The hook effect was a result of competitive interactions between free analytes, analyte-QD complexes at the test line where free analytes occupied binding sites of capture antibodies which would otherwise bound with analyte-QD complexes at high analyte concentrations. Addition of an intermediate pad treated with saturated sucrose solution delayed release of conjugate antibody and thus allowed free analytes to be captured at the text line before analyte-QD complexes were formed. Future LFAs may combine a new module consisting of saliva sampler and buffer storage to the LFA stripe to further reduce operations.

The thesis also studied a spontaneous anti-biofouling strategy by controlling oxygen vacancies in WO_3 nanosheets. Intrinsic surface oxygen vacancies in as-prepared WO_3 thin film led to hydrophilicity-superhydrophilicity transformation of WO_3 thin films by chemisorption of hydroxyl groups at the surface oxygen vacancy sites. Since a compact water layer was formed on superhydrophilic surfaces, superhydrophilic WO_3 thin films thus significantly adsorbed less proteins and exhibit longer electrode lifetime. Cellular toxicity of WO_3 was studied by exposing HUVECs to WO_3 nanosheets. Our findings suggest that WO_3 nanosheets have a biphasic effect on HUVECs, with concentrations below 0.5 μg/mL promoting cell growth and higher concentrations leading to significant apoptosis. Regarding antifouling strategies based on WO_3 to be used as implantable sensor electrodes, future studies need to answer (1) formation of

water layer on superhydrophilic V_O-rich WO_3 thin films at atomic scale, (2) composition of adsorbed protein layer in human blood and the relationship protein layer composition and biocompatibility of the thin film, and (3) the mechanism of WO_3 biphasic effect on HUVECs, especially its cellular toxicity at high concentration, which need to be studied from the aspects of protein corona formed around WO_3 nanosheets, uptake of WO_3 nanosheets into cells, and potential DNA damage after uptake.

5 References

(1) Kvedar, J. C.; Fogel, A. L.; Elenko, E.; Zohar, D. Digital Medicine's March on Chronic Disease. *Nat Biotechnol* **2016**, *34* (3), 239–246. https://doi.org/10.1038/nbt.3495.

(2) *The top 10 causes of death*. https://www.who.int/news-room/fact-sheets/detail/the-top-10-causes-of-death (accessed 2022-08-29).

(3) Celli, B. R.; Wedzicha, J. A. Update on Clinical Aspects of Chronic Obstructive Pulmonary Disease. *N Engl J Med* **2019**, *381* (13), 1257–1266. https://doi.org/10.1056/NEJMra1900500.

(4) *Chronic Obstructive Pulmonary Disease (COPD)*. Norwegian Institute of Public Health. https://www.fhi.no/en/op/hin/health-disease/copd/ (accessed 2022-08-30).

(5) Leung, J. M.; Niikura, M.; Yang, C. W. T.; Sin, D. D. COVID-19 and COPD. *European Respiratory Journal* **2020**, *56* (2). https://doi.org/10.1183/13993003.02108-2020.

(6) Zhao, Q.; Meng, M.; Kumar, R.; Wu, Y.; Huang, J.; Lian, N.; Deng, Y.; Lin, S. The Impact of COPD and Smoking History on the Severity of COVID-19: A Systemic Review and Meta-Analysis. *Journal of Medical Virology* **2020**, *92* (10), 1915–1921. https://doi.org/10.1002/jmv.25889.

(7) Guan, W.; Liang, W.; Zhao, Y.; Liang, H.; Chen, Z.; Li, Y.; Liu, X.; Chen, R.; Tang, C.; Wang, T.; Ou, C.; Li, L.; Chen, P.; Sang, L.; Wang, W.; Li, J.; Li, C.; Ou, L.; Cheng, B.; Xiong, S.; Ni, Z.; Xiang, J.; Hu, Y.; Liu, L.; Shan, H.; Lei, C.; Peng, Y.; Wei, L.; Liu, Y.; Hu, Y.; Peng, P.; Wang, J.; Liu, J.; Chen, Z.; Li, G.; Zheng, Z.; Qiu, S.; Luo, J.; Ye, C.; Zhu, S.; Cheng, L.; Ye, F.; Li, S.; Zheng, J.; Zhang, N.; Zhong, N.; He, J. Comorbidity and Its Impact on 1590 Patients with COVID-19 in China: A Nationwide Analysis. *European Respiratory Journal* **2020**, *55* (5). https://doi.org/10.1183/13993003.00547-2020.

(8) Patel, J. G.; Coutinho, A. D.; Lunacsek, O. E.; Dalal, A. A. COPD Affects Worker Productivity and Health Care Costs. *COPD* **2018**, *13*, 2301–2311. https://doi.org/10.2147/COPD.S163795.

(9) Kinge, J. M.; Sælensminde, K.; Dieleman, J.; Vollset, S. E.; Norheim, O. F. Economic Losses and Burden of Disease by Medical Conditions in Norway. *Health Policy* **2017**, *121* (6), 691–698. https://doi.org/10.1016/j.healthpol.2017.03.020.

(10) *Kommunehelsa*. http://khs.fhi.no/webview/ (accessed 2020-10-22).

(11) Wong, D. T. Towards a Simple, Saliva-Based Test for the Detection of Oral Cancer. *Expert Review of Molecular Diagnostics* **2006**, *6* (3), 267–272. https://doi.org/10.1586/14737159.6.3.267.

(12) Agustí, A.; Hogg, J. C. Update on the Pathogenesis of Chronic Obstructive Pulmonary Disease. *N Engl J Med* **2019**, *381* (13), 1248–1256. https://doi.org/10.1056/NEJMra1900475.

(13) He, G.; Dong, T.; Yang, Z.; Branstad, A.; Huang, L.; Jiang, Z. Point-of-Care COPD Diagnostics: Biomarkers, Sampling, Paper-Based Analytical Devices, and Perspectives. *Analyst* **2022**, *147* (7), 1273–1293. https://doi.org/10.1039/D1AN01702K.

(14) Martinez, F. D. Early-Life Origins of Chronic Obstructive Pulmonary Disease. *New England Journal of Medicine* **2016**, *375* (9), 871–878. https://doi.org/10.1056/NEJMra1603287.

(15) Boucher, R. C. Muco-Obstructive Lung Diseases. *New England Journal of Medicine* **2019**, *380*, 1941–1953. https://doi.org/10.1056/NEJMra1813799.

(16) Global Initiative for Chronic Obstructive Lung Disease. *Global Strategy for the Diagnosis, Management, and Prevention of Chronic Obstructive Pulmonary Disease (2022 Report)*; 2022. https://goldcopd.org/2022-gold-reports-2/ (accessed 2022-09-05).

(17) Sawyers, C. L. The Cancer Biomarker Problem. *Nature* **2008**, *452* (7187), 548–552. https://doi.org/10.1038/nature06913.

(18) Yu, J.-S.; Chen, Y.-T.; Chiang, W.-F.; Hsiao, Y.-C.; Chu, L. J.; See, L.-C.; Wu, C.-S.; Tu, H.-T.; Chen, H.-W.; Chen, C.-C.; Liao, W.-C.; Chang, Y.-T.; Wu, C.-C.; Lin, C.-Y.; Liu, S.-Y.; Chiou, S.-T.; Chia, S.-L.; Chang, K.-P.; Chien, C.-Y.; Chang, S.-W.; Chang, C.-J.; Young, J. D.; Pao, C. C.; Chang, Y.-S.; Hartwell, L. H. Saliva Protein Biomarkers to Detect Oral Squamous Cell Carcinoma in a High-Risk Population in Taiwan. *Proc Natl Acad Sci USA* **2016**, *113* (41), 11549–11554. https://doi.org/10.1073/pnas.1612368113.

(19) Faner, R.; Tal-Singer, R.; Riley, J. H.; Celli, B.; Vestbo, J.; MacNee, W.; Bakke, P.; Calverley, P. M. A.; Coxson, H.; Crim, C.; Edwards, L. D.; Locantore, N.; Lomas, D. A.; Miller, B. E.; Rennard, S. I.; Wouters, E. F. M.; Yates, J. C.; Silverman, E. K.; Agusti, A. Lessons from ECLIPSE: A Review of COPD Biomarkers. *Thorax* **2014**, *69* (7), 666–672. https://doi.org/10.1136/thoraxjnl-2013-204778.

(20) Grommes, J.; Soehnlein, O. Contribution of Neutrophils to Acute Lung Injury. *Mol Med* **2011**, *17* (3–4), 293–307. https://doi.org/10.2119/molmed.2010.00138.

(21) Heikenfeld, J.; Jajack, A.; Feldman, B.; Granger, S. W.; Gaitonde, S.; Begtrup, G.; Katchman, B. A. Accessing Analytes in Biofluids for Peripheral Biochemical Monitoring. *Nat Biotechnol* **2019**, *37* (4), 407–419. https://doi.org/10.1038/s41587-019-0040-3.

(22) Fang, L.; Gao, P.; Bao, H.; Tang, X.; Wang, B.; Feng, Y.; Cong, S.; Juan, J.; Fan, J.; Lu, K.; Wang, N.; Hu, Y.; Wang, L. Chronic Obstructive Pulmonary Disease in China: A Nationwide Prevalence Study. *The Lancet Respiratory Medicine* **2018**, *6* (6), 421–430. https://doi.org/10.1016/S2213-2600(18)30103-6.

(23) Cohen, L.; Walt, D. R. Highly Sensitive and Multiplexed Protein Measurements. *Chem. Rev.* **2019**, *119* (1), 293–321. https://doi.org/10.1021/acs.chemrev.8b00257.

(24) Gug, I. T.; Tertis, M.; Hosu, O.; Cristea, C. Salivary Biomarkers Detection: Analytical and Immunological Methods Overview. *TrAC Trends in Analytical Chemistry* **2019**, *113*, 301–316. https://doi.org/10.1016/j.trac.2019.02.020.

(25) Liao, S.-H.; Chen, K.-L.; Wang, C.-M.; Chieh, J.-J.; Horng, H.-E.; Wang, L.-M.; Wu, C. H.; Yang, H.-C. Using Bio-Functionalized Magnetic Nanoparticles and Dynamic Nuclear Magnetic Resonance to Characterize the Time-Dependent Spin-Spin Relaxation Time for Sensitive Bio-Detection. *Sensors* **2014**, *14* (11), 21409–21417. https://doi.org/10.3390/s141121409.

(26) Zhang, Y.; Bai, J.; Ying, J. Y. A Stacking Flow Immunoassay for the Detection of Dengue-Specific Immunoglobulins in Salivary Fluid. *Lab Chip* **2015**, *15* (6), 1465–1471. https://doi.org/10.1039/C4LC01127A.

(27) Barhoumi, L.; Baraket, A.; Bellagambi, F. G.; Karanasiou, G. S.; Ali, M. B.; Fotiadis, D. I.; Bausells, J.; Zine, N.; Sigaud, M.; Errachid, A. A Novel Chronoamperometric Immunosensor for Rapid Detection of TNF-α in Human Saliva. *Sensors and Actuators B: Chemical* **2018**, *266*, 477–484. https://doi.org/10.1016/j.snb.2018.03.135.

(28) Taylor, J. J.; Jaedicke, K. M.; van de Merwe, R. C.; Bissett, S. M.; Landsdowne, N.; Whall, K. M.; Pickering, K.; Thornton, V.; Lawson, V.; Yatsuda, H.; Kogai, T.; Shah, D.; Athey, D.; Preshaw, P. M. A Prototype Antibody-Based Biosensor for Measurement of Salivary

MMP-8 in Periodontitis Using Surface Acoustic Wave Technology. *Scientific Reports* **2019**, *9* (1), 1–9. https://doi.org/10.1038/s41598-019-47513-w.

(29) Elnathan, R.; Kwiat, M.; Pevzner, A.; Engel, Y.; Burstein, L.; Khatchtourints, A.; Lichtenstein, A.; Kantaev, R.; Patolsky, F. Biorecognition Layer Engineering: Overcoming Screening Limitations of Nanowire-Based FET Devices. *Nano Lett.* **2012**, *12* (10), 5245–5254. https://doi.org/10.1021/nl302434w.

(30) Ronkainen, N. J.; Halsall, H. B.; Heineman, W. R. Electrochemical Biosensors. *Chem. Soc. Rev.* **2010**, *39* (5), 1747. https://doi.org/10.1039/b714449k.

(31) Zang, Y.; Lei, J.; Hao, Q.; Ju, H. "Signal-On" Photoelectrochemical Sensing Strategy Based on Target-Dependent Aptamer Conformational Conversion for Selective Detection of Lead(II) Ion. *ACS Appl. Mater. Interfaces* **2014**, *6* (18), 15991–15997. https://doi.org/10.1021/am503804g.

(32) Fan, G.-C.; Zhu, H.; Shen, Q.; Han, L.; Zhao, M.; Zhang, J.-R.; Zhu, J.-J. Enhanced Photoelectrochemical Aptasensing Platform Based on Exciton Energy Transfer between CdSeTe Alloyed Quantum Dots and SiO_2 @Au Nanocomposites. *Chem. Commun.* **2015**, *51* (32), 7023–7026. https://doi.org/10.1039/C5CC01935D.

(33) Bevers, S.; Schutte, S.; McLaughlin, L. W. Naphthalene- and Perylene-Based Linkers for the Stabilization of Hairpin Triplexes. *J. Am. Chem. Soc.* **2000**, *122* (25), 5905–5915. https://doi.org/10.1021/ja0001714.

(34) Furst, A. L.; Muren, N. B.; Hill, M. G.; Barton, J. K. Label-Free Electrochemical Detection of Human Methyltransferase from Tumors. *PNAS* **2014**, *111* (42), 14985–14989. https://doi.org/10.1073/pnas.1417351111.

(35) O'Brien, E.; Holt, M. E.; Thompson, M. K.; Salay, L. E.; Ehlinger, A. C.; Chazin, W. J.; Barton, J. K. The [4Fe4S] Cluster of Human DNA Primase Functions as a Redox Switch Using DNA Charge Transport. *Science* **2017**, *355* (6327), eaag1789. https://doi.org/10.1126/science.aag1789.

(36) Slinker, J. D.; Muren, N. B.; Gorodetsky, A. A.; Barton, J. K. Multiplexed DNA-Modified Electrodes. *J. Am. Chem. Soc.* **2010**, *132* (8), 2769–2774. https://doi.org/10.1021/ja909915m.

(37) Hao, Z.; Pan, Y.; Shao, W.; Lin, Q.; Zhao, X. Graphene-Based Fully Integrated Portable Nanosensing System for on-Line Detection of Cytokine Biomarkers in Saliva. *Biosensors and Bioelectronics* **2019**, *134*, 16–23. https://doi.org/10.1016/j.bios.2019.03.053.

(38) Kim, Y.-H.; Lee, K.; Jung, H.; Kang, H. K.; Jo, J.; Park, I.-K.; Lee, H. H. Direct Immune-Detection of Cortisol by Chemiresistor Graphene Oxide Sensor. *Biosensors and Bioelectronics* **2017**, *98*, 473–477. https://doi.org/10.1016/j.bios.2017.07.017.

(39) Torrente-Rodríguez, R. M.; Campuzano, S.; Ruiz-Valdepeñas Montiel, V.; Gamella, M.; Pingarrón, J. M. Electrochemical Bioplatforms for the Simultaneous Determination of Interleukin (IL)-8 MRNA and IL-8 Protein Oral Cancer Biomarkers in Raw Saliva. *Biosensors and Bioelectronics* **2016**, *77*, 543–548. https://doi.org/10.1016/j.bios.2015.10.016.

(40) Yildiz, H. B.; Freeman, R.; Gill, R.; Willner, I. Electrochemical, Photoelectrochemical, and Piezoelectric Analysis of Tyrosinase Activity by Functionalized Nanoparticles. *Anal. Chem.* **2008**, *80* (8), 2811–2816. https://doi.org/10.1021/ac702401v.

(41) Sivula, K.; van de Krol, R. Semiconducting Materials for Photoelectrochemical Energy Conversion. *Nat Rev Mater* **2016**, *1* (2), 15010. https://doi.org/10.1038/natrevmats.2015.10.

(42) Wang, G.-L.; Liu, K.-L.; Dong, Y.-M.; Wu, X.-M.; Li, Z.-J.; Zhang, C. A New Approach to Light up the Application of Semiconductor Nanomaterials for Photoelectrochemical Biosensors: Using Self-Operating Photocathode as a Highly Selective Enzyme Sensor. *Biosensors and Bioelectronics* **2014**, *62*, 66–72. https://doi.org/10.1016/j.bios.2014.06.033.

(43) Bard, A. J. Photoelectrochemistry. *Science* **1980**, *207* (4427), 139–144. https://doi.org/10.1126/science.207.4427.139.

(44) Han, Q.; Wang, R.; Xing, B.; Zhang, T.; Khan, M. S.; Wu, D.; Wei, Q. Label-Free Photoelectrochemical Immunoassay for CEA Detection Based on CdS Sensitized WO3@BiOI Heterostructure Nanocomposite. *Biosensors and Bioelectronics* **2018**, *99*, 493–499. https://doi.org/10.1016/j.bios.2017.08.034.

(45) Fan, G.-C.; Shi, X.-M.; Zhang, J.-R.; Zhu, J.-J. Cathode Photoelectrochemical Immunosensing Platform Integrating Photocathode with Photoanode. *Anal. Chem.* **2016**, *88* (21), 10352–10356.

(46) Pardo-Yissar, V.; Katz, E.; Wasserman, J.; Willner, I. Acetylcholine Esterase-Labeled CdS Nanoparticles on Electrodes: Photoelectrochemical Sensing of the Enzyme Inhibitors. *J. Am. Chem. Soc.* **2003**, *125* (3), 622–623. https://doi.org/10.1021/ja028922k.

(47) Zhao, W.-W.; Ma, Z.-Y.; Yu, P.-P.; Dong, X.-Y.; Xu, J.-J.; Chen, H.-Y. Highly Sensitive Photoelectrochemical Immunoassay with Enhanced Amplification Using Horseradish Peroxidase Induced Biocatalytic Precipitation on a CdS Quantum Dots Multilayer Electrode. *Anal. Chem.* **2012**, *84* (2), 917–923. https://doi.org/10.1021/ac203184g.

(48) Victorious, A.; Saha, S.; Pandey, R.; Didar, T. F.; Soleymani, L. Affinity-Based Detection of Biomolecules Using Photo-Electrochemical Readout. *Front. Chem.* **2019**, *7*, 617. https://doi.org/10.3389/fchem.2019.00617.

(49) Arnold, A. R.; Zhou, A.; Barton, J. K. Characterization of the DNA-Mediated Oxidation of Dps, A Bacterial Ferritin. *J. Am. Chem. Soc.* **2016**, *138* (35), 11290–11298. https://doi.org/10.1021/jacs.6b06507.

(50) Chen, X.; Dong, T.; Wei, X.; Yang, Z.; Matos Pires, N. M.; Ren, J.; Jiang, Z. Electrochemical Methods for Detection of Biomarkers of Chronic Obstructive Pulmonary Disease in Serum and Saliva. *Biosensors and Bioelectronics* **2019**, *142*, 111453. https://doi.org/10.1016/j.bios.2019.111453.

(51) Bafadhel, M.; McKenna, S.; Terry, S.; Mistry, V.; Reid, C.; Haldar, P.; McCormick, M.; Haldar, K.; Kebadze, T.; Duvoix, A.; Lindblad, K.; Patel, H.; Rugman, P.; Dodson, P.; Jenkins, M.; Saunders, M.; Newbold, P.; Green, R. H.; Venge, P.; Lomas, D. A.; Barer, M. R.; Johnston, S. L.; Pavord, I. D.; Brightling, C. E. Acute Exacerbations of Chronic Obstructive Pulmonary Disease. *Am J Respir Crit Care Med* **2011**, *184* (6), 662–671. https://doi.org/10.1164/rccm.201104-0597OC.

(52) Wei, Y.; Wang, S.; Wang, D.; Liu, C. Expression and Clinical Significance of Serum Amyloid A and Interleukin‐6 in Patients with Acute Exacerbation of Chronic Obstructive Pulmonary Disease. *Experimental and Therapeutic Medicine* **2020**, *19* (3), 2089–2094. https://doi.org/10.3892/etm.2019.8366.

(53) Zhang, J.; Bai, C. The Significance of Serum Interleukin-8 in Acute Exacerbations of Chronic Obstructive Pulmonary Disease. *Tanaffos* **2018**, *17* (1), 13–21.

(54) Butler, C. C.; Gillespie, D.; White, P.; Bates, J.; Lowe, R.; Thomas-Jones, E.; Wootton, M.; Hood, K.; Phillips, R.; Melbye, H.; Llor, C.; Cals, J. W. L.; Naik, G.; Kirby, N.; Gal, M.; Riga, E.; Francis, N. A. C-Reactive Protein Testing to Guide Antibiotic Prescribing for COPD Exacerbations. *N Engl J Med* **2019**, *381* (2), 111–120. https://doi.org/10.1056/NEJMoa1803185.

(55) Agusti, A.; Faner, R.; Celli, B.; Rodriguez-Roisin, R. Precision Medicine in COPD Exacerbations. *The Lancet Respiratory Medicine* **2018**, *6* (9), 657–659. https://doi.org/10.1016/S2213-2600(18)30296-0.

(56) Patel, N.; Belcher, J.; Thorpe, G.; Forsyth, N. R.; Spiteri, M. A. Measurement of C-Reactive Protein, Procalcitonin and Neutrophil Elastase in Saliva of COPD Patients and Healthy Controls: Correlation to Self-Reported Wellbeing Parameters. *Respir Res* **2015**, *16* (1), 62. https://doi.org/10.1186/s12931-015-0219-1.

(57) Bircan, A.; Gokirmak, M.; Kilic, O.; Ozturk, O.; Akkaya, A. C-Reactive Protein Levels in Patients with Chronic Obstructive Pulmonary Disease: Role of Infection. *Med Princ Pract* **2008**, *17* (3), 202–208. https://doi.org/10.1159/000117793.

(58) Daniels, J. M. A.; Schoorl, M.; Snijders, D.; Knol, D. L.; Lutter, R.; Jansen, H. M.; Boersma, W. G. Procalcitonin vs C-Reactive Protein as Predictive Markers of Response to Antibiotic Therapy in Acute Exacerbations of COPD. *Chest* **2010**, *138* (5), 1108–1115. https://doi.org/10.1378/chest.09-2927.

(59) Bchir, S.; Nasr, H. ben; Bouchet, S.; Benzarti, M.; Garrouch, A.; Tabka, Z.; Susin, S.; Chahed, K.; Bauvois, B. Concomitant Elevations of MMP-9, NGAL, ProMMP-9/NGAL and Neutrophil Elastase in Serum of Smokers with Chronic Obstructive Pulmonary Disease. *Journal of Cellular and Molecular Medicine* **2017**, *21* (7), 1280–1291. https://doi.org/10.1111/jcmm.13057.

(60) Malo, O.; Sauleda, J.; Busquets, X.; Miralles, C.; Agustí, A. G. N.; Noguera, A. Systemic inflammation during exacerbations of chronic obstructive pulmonary disease. *Arch Bronconeumol* **2002**, *38* (4), 172–176.

(61) Land, K. J.; Boeras, D. I.; Chen, X.-S.; Ramsay, A. R.; Peeling, R. W. REASSURED Diagnostics to Inform Disease Control Strategies, Strengthen Health Systems and Improve Patient Outcomes. *Nat Microbiol* **2019**, *4* (1), 46–54. https://doi.org/10.1038/s41564-018-0295-3.

(62) Liu, G.-S.; Kong, Y.; Wang, Y.; Luo, Y.; Fan, X.; Xie, X.; Yang, B.-R.; Wu, M. X. Microneedles for Transdermal Diagnostics: Recent Advances and New Horizons. *Biomaterials* **2020**, *232*, 119740. https://doi.org/10.1016/j.biomaterials.2019.119740.

(63) Xue, P.; Zhang, L.; Xu, Z.; Yan, J.; Gu, Z.; Kang, Y. Blood Sampling Using Microneedles as a Minimally Invasive Platform for Biomedical Diagnostics. *Applied Materials Today* **2018**, *13*, 144–157. https://doi.org/10.1016/j.apmt.2018.08.013.

(64) Kim, Y.-C.; Park, J.-H.; Prausnitz, M. R. Microneedles for Drug and Vaccine Delivery. *Advanced Drug Delivery Reviews* **2012**, *64* (14), 1547–1568. https://doi.org/10.1016/j.addr.2012.04.005.

(65) Li, T.; Barnett, A.; L. Rogers, K.; B. Gianchandani, Y. A Blood Sampling Microsystem for Pharmacokinetic Applications: Design, Fabrication, and Initial Results. *Lab on a Chip* **2009**, *9* (24), 3495–3503. https://doi.org/10.1039/B910508E.

(66) Li, C. G.; Lee, K.; Lee, C. Y.; Dangol, M.; Jung, H. A Minimally Invasive Blood-Extraction System: Elastic Self-Recovery Actuator Integrated with an Ultrahigh- Aspect-Ratio Microneedle. *Advanced Materials* **2012**, *24* (33), 4583–4586. https://doi.org/10.1002/adma.201201109.

(67) Lee, D.-S.; Li, C. G.; Ihm, C.; Jung, H. A Three-Dimensional and Bevel-Angled Ultrahigh Aspect Ratio Microneedle for Minimally Invasive and Painless Blood Sampling. *Sensors and Actuators B: Chemical* **2018**, *255*, 384–390. https://doi.org/10.1016/j.snb.2017.08.030.

(68) Tsuchiya, K.; Nakanishi, N.; Uetsuji, Y.; Nakamachi, E. Development of Blood Extraction System for Health Monitoring System. *Biomed Microdevices* **2005**, *7* (4), 347–353. https://doi.org/10.1007/s10544-005-6077-8.

(69) Chaudhri, B. P.; Ceyssens, F.; Moor, P. D.; Hoof, C. V.; Puers, R. A High Aspect Ratio SU-8 Fabrication Technique for Hollow Microneedles for Transdermal Drug Delivery and Blood Extraction. *J. Micromech. Microeng.* **2010**, *20* (6), 064006. https://doi.org/10.1088/0960-1317/20/6/064006.

(70) Pérennès, F.; Marmiroli, B.; Matteucci, M.; Tormen, M.; Vaccari, L.; Fabrizio, E. D. Sharp Beveled Tip Hollow Microneedle Arrays Fabricated by LIGA and 3D Soft Lithography with Polyvinyl Alcohol. *J. Micromech. Microeng.* **2006**, *16* (3), 473–479. https://doi.org/10.1088/0960-1317/16/3/001.

(71) Izumi, H.; Yajima, T.; Aoyagi, S.; Tagawa, N.; Arai, Y.; Hirata, M.; Yorifuji, S. Combined Harpoonlike Jagged Microneedles Imitating Mosquito's Proboscis and Its Insertion Experiment with Vibration. *IEEJ Transactions on Electrical and Electronic Engineering* **2008**, *3* (4), 425–431. https://doi.org/10.1002/tee.20295.

(72) Aoyagi, S.; Izumi, H.; Fukuda, M. Biodegradable Polymer Needle with Various Tip Angles and Consideration on Insertion Mechanism of Mosquito's Proboscis. *Sensors and Actuators A: Physical* **2008**, *143* (1), 20–28. https://doi.org/10.1016/j.sna.2007.06.007.

(73) Blicharz, T. M.; Gong, P.; Bunner, B. M.; Chu, L. L.; Leonard, K. M.; Wakefield, J. A.; Williams, R. E.; Dadgar, M.; Tagliabue, C. A.; El Khaja, R.; Marlin, S. L.; Haghgooie, R.; Davis, S. P.; Chickering, D. E.; Bernstein, H. Microneedle-Based Device for the One-Step Painless Collection of Capillary Blood Samples. *Nat Biomed Eng* **2018**, *2* (3), 151–157. https://doi.org/10.1038/s41551-018-0194-1.

(74) Navazesh, M.; Kumar, S. K. S. Measuring Salivary Flow: Challenges and Opportunities. *The Journal of the American Dental Association* **2008**, *139*, 35S-40S. https://doi.org/10.14219/jada.archive.2008.0353.

(75) Denny, P.; Hagen, F. K.; Hardt, M.; Liao, L.; Yan, W.; Arellanno, M.; Bassilian, S.; Bedi, G. S.; Boontheung, P.; Cociorva, D.; Delahunty, C. M.; Denny, T.; Dunsmore, J.; Faull, K. F.; Gilligan, J.; Gonzalez-Begne, M.; Halgand, F.; Hall, S. C.; Han, X.; Henson, B.; Hewel, J.; Hu, S.; Jeffrey, S.; Jiang, J.; Loo, J. A.; Ogorzalek Loo, R. R.; Malamud, D.; Melvin, J. E.; Miroshnychenko, O.; Navazesh, M.; Niles, R.; Park, S. K.; Prakobphol, A.; Ramachandran, P.; Richert, M.; Robinson, S.; Sondej, M.; Souda, P.; Sullivan, M. A.; Takashima, J.; Than, S.; Wang, J.; Whitelegge, J. P.; Witkowska, H. E.; Wolinsky, L.; Xie, Y.; Xu, T.; Yu, W.; Ytterberg, J.; Wong, D. T.; Yates, J. R.; Fisher, S. J. The Proteomes of Human Parotid and Submandibular/Sublingual Gland Salivas Collected as the Ductal Secretions. *J. Proteome Res.* **2008**, *7* (5), 1994–2006. https://doi.org/10.1021/pr700764j.

(76) Porcheri, C.; Mitsiadis, T. A. Physiology, Pathology and Regeneration of Salivary Glands. *Cells* **2019**, *8* (9), 976. https://doi.org/10.3390/cells8090976.
(77) Humphrey, S. P.; Williamson, R. T. A Review of Saliva: Normal Composition, Flow, and Function. *The Journal of Prosthetic Dentistry* **2001**, *85* (2), 162–169. https://doi.org/10.1067/mpr.2001.113778.
(78) Soares Nunes, L. A.; Mussavira, S.; Sukumaran Bindhu, O. Clinical and Diagnostic Utility of Saliva as a Non-Invasive Diagnostic Fluid: A Systematic Review. *Biochemia Medica* **2015**, *25* (2), 177–192. https://doi.org/10.11613/BM.2015.018.
(79) Shannon, I. L.; Prigmore, J. R.; Chauncey, H. H. Modified Carlson-Crittenden Device for the Collection of Parotid Fluid. *J Dent Res* **1962**, *41* (4), 778–783. https://doi.org/10.1177/00220345620410040801.
(80) Stephen, K. W.; Speirs, C. F. Methods for Collecting Individual Components of Mixed Saliva: The Relevance to Clinical Pharmacology. *British Journal of Clinical Pharmacology* **1976**, *3* (2), 315–319. https://doi.org/10.1111/j.1365-2125.1976.tb00609.x.
(81) Johnson, D. A.; Yeh, C.-K.; Dodds, M. W. J. Effect of Donor Age on the Concentrations of Histatins in Human Parotid and Submandibular/Sublingual Saliva. *Archives of Oral Biology* **2000**, *45* (9), 731–740. https://doi.org/10.1016/S0003-9969(00)00047-9.
(82) Schneyer, L. H. Method for the Collection of Separate Submaxillary and Sublingual Salivas in Man. *J Dent Res* **1955**, *34* (2), 257–261. https://doi.org/10.1177/00220345550340021301.
(83) Bellagambi, F. G.; Lomonaco, T.; Salvo, P.; Vivaldi, F.; Hangouët, M.; Ghimenti, S.; Biagini, D.; Di Francesco, F.; Fuoco, R.; Errachid, A. Saliva Sampling: Methods and Devices. An Overview. *TrAC Trends in Analytical Chemistry* **2020**, *124*, 115781. https://doi.org/10.1016/j.trac.2019.115781.
(84) Soni, A.; Surana, R. K.; Jha, S. K. Smartphone Based Optical Biosensor for the Detection of Urea in Saliva. *Sensors and Actuators B: Chemical* **2018**, *269*, 346–353. https://doi.org/10.1016/j.snb.2018.04.108.
(85) Bellagambi, F. G.; Baraket, A.; Longo, A.; Vatteroni, M.; Zine, N.; Bausells, J.; Fuoco, R.; Di Francesco, F.; Salvo, P.; Karanasiou, G. S.; Fotiadis, D. I.; Menciassi, A.; Errachid, A. Electrochemical Biosensor Platform for TNF-α Cytokines Detection in Both Artificial and Human Saliva: Heart Failure. *Sensors and Actuators B: Chemical* **2017**, *251*, 1026–1033. https://doi.org/10.1016/j.snb.2017.05.169.
(86) dos Santos, W. T. P.; Compton, R. G. A Simple Method to Detect the Stimulant Modafinil in Authentic Saliva Using a Carbon-Nanotube Screen-Printed Electrode with Adsorptive Stripping Voltammetry. *Sensors and Actuators B: Chemical* **2019**, *285*, 137–144. https://doi.org/10.1016/j.snb.2019.01.047.
(87) Sánchez-Tirado, E.; Salvo, C.; González-Cortés, A.; Yáñez-Sedeño, P.; Langa, F.; Pingarrón, J. M. Electrochemical Immunosensor for Simultaneous Determination of Interleukin-1 Beta and Tumor Necrosis Factor Alpha in Serum and Saliva Using Dual Screen Printed Electrodes Modified with Functionalized Double–Walled Carbon Nanotubes. *Analytica Chimica Acta* **2017**, *959*, 66–73. https://doi.org/10.1016/j.aca.2016.12.034.
(88) Verma, S.; Singh, A.; Shukla, A.; Kaswan, J.; Arora, K.; Ramirez-Vick, J.; Singh, P.; Singh, S. P. Anti-IL8/AuNPs-RGO/ITO as an Immunosensing Platform for Noninvasive

Electrochemical Detection of Oral Cancer. *ACS Appl. Mater. Interfaces* **2017**, *9* (33), 27462–27474. https://doi.org/10.1021/acsami.7b06839.

(89) Joshi, S. R.; Sharma, A.; Kim, G.-H.; Jang, J. Low Cost Synthesis of Reduced Graphene Oxide Using Biopolymer for Influenza Virus Sensor. *Materials Science and Engineering: C* **2020**, *108*, 110465. https://doi.org/10.1016/j.msec.2019.110465.

(90) Manickam, P.; Fernandez, R. E.; Umasankar, Y.; Gurusamy, M.; Arizaleta, F.; Urizar, G.; Bhansali, S. Salivary Cortisol Analysis Using Metalloporphyrins and Multi-Walled Carbon Nanotubes Nanocomposite Functionalized Electrodes. *Sensors and Actuators B: Chemical* **2018**, *274*, 47–53. https://doi.org/10.1016/j.snb.2018.07.133.

(91) Sajid, M.; Kawde, A.-N.; Daud, M. Designs, Formats and Applications of Lateral Flow Assay: A Literature Review. *Journal of Saudi Chemical Society* **2015**, *19* (6), 689–705. https://doi.org/10.1016/j.jscs.2014.09.001.

(92) Mak, W. C.; Beni, V.; Turner, A. P. F. Lateral-Flow Technology: From Visual to Instrumental. *TrAC Trends in Analytical Chemistry* **2016**, *79*, 297–305. https://doi.org/10.1016/j.trac.2015.10.017.

(93) Hollander, Z.; DeMarco, M. L.; Sadatsafavi, M.; McManus, B. M.; Ng, R. T.; Sin, D. D. Biomarker Development in COPD. *Chest* **2017**, *151* (2), 455–467. https://doi.org/10.1016/j.chest.2016.09.012.

(94) Murphy, C. J.; Gole, A. M.; Stone, J. W.; Sisco, P. N.; Alkilany, A. M.; Goldsmith, E. C.; Baxter, S. C. Gold Nanoparticles in Biology: Beyond Toxicity to Cellular Imaging. *Acc. Chem. Res.* **2008**, *41* (12), 1721–1730. https://doi.org/10.1021/ar800035u.

(95) Hutter, E.; Fendler, J. H. Exploitation of Localized Surface Plasmon Resonance. *Advanced Materials* **2004**, *16* (19), 1685–1706. https://doi.org/10.1002/adma.200400271.

(96) Ge, C.; Yu, L.; Fang, Z.; Zeng, L. An Enhanced Strip Biosensor for Rapid and Sensitive Detection of Histone Methylation. *Anal. Chem.* **2013**, *85* (19), 9343–9349. https://doi.org/10.1021/ac402202x.

(97) Ahn, J. S.; Choi, S.; Jang, S. H.; Chang, H. J.; Kim, J. H.; Nahm, K. B.; Oh, S. W.; Choi, E. Y. Development of a Point-of-Care Assay System for High-Sensitivity C-Reactive Protein in Whole Blood. *Clinica Chimica Acta* **2003**, *332* (1), 51–59. https://doi.org/10.1016/S0009-8981(03)00113-X.

(98) Oh, Y. K.; Joung, H.-A.; Han, H. S.; Suk, H.-J.; Kim, M.-G. A Three-Line Lateral Flow Assay Strip for the Measurement of C-Reactive Protein Covering a Broad Physiological Concentration Range in Human Sera. *Biosensors and Bioelectronics* **2014**, *61*, 285–289. https://doi.org/10.1016/j.bios.2014.04.032.

(99) Hu, J.; Zhang, Z.-L.; Wen, C.-Y.; Tang, M.; Wu, L.-L.; Liu, C.; Zhu, L.; Pang, D.-W. Sensitive and Quantitative Detection of C-Reaction Protein Based on Immunofluorescent Nanospheres Coupled with Lateral Flow Test Strip. *Anal. Chem.* **2016**, *88* (12), 6577–6584. https://doi.org/10.1021/acs.analchem.6b01427.

(100) Li, Z.; Wang, Y.; Wang, J.; Tang, Z.; Pounds, J. G.; Lin, Y. Rapid and Sensitive Detection of Protein Biomarker Using a Portable Fluorescence Biosensor Based on Quantum Dots and a Lateral Flow Test Strip. *Anal. Chem.* **2010**, *82* (16), 7008–7014. https://doi.org/10.1021/ac101405a.

(101) Liu, X.; Yang, X.; Li, K.; Liu, H.; Xiao, R.; Wang, W.; Wang, C.; Wang, S. Fe3O4@Au SERS Tags-Based Lateral Flow Assay for Simultaneous Detection of Serum Amyloid A and C-

Reactive Protein in Unprocessed Blood Sample. *Sensors and Actuators B: Chemical* **2020**, *320*, 128350. https://doi.org/10.1016/j.snb.2020.128350.

(102) Rey, E. G.; O'Dell, D.; Mehta, S.; Erickson, D. Mitigating the Hook Effect in Lateral Flow Sandwich Immunoassays Using Real-Time Reaction Kinetics. *Anal. Chem.* **2017**, *89* (9), 5095–5100. https://doi.org/10.1021/acs.analchem.7b00638.

(103) Wu, R.; Zhou, S.; Chen, T.; Li, J.; Shen, H.; Chai, Y.; Li, L. S. Quantitative and Rapid Detection of C-Reactive Protein Using Quantum Dot-Based Lateral Flow Test Strip. *Analytica Chimica Acta* **2018**, *1008*, 1–7. https://doi.org/10.1016/j.aca.2017.12.031.

(104) Qi, X.; Huang, Y.; Lin, Z.; Xu, L.; Yu, H. Dual-Quantum-Dots-Labeled Lateral Flow Strip Rapidly Quantifies Procalcitonin and C-Reactive Protein. *Nanoscale Research Letters* **2016**, *11* (1), 167. https://doi.org/10.1186/s11671-016-1383-z.

(105) Taranova, N. A.; Urusov, A. E.; Sadykhov, E. G.; Zherdev, A. V.; Dzantiev, B. B. Bifunctional Gold Nanoparticles as an Agglomeration-Enhancing Tool for Highly Sensitive Lateral Flow Tests: A Case Study with Procalcitonin. *Microchim Acta* **2017**, *184* (10), 4189–4195. https://doi.org/10.1007/s00604-017-2355-4.

(106) Huang, D.; Ying, H.; Jiang, D.; Liu, F.; Tian, Y.; Du, C.; Zhang, L.; Pu, X. Rapid and Sensitive Detection of Interleukin-6 in Serum via Time-Resolved Lateral Flow Immunoassay. *Analytical Biochemistry* **2020**, *588*, 113468. https://doi.org/10.1016/j.ab.2019.113468.

(107) Yee, E. H.; Lathwal, S.; Shah, P. P.; Sikes, H. D. Detection of Biomarkers of Periodontal Disease in Human Saliva Using Stabilized, Vertical Flow Immunoassays. *ACS Sens.* **2017**, *2* (11), 1589–1593. https://doi.org/10.1021/acssensors.7b00745.

(108) Verma, M. S.; Tsaloglou, M.-N.; Sisley, T.; Christodouleas, D.; Chen, A.; Milette, J.; Whitesides, G. M. Sliding-Strip Microfluidic Device Enables ELISA on Paper. *Biosensors and Bioelectronics* **2018**, *99*, 77–84. https://doi.org/10.1016/j.bios.2017.07.034.

(109) Hu, J.; Choi, J. R.; Wang, S.; Gong, Y.; Feng, S.; Pingguan-Murphy, B.; Lu, T. J.; Xu, F. Multiple Test Zones for Improved Detection Performance in Lateral Flow Assays. *Sensors and Actuators B: Chemical* **2017**, *243*, 484–488. https://doi.org/10.1016/j.snb.2016.12.008.

(110) Gao, Y.; Zhu, Z.; Xi, X.; Cao, T.; Wen, W.; Zhang, X.; Wang, S. An Aptamer-Based Hook-Effect-Recognizable Three-Line Lateral Flow Biosensor for Rapid Detection of Thrombin. *Biosensors and Bioelectronics* **2019**, *133*, 177–182. https://doi.org/10.1016/j.bios.2019.03.036.

(111) Sathishkumar, N.; Toley, B. J. Development of an Experimental Method to Overcome the Hook Effect in Sandwich-Type Lateral Flow Immunoassays Guided by Computational Modelling. *Sensors and Actuators B: Chemical* **2020**, *324*, 128756. https://doi.org/10.1016/j.snb.2020.128756.

(112) Ross, G. M. S.; Filippini, D.; Nielen, M. W. F.; Salentijn, G. IJ. Unraveling the Hook Effect: A Comprehensive Study of High Antigen Concentration Effects in Sandwich Lateral Flow Immunoassays. *Anal. Chem.* **2020**, *92* (23), 15587–15595. https://doi.org/10.1021/acs.analchem.0c03740.

(113) Winder, A. D.; Mora, A. S.; Berry, E.; Lurain, J. R. The "Hook Effect" Causing a Negative Pregnancy Test in a Patient with an Advanced Molar Pregnancy. *Gynecologic Oncology Reports* **2017**, *21*, 34–36. https://doi.org/10.1016/j.gore.2017.06.008.

(114) Yeung, C.-W.; Cheung, A. N. Y. Negative Pregnancy Test in Patients with Trophoblastic Diseases. *Curr Obstet Gynecol Rep* **2014**, *3* (1), 102–106. https://doi.org/10.1007/s13669-013-0067-2.
(115) Póvoa, P.; Almeida, E.; Moreira, P.; Fernandes, A.; Mealha, R.; Aragão, A.; Sabino, H. C-Reactive Protein as an Indicator of Sepsis. *Intensive Care Med* **1998**, *24* (10), 1052–1056. https://doi.org/10.1007/s001340050715.
(116) Miles, L. E. M.; Lipschitz, D. A.; Bieber, C. P.; Cook, J. D. Measurement of Serum Ferritin by a 2-Site Immunoradiometric Assay. *Analytical Biochemistry* **1974**, *61* (1), 209–224. https://doi.org/10.1016/0003-2697(74)90347-9.
(117) Vaidya, H. C.; Wolf, B. A.; Garrett, N.; Catalona, W. J.; Clayman, R. V.; Nahm, M. H. Extremely High Values of Prostate-Specific Antigen in Patients with Adenocarcinoma of the Prostate; Demonstration of the "Hook Effect". *Clinical Chemistry* **1988**, *34* (10), 2175–2177. https://doi.org/10.1093/clinchem/34.10.2175.
(118) Ryall, R. G.; Story, C. J.; Turner, D. R. Reappraisal of the Causes of the "Hook Effect" in Two-Site Immunoradiometric Assays. *Analytical Biochemistry* **1982**, *127* (2), 308–315. https://doi.org/10.1016/0003-2697(82)90178-6.
(119) Lutz, B.; Liang, T.; Fu, E.; Ramachandran, S.; Kauffman, P.; Yager, P. Dissolvable Fluidic Time Delays for Programming Multi-Step Assays in Instrument-Free Paper Diagnostics. *Lab on a Chip* **2013**, *13* (14), 2840–2847. https://doi.org/10.1039/C3LC50178G.
(120) M. Whitesides, G. Viewpoint on "Dissolvable Fluidic Time Delays for Programming Multi-Step Assays in Instrument-Free Paper Diagnostics." *Lab on a Chip* **2013**, *13* (20), 4004–4005. https://doi.org/10.1039/C3LC90066E.
(121) Schreiber, G.; Haran, G.; Zhou, H.-X. Fundamental Aspects of Protein−protein Association Kinetics. *Chem. Rev.* **2009**, *109* (3), 839–860. https://doi.org/10.1021/cr800373w.
(122) Liang, T.; Robinson, R.; Houghtaling, J.; Fridley, G.; Ramsey, S. A.; Fu, E. Investigation of Reagent Delivery Formats in a Multivalent Malaria Sandwich Immunoassay and Implications for Assay Performance. *Anal. Chem.* **2016**, *88* (4), 2311–2320. https://doi.org/10.1021/acs.analchem.5b04222.
(123) Josephy, P. D.; Eling, T.; Mason, R. P. The Horseradish Peroxidase-Catalyzed Oxidation of 3,5,3',5'-Tetramethylbenzidine. Free Radical and Charge-Transfer Complex Intermediates. *J. Biol. Chem.* **1982**, *257* (7), 3669–3675.
(124) Lee, G.-Y.; Park, J.-H.; Chang, Y. W.; Cho, S.; Kang, M.-J.; Pyun, J.-C. Chronoamperometry-Based Redox Cycling for Application to Immunoassays. *ACS Sens.* **2018**, *3* (1), 106–112. https://doi.org/10.1021/acssensors.7b00681.
(125) Sinawang, P. D.; Rai, V.; Ionescu, R. E.; Marks, R. S. Electrochemical Lateral Flow Immunosensor for Detection and Quantification of Dengue NS1 Protein. *Biosensors and Bioelectronics* **2016**, *77*, 400–408. https://doi.org/10.1016/j.bios.2015.09.048.
(126) Renault, C.; Anderson, M. J.; Crooks, R. M. Electrochemistry in Hollow-Channel Paper Analytical Devices. *J. Am. Chem. Soc.* **2014**, *136* (12), 4616–4623. https://doi.org/10.1021/ja4118544.
(127) Glavan, A. C.; Christodouleas, D. C.; Mosadegh, B.; Yu, H. D.; Smith, B. S.; Lessing, J.; Fernández-Abedul, M. T.; Whitesides, G. M. Folding Analytical Devices for Electrochemical ELISA in Hydrophobic RH Paper. *Anal. Chem.* **2014**, *86* (24), 11999–12007. https://doi.org/10.1021/ac5020782.

(128) Gasperino, D.; Baughman, T.; Hsieh, H. V.; Bell, D.; Weigl, B. H. Improving Lateral Flow Assay Performance Using Computational Modeling. *Annual Rev. Anal. Chem.* **2018**, *11* (1), 219–244. https://doi.org/10.1146/annurev-anchem-061417-125737.
(129) He, G.; Dong, T.; Yang, Z.; Branstad, A.; Huang, L.; Jiang, Z. Point-of-Care COPD Diagnostics: Biomarkers, Sampling, Paper-Based Analytical Devices, and Perspectives. *Analyst* **2022**. https://doi.org/10.1039/D1AN01702K.
(130) He, G.; Dong, T.; Yang, Z.; Jiang, Z. Mitigating Hook Effect in One-Step Quantitative Sandwich Lateral Flow Assay by Timed Conjugate Release. *Talanta* **2022**, *240*, 123157. https://doi.org/10.1016/j.talanta.2021.123157.
(131) Jaffer, I. H.; Weitz, J. I. The Blood Compatibility Challenge. Part 1: Blood-Contacting Medical Devices: The Scope of the Problem. *Acta Biomaterialia* **2019**, *94*, 2–10. https://doi.org/10.1016/j.actbio.2019.06.021.
(132) Vogler, E. A. Protein Adsorption in Three Dimensions. *Biomaterials* **2012**, *33* (5), 1201–1237. https://doi.org/10.1016/j.biomaterials.2011.10.059.
(133) Brash, J. L.; Horbett, T. A.; Latour, R. A.; Tengvall, P. The Blood Compatibility Challenge. Part 2: Protein Adsorption Phenomena Governing Blood Reactivity. *Acta Biomaterialia* **2019**, *94*, 11–24. https://doi.org/10.1016/j.actbio.2019.06.022.
(134) Wilson, C. J.; Clegg, R. E.; Leavesley, D. I.; Pearcy, M. J. Mediation of Biomaterial–Cell Interactions by Adsorbed Proteins: A Review. *Tissue Engineering* **2005**, *11* (1–2), 1–18. https://doi.org/10.1089/ten.2005.11.1.
(135) Gorbet, M.; Sperling, C.; Maitz, M. F.; Siedlecki, C. A.; Werner, C.; Sefton, M. V. The Blood Compatibility Challenge. Part 3: Material Associated Activation of Blood Cascades and Cells. *Acta Biomaterialia* **2019**, *94*, 25–32. https://doi.org/10.1016/j.actbio.2019.06.020.
(136) *Proteins at Interfaces III State of the Art 2012*; Horbett, T., Brash, J. L., Norde, W., Eds.; American Chemical Society, Series Ed.; ACS Symposium Series; American Chemical Society: Washington, DC, 2012; Vol. 1120. https://doi.org/10.1021/bk-2012-1120.
(137) Gooding, J. J. Finally, a Simple Solution to Biofouling. *Nat. Nanotechnol.* **2019**, *14* (12), 1089–1090. https://doi.org/10.1038/s41565-019-0573-0.
(138) Ostuni, E.; Chapman, R. G.; Holmlin, R. E.; Takayama, S.; Whitesides, G. M. A Survey of Structure−Property Relationships of Surfaces That Resist the Adsorption of Protein. *Langmuir* **2001**, *17* (18), 5605–5620. https://doi.org/10.1021/la010384m.
(139) Hirsh, J. Oral Anticoagulant Drugs. *New England Journal of Medicine* **1991**, *324* (26), 1865–1875. https://doi.org/10.1056/NEJM199106273242606.
(140) Holmes, D. R.; Kereiakes, D. J.; Garg, S.; Serruys, P. W.; Dehmer, G. J.; Ellis, S. G.; Williams, D. O.; Kimura, T.; Moliterno, D. J. Stent Thrombosis. *Journal of the American College of Cardiology* **2010**, *56* (17), 1357–1365. https://doi.org/10.1016/j.jacc.2010.07.016.
(141) Barfidokht, A.; Gooding, J. J. Approaches Toward Allowing Electroanalytical Devices to Be Used in Biological Fluids. *Electroanalysis* **2014**, *26* (6), 1182–1196. https://doi.org/10.1002/elan.201400097.
(142) Arroyo-Currás, N.; Somerson, J.; Vieira, P. A.; Ploense, K. L.; Kippin, T. E.; Plaxco, K. W. Real-Time Measurement of Small Molecules Directly in Awake, Ambulatory Animals. *Proc. Natl. Acad. Sci. U.S.A.* **2017**, *114* (4), 645–650. https://doi.org/10.1073/pnas.1613458114.

(143) Chuah, K.; Wu, Y.; Vivekchand, S. R. C.; Gaus, K.; Reece, P. J.; Micolich, A. P.; Gooding, J. J. Nanopore Blockade Sensors for Ultrasensitive Detection of Proteins in Complex Biological Samples. *Nat Commun* **2019**, *10* (1), 2109. https://doi.org/10.1038/s41467-019-10147-7.

(144) Sabaté del Río, J.; Henry, O. Y. F.; Jolly, P.; Ingber, D. E. An Antifouling Coating That Enables Affinity-Based Electrochemical Biosensing in Complex Biological Fluids. *Nat. Nanotechnol.* **2019**, *14* (12), 1143–1149. https://doi.org/10.1038/s41565-019-0566-z.

(145) Jiang, C.; Wang, G.; Hein, R.; Liu, N.; Luo, X.; Davis, J. J. Antifouling Strategies for Selective *In Vitro* and *In Vivo* Sensing. *Chem. Rev.* **2020**, *120* (8), 3852–3889. https://doi.org/10.1021/acs.chemrev.9b00739.

(146) Ostuni, E.; Chapman, R. G.; Liang, M. N.; Meluleni, G.; Pier, G.; Ingber, D. E.; Whitesides, G. M. Self-Assembled Monolayers That Resist the Adsorption of Proteins and the Adhesion of Bacterial and Mammalian Cells. *Langmuir* **2001**, *17* (20), 6336–6343. https://doi.org/10.1021/la010552a.

(147) Holmlin, R. E.; Chen, X.; Chapman, R. G.; Takayama, S.; Whitesides, G. M. Zwitterionic SAMs That Resist Nonspecific Adsorption of Protein from Aqueous Buffer. *Langmuir* **2001**, *17* (9), 2841–2850. https://doi.org/10.1021/la0015258.

(148) Chen, S.; Cao, Z.; Jiang, S. Ultra-Low Fouling Peptide Surfaces Derived from Natural Amino Acids. *Biomaterials* **2009**, *30* (29), 5892–5896. https://doi.org/10.1016/j.biomaterials.2009.07.001.

(149) Schöttler, S.; Becker, G.; Winzen, S.; Steinbach, T.; Mohr, K.; Landfester, K.; Mailänder, V.; Wurm, F. R. Protein Adsorption Is Required for Stealth Effect of Poly(Ethylene Glycol)- and Poly(Phosphoester)-Coated Nanocarriers. *Nature Nanotech* **2016**, *11* (4), 372–377. https://doi.org/10.1038/nnano.2015.330.

(150) Pelegri-O'Day, E. M.; Lin, E.-W.; Maynard, H. D. Therapeutic Protein–Polymer Conjugates: Advancing Beyond PEGylation. *J. Am. Chem. Soc.* **2014**, *136* (41), 14323–14332. https://doi.org/10.1021/ja504390x.

(151) Ishida, T.; Kiwada, H. Anti-Polyethyleneglycol Antibody Response to PEGylated Substances. *Biological and Pharmaceutical Bulletin* **2013**, *36* (6), 889–891. https://doi.org/10.1248/bpb.b13-00107.

(152) Zhang, Z.; Zhang, M.; Chen, S.; Horbett, T. A.; Ratner, B. D.; Jiang, S. Blood Compatibility of Surfaces with Superlow Protein Adsorption. *Biomaterials* **2008**, *29* (32), 4285–4291. https://doi.org/10.1016/j.biomaterials.2008.07.039.

(153) Choi, H. G.; Jung, Y. H.; Kim, D. K. Solvothermal Synthesis of Tungsten Oxide Nanorod/Nanowire/Nanosheet. *Journal of the American Ceramic Society* **2005**, *88* (6), 1684–1686. https://doi.org/10.1111/j.1551-2916.2005.00341.x.

(154) Kalantar-zadeh, K.; Vijayaraghavan, A.; Ham, M.-H.; Zheng, H.; Breedon, M.; Strano, M. S. Synthesis of Atomically Thin WO_3 Sheets from Hydrated Tungsten Trioxide. *Chem. Mater.* **2010**, *22* (19), 5660–5666. https://doi.org/10.1021/cm1019603.

(155) Wang, Y.; Cai, J.; Wu, M.; Chen, J.; Zhao, W.; Tian, Y.; Ding, T.; Zhang, J.; Jiang, Z.; Li, X. Rational Construction of Oxygen Vacancies onto Tungsten Trioxide to Improve Visible Light Photocatalytic Water Oxidation Reaction. *Applied Catalysis B: Environmental* **2018**, *239*, 398–407. https://doi.org/10.1016/j.apcatb.2018.08.029.

(156) Zhang, N.; Li, X.; Ye, H.; Chen, S.; Ju, H.; Liu, D.; Lin, Y.; Ye, W.; Wang, C.; Xu, Q.; Zhu, J.; Song, L.; Jiang, J.; Xiong, Y. Oxide Defect Engineering Enables to Couple Solar Energy

into Oxygen Activation. *J. Am. Chem. Soc.* **2016**, *138* (28), 8928–8935. https://doi.org/10.1021/jacs.6b04629.

(157) Liang, L.; Li, X.; Sun, Y.; Tan, Y.; Jiao, X.; Ju, H.; Qi, Z.; Zhu, J.; Xie, Y. Infrared Light-Driven CO2 Overall Splitting at Room Temperature. *Joule* **2018**, *2* (5), 1004–1016. https://doi.org/10.1016/j.joule.2018.02.019.

Article 1

He, G., Dong, T., Yang, Z., Branstad, A., Huang, L., Jiang, Z., (2022). Point-of-care COPD diagnostics: Biomarkers, sampling, paper-based analytical devices, and perspectives, Analyst, 147, 1273-1293. Doi: 10.1039/D1AN01702K

Article 2

He, G., Dong, T., Yang, Z., Jiang, Z., (2022) Mitigating hook effect in one-step quantitative sandwich lateral flow assay by timed conjugate release, Talanta, 240, 123157. Doi: 10.1016/j.talanta.2021.123157

Talanta 240 (2022) 123157

Contents lists available at ScienceDirect

Talanta

journal homepage: www.elsevier.com/locate/talanta

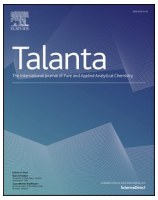

Mitigating hook effect in one-step quantitative sandwich lateral flow assay by timed conjugate release

Guozhen He [a,b], Tao Dong [b,*], Zhaochu Yang [a], Zhuangde Jiang [a]

[a] Chongqing Key Laboratory of Micro-Nano Systems and Smart Transduction, Chongqing Key Laboratory of Colleges and Universities on Micro-Nano Systems Technology and Smart Transducing, Collaborative Innovation Center on Micro-Nano Transduction and Intelligent Eco-Internet of Things, Chongqing Academician and Expert Workstation, Chongqing Technology and Business University, Nan'an District, Chongqing, 400067, China

[b] Department of Microsystems (IMS), Faculty of Technology, Natural Sciences and Maritime Sciences, University of South-Eastern Norway, Postboks 235, 3603, Kongsberg, Norway

ARTICLE INFO

Keywords:
Lateral flow assay
Hook effect
Time conjugate release
Salivary assay
Fluorescence

ABSTRACT

Sandwich lateral flow assay (LFA) is one of the most successfully commercialized paper-based biosensors, which offers a rapid, low-cost, one-step assay. Despite its advantages, conventional sandwich LFA is fundamentally limited by the high-dose "hook" effect—a phenomenon that occurs at very high analyte concentrations and results in false-negative results. In this paper, we present a novel strategy of automatic timed detection antibody release to mitigate the hook effect in sandwich LFA without additional manual steps. We introduced an intermediate pad treated with saturated sucrose solution to regulate the flow between the nitrocellulose membrane and the conjugate pad in order to delay the reaction between detection antibodies and analytes. Using C-reactive protein (CRP) as a representative analyte, we demonstrated that our strategy exhibited a range of detection 10 times wider than that of our conventional LFA, without sacrificing the limit of detection. Comparing to other published strategies, our work could offer a one-step, cost-effective approach that is closely unified with the benefits of the LFA.

1. Introduction

Sandwich lateral flow assay (LFA) has been widely applied in the rapid point-of-care (POC) testing industry due to its low cost, rapid response, and one-step operation [1]. Despite the advantages and the broad applications, sandwich LFAs produce false-negative results at very high concentrations of analytes, which is described as the high-dose "hook effect" [2–8]. T/C intensity initially increases monotonically but eventually decreases when the analyte concentration surpasses a certain level, exhibiting a hook-like curve in the T/C intensity vs. analyte concentration diagram. First observed in one-step sandwich immunoassays in the 1980s, the hook effect is an intrinsic phenomenon in sandwich assays [9]. Assuming analytes bind to detection antibodies and capture antibodies simultaneously, the widely accepted explanation is that unlabeled analytes occupy sites at the test line that would have captured labeled analytes. In other words, there is a shortage of free detection antibodies to bind analytes, which are captured at the test lines. Hook effect limits the clinical applications of LFA where biomarkers in real human samples could increase significantly when patients were experiencing severe diseases. Taking the example of C-reactive protein (CRP) concentration in serum, it is below 1 mg/mL for healthy people but can roar up to more than 250 mg/mL in case of severe infection [10].

In conventional sandwich immunoassays, the problem is solved by sample dilution [11], addition washing step [12], and increasing concentrations of detection antibody [13]. Similar strategies have also been applied in LFAs [6]. Increasing detection antibody leads to higher background noise that limits the lower limit of detection. Attempts have been made to alleviate the hook effect by adding a third line that only binds conjugates [14] and introducing multiple test zones for one analyte [5]. E.G. Rey et al. adapted kinetic measurement with an algorithm to measure the speed at which both sample and control line develop instead of measuring the final intensity [4]. Other researchers also tried to provide theoretical explanations of the "hook" effect in LFAs due to high analyte concentration [3,6]. Hook effect is affected by the capture antibody's avidity to both free analyte and analyte-detection antibody complex [6], while in most cases, both avidities need to be measured experimentally. Oh et al. reported a timed reagent release strategy by

* Corresponding author.
E-mail address: Tao.Dong@usn.no (T. Dong).

https://doi.org/10.1016/j.talanta.2021.123157
Received 21 September 2021; Received in revised form 15 December 2021; Accepted 16 December 2021
Available online 17 December 2021

adding a sample injection zone in the middle of the strip while placing a commercial asymmetric polysulfone membrane (ASPM) with asymmetric pole distribution located horizontally between the buffer pad and sample pad to delay the conjugate release [15].

To resolve the hook effect in sandwich LFA without additional steps and costs, we proposed a strategy based on delaying the release of detection antibodies from the conjugate pad to avoid the competition between free and labeled analytes at the test line. We hypothesized that by avoiding the competitive reactions between the analyte, capture antibody, and detection antibody, the hook effect could be mitigated. We re-designed the lateral flow assay and introduced an intermediate pad treated with sucrose between the nitrocellulose membrane and the conjugated pad to demonstrate our strategy. The intermediate pad regulated the liquid flow into the conjugated pad [16] to achieve the timed-release of detection antibody. The advantage of sucrose treatment was that the sucrose did not interfere with the CRP-antibody binding, while the cost of sucrose treatment was neglectable. We experimentally proved that our designated LFA mitigated false-negative results caused by the high-dose hook effect.

2. Experimental section

2.1. Reagents and instruments

Anti-CRP antibody [C2] (ab136176), anti-CRP antibody [C6] (ab8278) were purchased from Abcam in both Norway and China. High purity native CRP purified from human serum was purchased from Sigma Aldrich (both Norway and China). Nitrocellulose (NC) membranes CN140 of 25 mm width were purchased from sartorius. Glass fiber membranes, polyester fiber membranes, absorbent pads, and adhesive backing cards were purchased from Jieyi Biotech. CO., LTD. Bovine serum albumin (BSA) and Tween 20 were purchased from Beijing Solarbio Science & Technology Co., Ltd.

Saliva oral swab was purchased from Salimetrics, State College, PA. Sucrose (S0389) was purchased from Sigma Aldrich. CdSe-TiO_2 quantum dots were purchased from Kundao Biotech, Shanghai. CRP human ELISA kits were purchased from Thermo Fisher.

2.2. Quantum dots conjugation

We used a commercial CdSe-TiO_2 core-shell quantum dot with polyethylene glycol (PEG) modification as the fluorescence label. Ultraviolet (UV) light was applied as the light source for excitation. The commercial CdSe QD exhibited an excitation range between 365 and 450 nm and a fluorescence peak at 570 nm. No photobleaching was observed. As-purchased QDs were linked to anti-CRP antibody C6 (detection antibody, CdSe-C6) via EDC-NHS linking. CdSe-C6 was immobilized onto the glass fiber conjugate pad.

2.3. Preparation of the intermediate pad

We compared cellulose membranes treated with different sucrose saturation as the intermediate pad. To treat cellulose membranes with sucrose, we first dissolved excess sucrose in deionized water (DI water) at room temperature for several days to create a saturated sucrose water solution. Sucrose settlements were removed from the saturated solution. Subsequently, the saturated sucrose solution was diluted to prepare 10%–100% saturated solution. Cellulose membranes were also treated with DI water for comparison, noted as 0% saturation. Cellulose membranes were firstly wicked from the edges and then immersed into the sucrose solution. After that, cellulose membranes were dried in a vacuum chamber at 36 °C until they were completely dried.

2.4. Preparation of the lateral flow strips

The lateral flow strip is assembled with a sample pad, a conjugate pad, an NC membrane, an absorbent pad, and an intermediate pad (Fig. 1). Anti-CRP antibody C2 is applied as the capture antibody (500 μg/mL in 0.01 M phosphate-buffered saline (PBS) solution, pH 7.4), which was dispensed in a line onto CN140 NC membranes at a jetting rate of 0.5 μL/cm. The NC membranes were subsequently dried at 37 °C for 2 h in vacuum. NC membranes immobilized capture antibodies were blocked with 2% w/v BSA and 0.02% w/v Tween-20 in 0.01 M PBS solution (pH 7.2) at room temperate. Both sample pad and conjugate pad are made of glass fiber membranes. To realize timed-release of detection antibody, an intermediate pad was placed at the bottom of the conjugate pad.

2.5. Sampling of human saliva

Human saliva samples were taken from three nominally healthy volunteers using SalivaBio Oral Swabs. We received consent from the volunteers to use their saliva for research. Before each sampling, volunteers were restrained from food, alcoholic or carbonated drinks, smoking, and physical exercises. The protocol of sample collection followed recommended instructions from Salimetrics, through which the volunteer kept the oral swab in the mouth for 2 min. The swab was immediately transferred to a centrifuge tube after sampling. To extract the saliva, the swab was centrifuged at 1500 g for 15 min. Saliva samples were stored at −20 °C and analyzed within 4 months. Saliva samples were defrosted before each assay. Initial CRP concentrations in saliva were determined using ELISA human CRP kits, following the test protocol provided by the supplier. CRP was subsequently spiked into saliva samples to reach desired concentrations. Sampling and storage of human saliva were approved by the Regional Committees for Medical and Health Research Ethics. Data were stored according to the regulations of the Norwegian Center for Research Data.

2.6. Detection of CRP in artificial saliva and human saliva using fluorescence lateral flow strips

Due to the scarcity of human saliva samples, we prepared artificial saliva to develop LFAs. Mucin-based artificial saliva was prepared according to a reported method [17]. Human saliva was used during the validation of LFA. Both artificial and human saliva were spiked with CRP. Initial CRP concentrations in human saliva were measured by ELISA. For each assay, we added 200 μL sample solution with desired amounts of CRP onto the sample pad. Fluorescence was recorded by a single-lens reflex camera. Images were first transformed into grayscale,

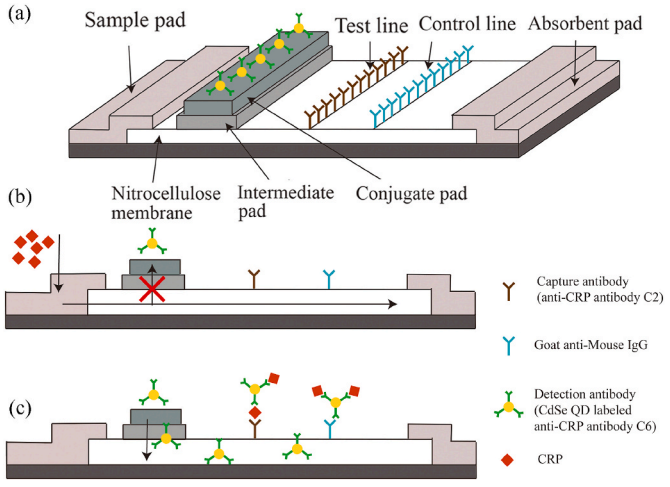

Fig. 1. (a) Scheme of the lateral flow assay structure with an intermediate pad. (b) Wetting of the conjugate pad was initially prevented by the hindrance induced by the sucrose-treated intermediate pad. (c) Release of detection antibody was delayed in order to mitigate the hook effect.

and fluorescence intensities were obtained using the measurement function in ImageJ. Intensities of T lines and C lines were calculated by subtracting background fluorescence intensity from the overall integrated intensity of the selected areas.

3. Results and discussion

3.1. Principle of the lateral flow assay with timed conjugate release

In conventional lateral flow sandwich assays, a conjugated pad is placed directly between the sample pad and nitrocellulose membrane so that detection antibodies flow with the analyte together when the conjugate pad is wetted. In this scenario, analytes will bind both detection antibody and capture antibody simultaneously [18,19]. At high analyte concentrations, when the detection antibody is deficient, unlabeled analytes compete with analytes bound to detection antibody at the test line, leading to false-negative results.

To resolve this hook effect, we hypothesized that by delaying the detection antibody entering the sandwich assay system, the competition between CRP captured at the test line and free CRP could be potentially avoided. In other words, reactions between CRP at the test line and detection antibody would be favored by setting a time interval between the presence of CRP and detection antibody at the sandwich assay system. We studied two approaches— (1) manually adding CRP and detection antibody in sequence; adding an intermediate pad that is (2) treated by sucrose to delay the release of detection antibody—to step-by-step verify our hypothesis. We deployed an intermediate pad with flow-tuning characteristics to bridge the sample pad and nitrocellulose membrane (Fig. 1). The intermediate pad sits above the conjugate pad in which the detection antibody is immobilized. Such an intermediate pad exhibits a slower vertical flow rate than its lateral counterparts to delay the flow entering the conjugate pad. Detection antibody is released at certain times when analytes are mostly bound to the test line to avoid competitive reactions.

3.2. Intermediate pad treatment with sucrose solution

We dedicatedly designed the intermediate pad by testing different materials and treatments to control the release time smartly. We finally selected a commercial cellulose membrane treated with sucrose to treat the pad. The intermediate pad should not affect the antibody-antigen reaction. It excludes the pad to be treated with most salts since salts significantly affect antibody conformation and their reactions with antigens. Sucrose was selected due to its low price and biocompatibility [16]. Sucrose did not interfere with the CRP-antibody binding, nor did it induce false-positive results. It is also believed to be an inexpensive stabilizer against degradation of proteins dried on paper substrates [20]. A barrier with tunable permeability is desired for lateral flow assays to control the delayed release of detection antibody smartly. For this purpose, we investigated paper-based barriers consisting of cellulose membrane treated with sucrose solution. We compared cellulose membrane treated with different concentrations as the intermediate layer bridging the sample-conducting nitrocellulose membrane and conjugate pad. We treated 330 μm thick cellulose membranes with DI water (which was considered as the blank group with 0% sucrose) and 10%–100% sucrose saturated solutions. We mixed red dye with sample solutions before wicking the LFA strips. The wetting performance was evaluated by recording the time spent before intermediate pad completely turned red (Fig. 2). For a blank intermediate pad without sucrose, it took around 4 min to turn red completely. At the interface between the intermediate pad and the NC membrane, the vertical fluidic resistance was larger than the horizontal fluidic resistance due to gravity and permeability difference in different porous materials. Thus, the fluid initially traveled in the horizontal direction. The intermediate pad also stored solution before it fully turned red. As the sucrose saturation percentage increased, it gradually took more time to completely color

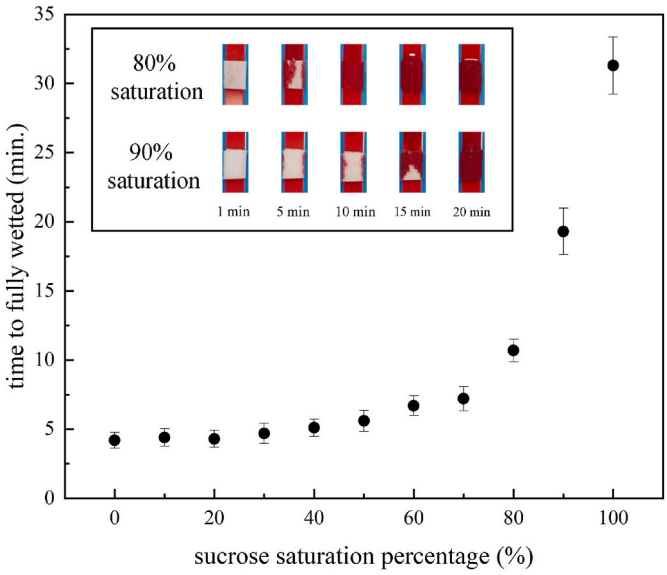

Fig. 2. Characterization of time spent to fully wet intermediate pads treated with sucrose solution at different saturation percentages (n = 3). The inset shows representative images of characterization taken from intermediate pads treated by 80% and 90% sucrose saturated solution.

the intermediate pad, which could be considered as an increase in the ability of fluidic hindrance. As the saturation percentage exceeded 70%, the wetting time increased dramatically, from 7.2 min (70% saturation) to 31.3 min (100% saturation). We considered that saturation between 70% and 90% led to moderate time delays between 7.2 min and 19.3 min, which were chosen for further studied for timed-release of detection antibody. Such hindrance to the flow could be potentially attributed to two reasons. Firstly, sucrose from the highly saturated solutions was dried and subsequently formed large amounts of small crystals within the pores of cellulose membranes. When sucrose encountered the flow, sucrose started to dissolve quickly, resulting in a local region with saturated sucrose concentration. Therefore, further dissolution of sucrose was prohibited until local concentration was decreased due to diffusion of sucrose molecules to areas where sucrose concentration was low. Sucrose crystals blocked the solution into the conjugate pad, forming a temporally water-proof barrier. On the other hand, the local region with saturated sucrose concentration exhibited a high viscosity and exerted high flow resistances that delayed the flow through the pad [16]. When sucrose crystals gradually dissolved upon contact with the aqueous solution, a route would be opened to release detection antibodies in the conjugate pad into the assay.

3.3. Hook effect in conventional lateral flow assay

The conventional format of a lateral flow assay consists of a sample pad, a conjugate pad, a nitrocellulose membrane immobilized with both a test line and a control line, and a wick (adsorbent) pad. When a sample was added to the test strip, it flowed uniformly without any delay in the release of the detection antibody (detection antibody is also often called the conjugate). To determine analyte concentrations quantitatively, researchers often measure either the test line intensity or the ratio of the test line intensity over the control line intensity (T/C). We compared both the test line intensity and the T/C ratios to study their contributions in the hook effect. We noticed that the test line intensity increased monotonically for CRP detection as CRP concentration increased within the region between 1 ng/mL to 1 μg/mL (Fig. 3a and b). The test line intensity reached the peak and saturated around 1 μg/mL. As the CRP concentration continued to increase, the test line intensity started to drop.

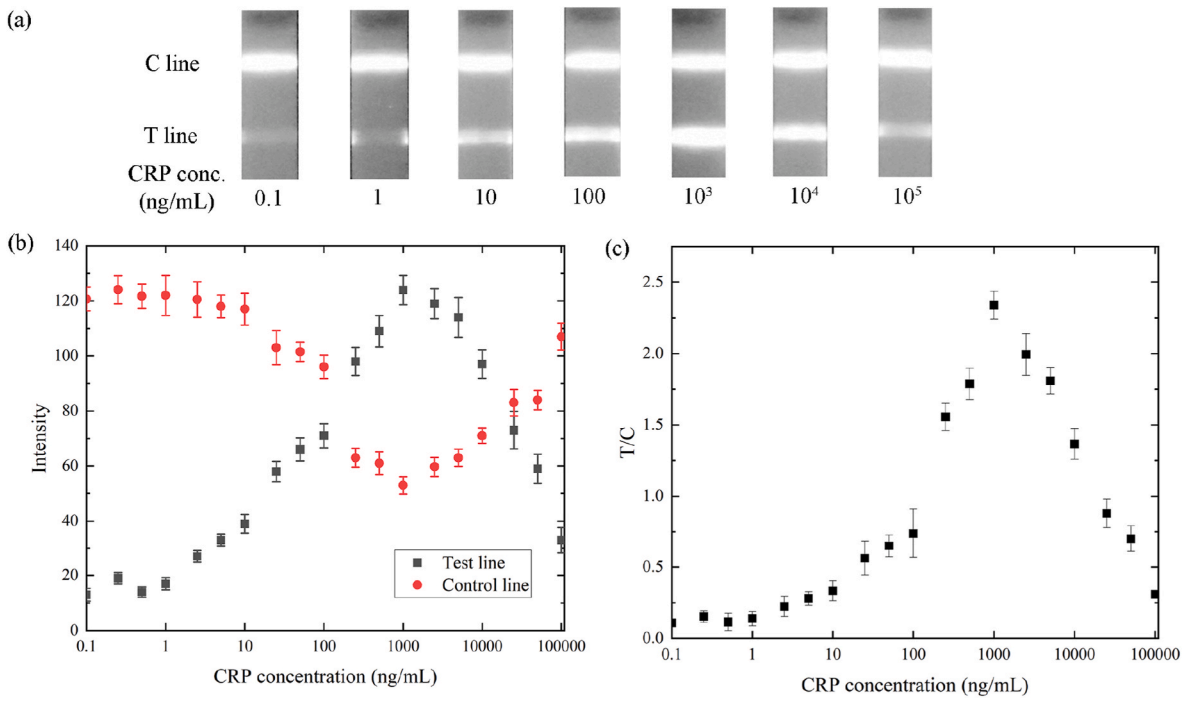

Fig. 3. (a) Greyscale photos of T and C line at different CRP concentrations. Calibration curve of conventional CRP LFA testing CRP in artificial saliva: (b) intensity of test line and control at different CRP concentrations; (c) T/C ratios at different CRP concentrations. (n = 3).

On the other hand, the control line intensity started at the highest intensity and decreased as CRP concentration increased in the region between 1 ng/mL to 1 μg/mL. However, the control line intensity reached the lowest point at around 1 μg/mL while the test line intensity reached the highest peak. With a further increase in CRP concentration, the control line intensity increased while the test line intensity decreased. T/C ratios exhibited a similar trend to the test line intensity and reached a peak around 1000 ng/mL (Fig. 3c). A clear hook was observed in both T line and T/C ratios (Fig. 3b and c). When CRP increased above 1000 ng/mL, the lateral flow assay gave false-negative results. Using T/C as the calibration curve did not exhibit any obvious advantage comparing using the T line intensity. After the hook effect happened around 1000 ng/mL CRP concentration, T intensity and T/C ratios dramatically dropped.

The most widely-accepted explanation is that the hook effect is a concentration effect [9,13]. Excess analytes hinder simultaneous binding of CRP to both capture antibody at the test line and detection antibody in solution. In conventional lateral flow assays, the detection antibody dried on the conjugate pad diffused in the nitrocellulose membrane with free CRP molecules together. Both detection antibody and capture antibody may recognize more than one epitope of CRP. Besides, one quantum dot was linked to three detection antibodies (C6) on average through our protocol. The multivalent reaction may result in higher-order antibody-CRP complexed and multiple configurations with different binding affinities or associations. The antibody-CRP association may also go through an intermediate state, forming a transient complex [21]. For simplicity, we assume CRP-C2 binding and CRP-C6 binding are both a one-step reaction and result in a single configuration for either CRP-C2 complex or CRP-C6 complex. Then, we will have four association constants for four different reactions in the lateral flow assay. We note these constants as K_a for the reaction between free CRP and capture antibody C2 immobilized at the test line, K_b for the reaction between free CRP and detection antibody C6-QD conjugate in the solution, K_c for the reaction between C6-QD conjugate and CRP-C2 at the test line, and K_d for the reaction between CRP-C6-QD complex and antibody C2 at the test line. The magnitudes of these association constants often lie in the following sequence: $K_c > K_a > K_b > K_d$ [22]. It suggested that the association rate constant of analyte binding to either detection antibody in solution or immobilized capture antibody was around the same level. In contrast, these two constants would be 3 to 4 magnitude higher than the association rate constant of detection antibody-analyte conjugate binding to capture antibody [22]. We can also expect more free CRP molecules to bind to the conjugates in solution than they bind to the detection antibody. In case of excess CRP, the binding equilibrium may shift further to the formation of CRP-C6 complexes.

The hook effect observed in the T/C ratio is a synergistic effect of both test line and control line. Before the saturation point at 1000 ng/mL, the test line intensity increased because of an increasing number of C2-CRP-C6 complexes formed at the test line, while the control line intensity decreased due to less available C6 conjugate could be captured at the control line. It resulted in a monotonic increase in T/C ratios before the hook effect. When the hook effect happened at CRP concentrations higher than 1000 ng/mL, unlabeled CRP molecules blocked sites that would have captured CRP-C6-QD conjugates. It resulted in increasing numbers of conjugates bound to the control line and an increase in control line intensity. The C6-CRP complex usually has a lower avidity than the free C6 antibody does when binding to IgG antibodies at the control line [22]. It may explain that the control line intensity at CRP concentrations between 10 and 100 μg was lower than its intensity at CRP concentrations below 10 ng/mL.

Influence of timed conjugate release on the hook effect in artificial saliva samples and human saliva samples.

Since K_c is often larger than K_a, we came up with a strategy to mitigate the hook effect by avoiding the competition between CRP-C2 binding and CRP-C6 binding. We verified this strategy by comparing premixing to sequentially adding CRP and detection antibodies (Fig. 4a). By increasing the interval between adding CRP and detection antibody, CRP is allowed to associate solely with the capture antibody C2 without interferences from detection antibody C6. We observed the “hook” peak gradually shifted to higher CRP concentrations and eventually disappeared by prolonging the time interval (Fig. 4a). T/C signals started to saturate after 10 μg/mL with a 15-min interval. To avoid manually adding detection antibody at certain time intervals, we studied the

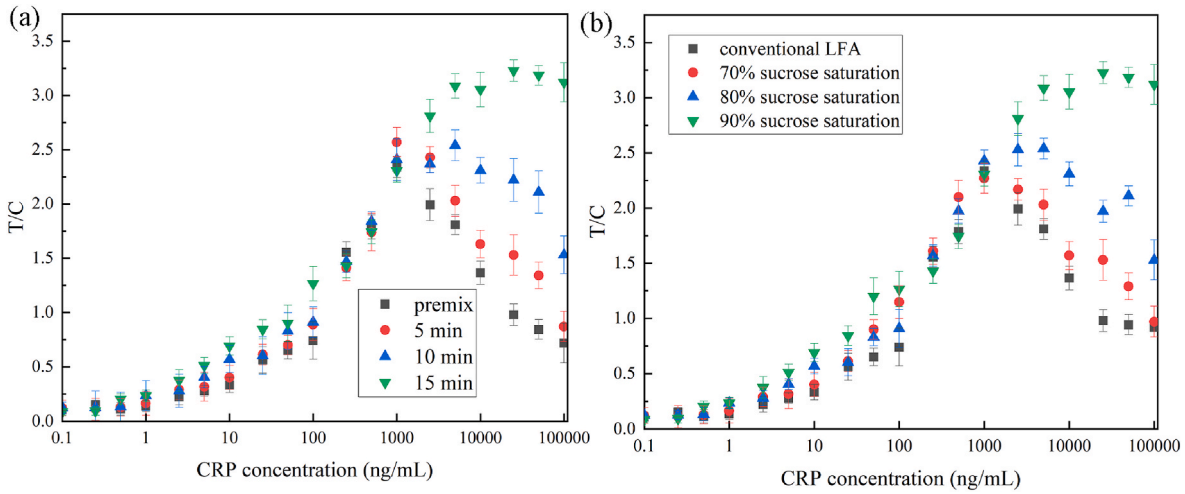

Fig. 4. Calibration curve of (a) conventional LFAs testing premixed and sequential addition of CRP and detection antibody with manual time intervals; (b) LFAs integrated with intermediate pads treated with saturated sucrose solution. Results were measured using artificial saliva (n = 3).

timed conjugate release controlled by intermediate pads treated with sucrose solution. By increasing the sucrose concentration, the intermediate pad exerted more resistance to the flow passing through and increased the delayed time to release detection antibodies from the conjugate pad. The "hook" peak moved to higher concentrations (Fig. 4b) and eventually disappeared, which exhibited a similar trend to Fig. 4a. The hook effect was resolved by our timed released strategy. What's more, sucrose treatment didn't exert any negative influence on CRP detection.

To elucidate the mitigation of the hook effect, we studied the development of both T line and C line in a lateral flow assay with the structure shown in Fig. 1. As the CRP concentration increased in the

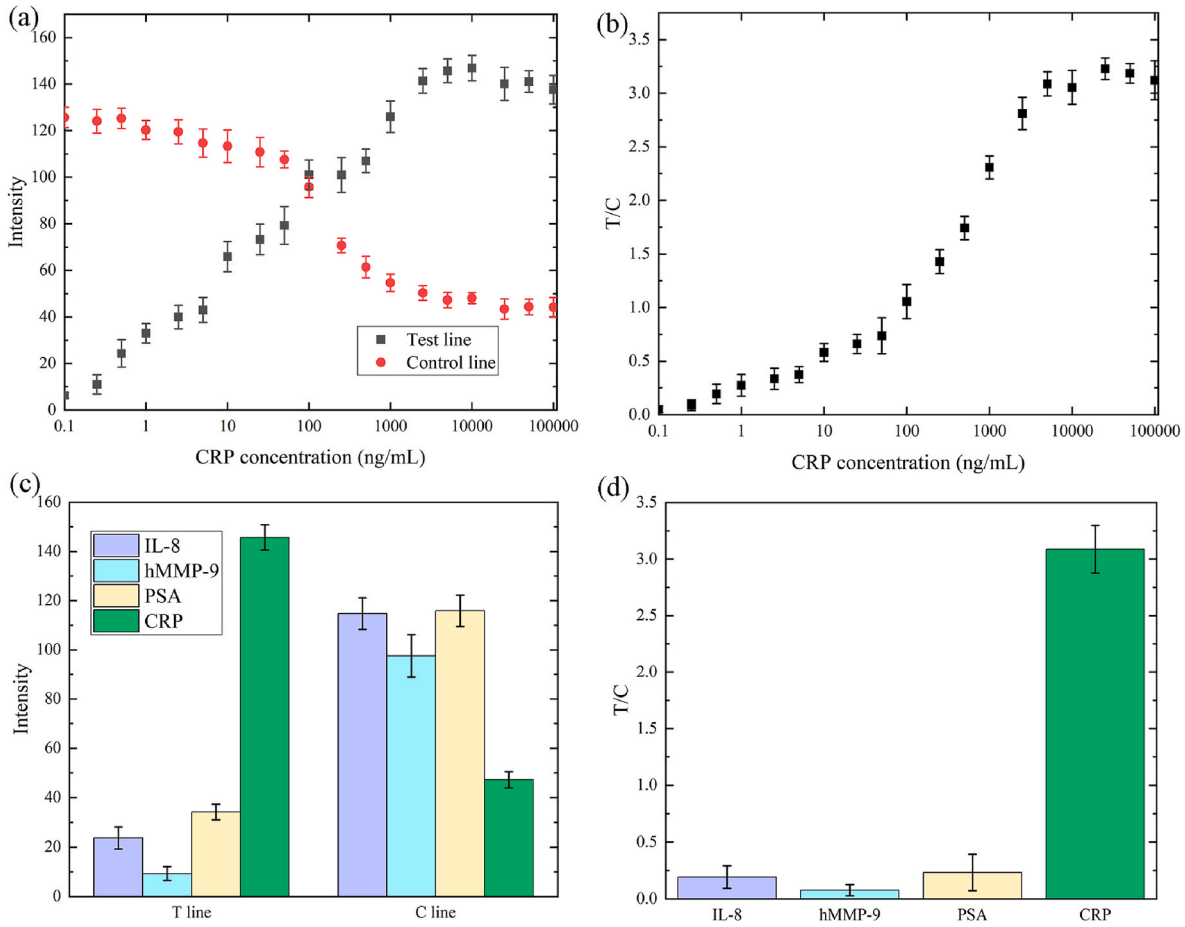

Fig. 5. Calibration curve of the CRP LFA with intermediate pad treated with 90% sucrose saturation, (a) test line and control line intensities, and (b) T/C ratios at different CRP concentrations. Histogram of the specificity of the CRP LFA with intermediate pad, (c) test line and control line intensities, and (d) T/C ratios at analyte concentrations of 5 μg/mL. Results were obtained using artificial saliva (n = 3).

region between 1 ng/mL to 10 μg/mL, we observed a monotonic increase in the test line intensity and a gradual decrease in the control line intensity (Fig. 5a). The test line intensity stopped to increase in the region between 25 μg/mL to 100 μg/mL. It also leads to a continuous increase in the T/C ratios (Fig. 5b). As the CRP concentration continued to increase from 100 μg/mL to 1000 μg/mL, we observed a plateau in both the test line intensity and the T/C ratios. No clear hook effect was observed.

In conventional lateral flow assays with high-dose CRP, free CRP competes with CRP-C6-QD conjugate at the test line. Free CRP molecules will always exist at the test line regardless of the concentrations. Since $K_c > K_a > K_b > K_d$, more CRP will be associated with C6-QD than bind with the test line. Around the saturated CRP concentration where the hook effect happened (1000 ng/mL in Fig. 3), the test line intensity would be largely governed by K_d. In the timed-release format (Fig. 5a and b), the test line intensity would be primarily governed by K_b. It may explain that timed-release of detection antibody not only mitigated the hook effect but also resulted in a wider range of detection than its conventional counterpart. The mechanism to avoid the hook effect is still under debate [6,22,23]. Before the 1990s, it was widely accepted that one-step sandwich assays were severely affected by the hook effect, while two-step sandwich assays were generally hook-effect-free [9]. When researchers reexamined the hook effect in immunoassays in the 1990s, S.A. Fernando and G.S. Wilson argued that two-step immunoassays also exhibited the hook effect, if analytes underwent multiple epitope interaction with detection antibodies [23]. However, recent studies based on simulation and surface plasmon resonance suggested that sequential injection of analytes and detection antibody could not only avoid the hook effect but improve the limit of detection as well [6,22], which agreed with our study. Usage of sucrose treatment did not comprise the limit of detection to trade for a wide working range (Table 1). Among all the strategies, sample dilution and washing step are the simplest approaches to mitigate hook effect. Nevertheless, both strategies introduced an additional manual step, which was contrary to the designing principles and benefits of LFAs—an easy, inexpensive, and one-step assay. Increasing detection antibodies and adding a third line on the membrane would significantly increase the manufacture expense due to the high cost of monoclonal antibodies. Antibody cost plays a major role in expenses of raw materials. Among current strategies, kinetic measurement is the most cost-effective approach which requires no additional manual step nor significantly increase in cost. The drawback of current kinetic measurement is that the geometric derivative of T/C is negatively correlated to the analyte concentration. The negative correlation may limit the range of detection when a wide range detection is needed. Oh et al. successful reduced the hook effect by applying strategy was based on a two-step assay [15]. In their strategy, sample and buffer solution were added onto a sample pad and a buffer pad respectively. Since the sample pad was located between two NC membranes, samples would flow in both directions. It induced potential reaction between the analytes and conjugated antibodies, which would lead to the hook effect. Even though our working range is no better than the three-line LFA [14] or the multiple-zone LFA [5], our strategy offers a cost-effective approach to avoid the hook effect. In the three-line LFA [14] and the multiple-zone LFA [5], the amounts of detection antibodies were significantly increased, which would greatly increase manufacturing cost and hinder further commercialization. Compared to other strategies without dramatically increase the amount of detection antibody [4,15], our strategy successfully lower the limit of detection by two-fold without compromising the working range.

Followingly, we tested the specificity of our improved hook-effect-free lateral flow assay against other common protein analytes that exist in human blood and saliva (Fig. 5c and d). We selected IL-8, hMMP-9, and PSA, which co-exist in both saliva and serum of patients with heart disease and chronic obstructive pulmonary disease, to verify the potential of our modified lateral flow assay in screening chronic diseases. Concentrations of these interferents and CRP were set to 5 μg/mL for comparison. The T/C ratio of CRP test was around 100-fold higher than the T/C ratios of IL-8, hMMP-9 and PSA tests. The interference was neglectable comparing to the CRP result.

Lastly, we tested saliva samples to verify to hook-effect-free performance of our LFA strips with an intermediate pad. Saliva samples were collected from nominally healthy volunteers using Saliva oral swabs. Initial CRP concentrations in saliva were determined using ELISA. CRP was subsequently spiked into saliva samples to reach desired concentrations. As shown in Figure S1, no hook effect was observed at the test line in the range between 1 ng/mL to 10 μg/mL; however, fluctuation in T/C ratios was observed between 10 μg/mL to 100 μg/mL when fluorescence intensities at T and C lines reached their limits. It resulted from the changes in C line intensity while T line intensity gradually reached a plateau. After all, T/C ratio was more sensitive to the variations than the T line intensity. Accuracy of LFA strips with intermediate pad treated with 90% saturation was evaluated against ELISA with human saliva samples (Table S1). The relative errors of our method against ELISA were lower than 15%.

4. Conclusions

We reported a new strategy based on automatic timed release of detection antibody in sandwich lateral flow assay to resolve the hook effect without additional manual operation. In our approach, timed release was achieved by an intermediate pad between the nitrocellulose membrane and the conjugate pad to regulate the flow and delay the release of the detection antibody. We investigated sucrose treatment of the cellulose membrane as the intermediate pad. Sucrose crystals served as barriers to liquid displacement. Our improved LFA exhibited a working range between 0.5 ng/mL–10 μg/mL, without observing the

Table 1
Comparison between our strategy and other strategies to mitigate the hook effect.

Strategy	Limit of detection	Working range	Linear range	Comments	Ref.
Colorimetric three-line LFA	0.649 ng/mL	0.69 ng/mL–1.02 mg/mL; 0.4–84.7 μg/mL in clinical samples.	1 ng/mL–500 μg/mL	A third line of antibody would increase fabrication cost. It requires suitable algorithm to calculate test results.	[14]
Colorimetric multiple-zone LFA	0.2875 ng/mL	0.575 ng/L–1150 mg/L	Not mentioned.	Multiple test zones in circular shape would significantly increase fabrication cost. Hook effect still exists.	[5]
Colorimetric LFA with kinetic measurement	not mentioned	not mentioned	10–255 ng/mL	kinetic measurement may result in complicity in readouts and large method bias.	[4]
Fluorescence LFA with sequential sample and buffer injection	43 ng/mL	119 ng/mL–100 μg/mL	not mentioned	Sample and buffered solution are added separately.	[15]
Fluorescence LFA with intermediate pad	0.5 ng/mL	0.5 ng/mL–10 μg/mL	50 ng/mL – 2.5 μg/mL		This work

*Note: due to varieties of units being used in the references, we adapt molar concentration for better comparison. Since it was not classified whether monomeric or pentameric CRP was studied in the references, we assume that pentameric CRP (115 kDa) was under investigation.

hook effect. Compared to other published strategies, our work offers a cost-effective, one-step approach that is closely unified with the benefits of LFA.

In the future, researchers may combine new label-free strategies based on acoustic, thermal, and other principles to replace the sandwich format in LFAs. Other attempts may be made in researching new bio-recognition elements compatible with LFA or other paper-based assays. Researchers also need to better explain the delivery and distribution of both analytes and detection antibodies and their reactions with each other in the porous medium. After all, LFA is one of the most developed and commercialized paper-based biosensors. Improving LFA is still by large an empirical process. Input-output ratio (in this case, expense-profit ratio) is always an essential factor to be considered when studying the LFA and other paper-based biosensors.

Credit author statement

Guozhen He: Conceptualization, Methodology, Software, Validation, Formal analysis, Investigation, Resources, Writing – review & editing, Visualization. Tao Dong: Data curation, Writing – review & editing, Supervision, Project administration, Funding acquisition. Zhaochu Yang: Writing – review & editing, Supervision, Project administration, Resources. Zhuangde Jiang: Supervision, Funding acquisition.

Declaration of competing interest

The authors declare that they have no known competing financial interests or personal relationships that could have appeared to influence the work reported in this paper.

Acknowledgements

This work was supported by projects of RFF Forskningsfond Oslofjordfondet (Project No. 285575), Regionalt forskningsfond Vestfold og Telemark (Project No. 321814), The support from Chongqing Research Program of Basic Research and Frontier Technology (Project No. cstc2019jcyj-msxmX0776 and cstc2021jcyj-msxmX1038), and Chongqing Education Commission – Science and Technology Research Program (Project Nos. KJZD-K201800802, KJZD-K201900802, and KLZD-K202000805) is also acknowledged.

Appendix A. Supplementary data

Supplementary data to this article can be found online at https://doi.org/10.1016/j.talanta.2021.123157.

References

[1] M. Sajid, A.-N. Kawde, M. Daud, Designs, formats and applications of lateral flow assay: a literature review, J. Saudi Chem. Soc. 19 (2015) 689–705, https://doi.org/10.1016/j.jscs.2014.09.001.

[2] Y. Gao, Z. Zhu, X. Xi, T. Cao, W. Wen, X. Zhang, S. Wang, An aptamer-based hook-effect-recognizable three-line lateral flow biosensor for rapid detection of thrombin, Biosens. Bioelectron. 133 (2019) 177–182, https://doi.org/10.1016/j.bios.2019.03.036.

[3] N. Sathishkumar, B.J. Toley, Development of an experimental method to overcome the hook effect in sandwich-type lateral flow immunoassays guided by computational modelling, Sensor. Actuator. B Chem. 324 (2020), 128756, https://doi.org/10.1016/j.snb.2020.128756.

[4] E.G. Rey, D. O'Dell, S. Mehta, D. Erickson, Mitigating the hook effect in lateral flow sandwich immunoassays using real-time reaction kinetics, Anal. Chem. 89 (2017) 5095–5100, https://doi.org/10.1021/acs.analchem.7b00638.

[5] J. Hu, J.R. Choi, S. Wang, Y. Gong, S. Feng, B. Pingguan-Murphy, T.J. Lu, F. Xu, Multiple test zones for improved detection performance in lateral flow assays, Sensor. Actuator. B Chem. 243 (2017) 484–488, https://doi.org/10.1016/j.snb.2016.12.008.

[6] G.M.S. Ross, D. Filippini, M.W.F. Nielen, G.I.J. Salentijn, Unraveling the hook effect: a comprehensive study of high antigen concentration effects in sandwich lateral flow immunoassays, Anal. Chem. 92 (2020) 15587–15595, https://doi.org/10.1021/acs.analchem.0c03740.

[7] A.D. Winder, A.S. Mora, E. Berry, J.R. Lurain, The "hook effect" causing a negative pregnancy test in a patient with an advanced molar pregnancy, Gynecol. Oncol. Rep. 21 (2017) 34–36, https://doi.org/10.1016/j.gore.2017.06.008.

[8] C.-W. Yeung, A.N.Y. Cheung, Negative pregnancy test in patients with trophoblastic diseases, Curr. Obstet. Gynecol. Rep. 3 (2014) 102–106, https://doi.org/10.1007/s13669-013-0067-2.

[9] S. Amarasiri Fernando, G.S. Wilson, Studies of the 'hook' effect in the one-step sandwich immunoassay, J. Immunol. Methods 151 (1992) 47–66, https://doi.org/10.1016/0022-1759(92)90104-2.

[10] P. Póvoa, E. Almeida, P. Moreira, A. Fernandes, R. Mealha, A. Aragão, H. Sabino, C-reactive protein as an indicator of sepsis, Intensive Care Med. 24 (1998) 1052–1056, https://doi.org/10.1007/s001340050715.

[11] L.E.M. Miles, D.A. Lipschitz, C.P. Bieber, J.D. Cook, Measurement of serum ferritin by a 2-site immunoradiometric assay, Anal. Biochem. 61 (1974) 209–224, https://doi.org/10.1016/0003-2697(74)90347-9.

[12] H.C. Vaidya, B.A. Wolf, N. Garrett, W.J. Catalona, R.V. Clayman, M.H. Nahm, Extremely high values of prostate-specific antigen in patients with adenocarcinoma of the prostate; demonstration of the "hook effect", Clin. Chem. 34 (1988) 2175–2177, https://doi.org/10.1093/clinchem/34.10.2175.

[13] R.G. Ryall, C.J. Story, D.R. Turner, Reappraisal of the causes of the "hook effect" in two-site immunoradiometric assays, Anal. Biochem. 127 (1982) 308–315, https://doi.org/10.1016/0003-2697(82)90178-6.

[14] Y.K. Oh, H.-A. Joung, H.S. Han, H.-J. Suk, M.-G. Kim, A three-line lateral flow assay strip for the measurement of C-reactive protein covering a broad physiological concentration range in human sera, Biosens. Bioelectron. 61 (2014) 285–289, https://doi.org/10.1016/j.bios.2014.04.032.

[15] J. Oh, H.-A. Joung, H.S. Han, J.K. Kim, M.-G. Kim, A hook effect-free immunochromatographic assay (HEF-ICA) for measuring the C-reactive protein concentration in one drop of human serum, Theranostics 8 (2018) 3189–3197, https://doi.org/10.7150/thno.24034.

[16] B. Lutz, T. Liang, E. Fu, S. Ramachandran, P. Kauffman, P. Yager, Dissolvable fluidic time delays for programming multi-step assays in instrument-free paper diagnostics, Lab Chip 13 (2013) 2840–2847, https://doi.org/10.1039/C3LC50178G.

[17] J.J. Pytko-Polonczyk, A. Jakubik, A. Przeklasa-Bierowiec, B. Muszynska, Artificial saliva and its use in biological experiments, J. Physiol. Pharmacol. Off. J. Pol. Physiol. Soc. 68 (2017) 807–813.

[18] D. Gasperino, T. Baughman, H.V. Hsieh, D. Bell, B.H. Weigl, Improving lateral flow assay performance using computational modeling, Annu. Rev. Anal. Chem. 11 (2018) 219–244, https://doi.org/10.1146/annurev-anchem-061417-125737.

[19] M.M. Gong, D. Sinton, Turning the page: advancing paper-based microfluidics for broad diagnostic application, Chem. Rev. 117 (2017) 8447–8480, https://doi.org/10.1021/acs.chemrev.7b00024.

[20] G.M. Whitesides, Viewpoint on "Dissolvable fluidic time delays for programming multi-step assays in instrument-free paper diagnostics, Lab Chip 13 (2013) 4004–4005, https://doi.org/10.1039/C3LC90066E.

[21] G. Schreiber, G. Haran, H.-X. Zhou, Fundamental aspects of protein−protein association kinetics, Chem. Rev. 109 (2009) 839–860, https://doi.org/10.1021/cr800373w.

[22] T. Liang, R. Robinson, J. Houghtaling, G. Fridley, S.A. Ramsey, E. Fu, Investigation of reagent delivery formats in a multivalent malaria sandwich immunoassay and implications for assay performance, Anal. Chem. 88 (2016) 2311–2320, https://doi.org/10.1021/acs.analchem.5b04222.

[23] S. Amarasiri Fernando, G.S. Wilson, Multiple epitope interactions in the two-step sandwich immunoassay, J. Immunol. Methods 151 (1992) 67–86, https://doi.org/10.1016/0022-1759(92)90105-3.

Article 3

He, G., Dong, T., Yang, Z., Ohlckers, P., (2019) Tuning 2D Black Phosphorus: defect tailoring and surface functionalization, Chemistry of Materials, 31(24), 9917-9938. Doi: 10.1021/acs.chemmater.9b03639

Article 4

He, G., Dong, T., et al., (2023) oxygen-vacancy-engineered tungsten trioxide coating with ultra-high resistance against adhesion of fouling proteins for biomedical sensor surfaces.

Article 5 (IEEE Conference)

He, G., Dong, T., Yang, Z., (2022) Probe sonication to prepare homogenous WO_3 nanosheet inks for energy conversion and biosensing applications, 20th International Conference on Mechatronics-Mechatronika, pp. 1-4. IEEE. DOI: 10.1109/ME54704.2022.9982863.

Doctoral dissertation no. 167
2023
—

Point of Care COPD Diagnostics Based on Paper-based Assay and Biofluid Sensing

Dissertation for the degree of PhD

—

Guozhen He

—

ISBN 978-82-7206-783-9 (print)
ISBN 978-82-7206-782-2 (online)

usn.no